Pseudo-First-Order Stark Effect in Symmetric-Top Molecules

Marko Härtelt

Diploma Thesis

Pseudo-First-Order Stark Effect in Symmetric-Top Molecules

Marko Härtelt

Fachbereich Physik
Technische Universität Berlin, Germany

Research performed at:
Fritz-Haber-Institut der Max-Planck-Gesellschaft
Department of Molecular Physics

Thesis supervisor: Prof. Dr. Bretislav Friedrich
Reviewer: Prof. Dr. Thomas Möller

March 28, 2008

Zusammenfassung

Befinden sich Moleküle in einem Molekularstrahl, so sind ihre Molekülachsen beliebig im Raum orientiert. Aufgrund dieser statistischen Verteilung der Molekülachsen können winkelabhängige Eigenschaften nicht direkt untersucht werden. Diese sind jedoch von grundlegender Bedeutung für die detaillierte Untersuchung von Molekülkollisionen und Photodissoziationsprozessen als auch in spektroskopischen Experimenten. Durch äußere Felder lassen sich die Moleküle im Laborsystem ausrichten. Dabei werden zwei fundamental verschiedene Methoden unterschieden. Zum einen können präzidierende Rotationszustände von symmetrischen Kreiselmolekülen in einem Hexapol selektiert werden, wobei Moleküle des selben Rotationszustandes die selbe Orientierung aufweisen. Zum anderen kann die Rotationsbewegung der Moleküle aller Zustände durch elektrostatische oder AC elektrische Felder, zum Beispiel durch einen Laser, beeinflusst werden. Elektrostatische Felder richten das Dipolmoment polarer Moleküle entlang der Feldrichtung aus. Der Grad der Orientierung hängt aber stark von der Temperatur des Ensembles, dem Dipolmoment und der Rotationskonstanten ab. In Laserfeldern hingegen wird die Anisotropie der Polarisierbarkeit von Molekülen ausgenutzt. Damit ist es möglich Moleküle auszurichten, im allgemeinen jedoch nicht zu orientieren.

Im Jahr 1999 hatten B. Friedrich und D. Herschbach die Idee, elektrostatische und nichtresonante Laserfelder zu überlagern. Lineare Moleküle in nichtresonanten Laserfeldern bilden quasientartete Zustände aus, sogenannte „tunneling doublets“, welche mit Hilfe eines schwachen elektrischen Feldes durch den „pseudo-first-order“ Stark Effekt gekoppelt werden. Die entstehenden Zustände sind entgegengesetzt zueinander stark orientiert. Der Grad an Orientierung, der in den kombinierten Feldern erreicht werden kann, übertrifft den in elektrostatischen Feldern. Bisher wurde die Idee nur für lineare Moleküle ausgearbeitet und experimentell bestätigt. Die theoretische Verallgemeinerung dieser Methode auf das komplexere System der symmetrischen Kreiselmoleküle, ist das Thema dieser Diplomarbeit.

In Abhängigkeit von den Trägheitsmomenten und den Polarisierbarkeiten, die jeweils prolat oder oblat sein können, lassen sich vier verschiedene Typen von symmetrischen Kreiseln unterscheiden. Untersucht wurde die Wirkung von kollinear und senkrecht kombinierten Feldern auf die niedrigsten Rotationszustände dieser verschiedenen Typen. Zur

Auswertung wurden bisher vorhandene Modelle, die das Verhalten der Zustände in einzelnen Feldern beschreiben, herangezogen. Für sehr große Feldstärken erhält man im Grenzfall jeweils einen harmonischen Oszillator. Korrelationsdiagramme, welche die feldfreien Zustände mit ihren Grenzwerten verbinden, dienen dazu, verschiedene Typen von Zuständen zu unterscheiden. Für kollineare Felder konnte außerdem die Schrödingergleichung auf eine eindimensionale Bewegungsgleichung reduziert und ein effektives Potential hergeleitet werden, das eine einfachere Deutung der Ergebnisse ermöglicht.

Die kollinearen bzw. senkrechten Felder richten das Dipolmoment von Molekülen mit einer oblaten bzw. prolaten Anisotropie der Polarisierbarkeit entlang des elektrostatischen Feldes aus. Für Moleküle mit einer oblaten Polarisierbarkeitsanisotropie wirkt für Zustände mit $\tilde{J} \geq |K| + |M|$ der gleiche Verstärkungsmechanismus, der auch bei linearen Molekülen die Verstärkung der Orientierung verursacht. Das elektrostatische Feld koppelt die im Laserfeld entstandenen „tunneling doublets“ und richtet sie entgegengesetzt aus. Zustände mit $\tilde{J} < |K| + |M|$ hingegen haben kein Äquivalent im linearen Molekül. Im Feld eines Lasers treten sie als zweifach exakt entartete Zustände („degenerate doublets“) auf, die entgegengesetzt zueinander entlang der Polarisationsrichtung des Lasers stark orientiert sind. Starke elektrische Felder sorgen für ein Umklappen der entgegengesetzt zum elektrischen Feld orientierten Zustände. Für eine prolate Anisotropie der Polarisierbarkeit gibt es vergleichbare Verstärkungsmechanismen in den senkrechten Feldern.

Die Analyse der gegeneinander geneigten Felder wird durch die Aufhebung der Zylindersymmetrie erschwert. Werden zwei der Parameter - Feldstärken und Neigungswinkel - verändert, führt dies zu einer Veränderung des Verhaltens an einer Kreuzung. Aus vermiedenen Kreuzungen können echte Kreuzungen werden. Die verwendeten adiabatischen Bezeichnungen („label“) der Zustände hängen von dem gewählten Pfad im Parameterraum ab und können untereinander tauschen („label switching“). Für vergleichbare Systeme wurde ein derartiges Verhalten bisher nicht dokumentiert. Eine Ursache für das „label switching“ ist die Brechung der Symmetrie. Eine ausreichende Erklärung liefert dies jedoch nicht, da nur bei Beteiligung des elektrischen Feldes die „label“ tauschen. Werden nur die Strahlungsintensität und der Neigungswinkel verändert, kommt es trotz Symmetrieveränderung nicht zum Tausch.

Ein weiterer Grund könnte das chaotische Verhalten dieses quantenmechanischen Systems sein, wofür in anderen Arbeiten Hinweise gefunden wurden. Zusätzlich könnte Monodromie, welche für den symmetrischen Kreisel in elektrostatischen Feldern bereits nachgewiesen wurde, eine Ursache sein. Monodromie verhindert in der Quantenmechanik das Auffinden einer globalen und glatten Funktion, mit deren Hilfe die Energien aller Zustände als Funktion der Quantenzahlen dargestellt werden können. Alle bisherigen Untersuchungen an zweiatomigen und symmetrischen Kreiselmolekülen sowie vergleichbaren Systemen

basieren jedoch auf Betrachtungen für feste Werte der Feldstärke(n) und des Neigungswinkels. Das Phänomen des „label switchings“ tritt jedoch erst beim Variieren von Parametern auf.

In dieser Arbeit wurden erste quantenmechanische Untersuchungen des Monodromieverhaltens vorgenommen. Dabei konnte gezeigt werden, dass Monodromie auch im reinen AC-Feld eines Lasers bei einer prolaten Polarisierbarkeitsanisotropie des symmetrischen Kreisels auftritt. In den kombinierten und geneigten Feldern wurden Hinweise für einen fundamentalen Wechsel der Art der Monodromie gefunden. Eine genauere Analyse setzt jedoch den Vergleich mit dem klassischen System voraus und das Konzept der Monodromie muss auf variierende Parameter erweitert werden. Ob damit das Tauschen der Bezeichner erklärt werden kann, konnte nicht abschließend bewiesen werden. Das betrachtete System wirft viele interessante Fragestellungen auf, die weitere Untersuchungen lohnenswert erscheinen lassen.

Contents

1 Introduction

1.1 Why would one wish to orient molecules?

The uncertainty principle ensures that molecules are perpetually restless. Any attempt at fixing a molecular position is penalized by widening the spread in the conjugate momentum. Or *vice versa*. This is exemplified by the free rotation of a gaseous molecule about its center of mass: since such a motion is characterized by a fixed value of the rotational angular momentum, the conjugate angle that describes the position of the molecular frame in the laboratory is arbitrary. This has a dramatic consequence: molecular rotation averages out any orientational dependence of the interactions the molecule may partake in and makes it act in the laboratory frame as if it were isotropic, *i.e.*, as if the shape of the molecule were spherical. Although gas phase molecules are unperturbed and, therefore, suitable for studies of fundamental molecular properties and interactions, molecular rotation blurs much of the directional information that can be obtained about molecules, including information about molecular structure. In this thesis, we extend a new techniques that makes it possible to do away with rotational averaging of interactions in the gas phase. We expect that the technique will find applications in stereo- and photo-dissociation dynamics, spectroscopy, and in manipulation of molecules.

In order to reveal the spatial properties of the interactions of gaseous molecules with one another or with radiation, two major techniques have been developed to orient the molecules in the laboratory frame. The first such technique is based on the focusing properties of a hexapole electric field that can be used to state-select *precessing states* of polar symmetric top molecules (or equivalent) [1, 2]. Precessing states are characterized by nonzero values of all the symmetric-top quantum numbers, J, M, and K; as a result, molecules in such states are inherently oriented in the laboratory frame. However, when $K = 0$, all M-states are only aligned and so state-selection of these tumbling states cannot produce orientation. That is, *unless* the states become perturbed by their interaction with an external field ...

This thesis is concerned with an orientation/alignment technique based on a controlled perturbation of molecular rotation by external fields. This technique is applicable to any non-spherical molecules. Like the classical pendulum or the needle of a compass, the molecular dipole moment is acted upon by a torque exerted by the external field which forces it to

line up with the field. Because of the limitations imposed by the uncertainty principle, the molecular dipole in fact librates (oscillates) about the field direction like a pendulum. This technique was first implemented for polar molecules whose free rotation was transformed into a pendular motion by a static electric field [3, 4].

Developed in spite of the lamentations that "even a strong field would achieve only a tiny orientation" [5], the *pendular orientation* technique has now been widely accepted, and implemented in many laboratories. It makes it possible to orient or align the figure axis of a host of polar [4] or paramagnetic molecules [6] (as well as of paramagnetic ions), including linear and asymmetric top species [7, 8]. For the technique to be applicable, the dipole moment must be coupled to one of the molecular axes so that the resulting interaction be proportional to the cosine of the angle between the body- and space-fixed axes. While the electric dipole moment is always coupled to the molecular frame, this is not generally the case for the magnetic moment. However, for instance for linear molecules with nonzero electronic angular momentum which is coupled to the molecular axis, the corresponding electronic magnetic moment lies along the internuclear axis as well and, therefore, pendular states can be created even in a magnetic field [9]. In the pendular mode, the molecular axis librates about the field vector and thus is oriented (in the case of the electric dipole interaction) or aligned (in the magnetic case, due to the equiprobable projections of the electronic angular momentum on the internuclear axis in either direction).

The directionality of pendular states arises from hybridization (linear superposition) of the field-free rotor states which are coupled by the cosine interaction. Since the hybridization occurs most easily for the lowest rotational states, a key ingredient of pendular orientation/alignment is condensation of the molecules into these lowest rotational states, *i.e.*, rotational cooling. Pendular orientation has been employed in a variety of studies, including spectroscopy of molecules [10, 11] and clusters [12, 13], collision stereodynamics [14], and photodissociation [15, 16]. The anisotropic distribution of pendular molecules has been also demonstrated by observing the concomitant optical anisotropy using polarization spectroscopy [17]. The polarization spectra were found to have a sparse structure that can be easily assigned and, therefore, polarization spectroscopy of pendular molecules is being developed as a tool for the study of the otherwise congested spectra of polyatomic molecules.

Pendular hybridization of a different kind can be achieved by the interaction of a nonresonant laser field with the anisotropic molecular polarizability [18, 19]. This method is applicable regardless of whether or not the molecule is polar or paramagnetic and can be used to extend rotational spectroscopy [20], suppress rotational tumbling [21, 22] focus molecules [23, 24], or to attain spatial trapping of molecules [18, 25].

Recently, two general approaches to enhance orientation and alignment have been developed, which are amenable to a wide variety of molecules and applications [26, 27]. The key aspect is to endow a polar molecule with what resembles a precessing state. Such molecules, whether linear or asymmetric, in effect can be made to act almost like a symmetric top. The enhanced interaction with external fields thereby provided can be exploited in many methods to control or restrict molecular orientation or translation.

1.2 Previous theoretical and experimental work

The mutual orientation of the reactants in a collisional experiment has a major influence on the reaction cross section. This can be clearly seen for the case of a collision between an atom and a heteronuclear diatomic molecule. The outcome of the collision depends on whether the molecule 'strikes' the atom with its head or tail, $A + BC \rightarrow AB + C$ or $A + CB \rightarrow AC + B$. Scattering experiment with oriented molecules have been in progress since the 1960s using the technique of hexapole focusing, to select precessing states of symmetric top molecules [2, 28, 29, 30, 31].

Likewise, photodissociation or photoabsorbtion depends on the relative orientation of the transition dipole moment and the direction of the polarization vector of the radiation. An ion imaging experiment [32] delivers the full product velocity distribution of a photodissociation event. Examples include the $ABC + h\nu \rightarrow ABC^* \rightarrow A + BC$ reaction, where the dynamics of the photo-induced bond breaking could be studied [33]. The random orientation of the molecular axis conceals the spatial aspects of the dynamics. In order to reveal them, the molecules have to be oriented [34].

In 1990 Loesch and Remscheid [3] and, independently, Friedrich and Herschbach [4] came up with the idea to angularly trap the dipole of a polar molecule by a pendulum potential created by the interaction with an electrostatic field. This method, *pendular orientation* (also known as the 'brute-force method') is more versatile than hexapole focusing, applicable to linear molecules as well as to symmetric and asymmetric tops [7, 8], but works only for molecules with a large value of the ratio of the body-fixed dipole moment to the rotational constant. Since only low lying rotational states are oriented, the method is only suitable for molecules that can be strongly rotationally cooled in a supersonic nozzle expansion. There is a host of experiments which made use of pendular orientation, e.g., to separate cofragments from photodissociation of van der Waals clusters, stereodynamics of molecular collisions, or spectroscopy of 'pendular states' for all species of molecules from linear to asymmetric tops [35].

For nonpolar molecules, Friedrich and Herschbach [18] proposed to use the interaction of the anisotropic molecular polarizability with a nonresonant laser field to achieve *pendular alignment* of the molecular axis. Pendular alignment has been applied to all kinds of molecules in a variety of experiments. Combined laser fields have been used to achieve three-dimensional alignment, while short pulses can be used to create aligned molecules in a field-free region. For a recent review see [36, 37].

The emergence of methods for slowing, trapping and manipulating gaseous species has led to a renaissance in atomic physics which is now progressing into molecular/chemical physics as well. Since molecules offer a vast range of properties not available with atoms, explorations of ultracold molecules hold the promise of not just widening the scope of atomic phenomena (such as Bose-Einstein condensation) but of reaching entirely new territories. For instance, energy transfer processes and chemical reactions would exhibit pronounced quantum dynamics if molecular translation can be slowed enough to endow the molecules with de Broglie wavelengths large compared with the size of the molecules [38].

Since the forces available to trap neutral atoms or molecules are weak, a key requisite for trapping is a means to lower markedly their translational energy, typically below 1 K. This can be accomplished with a variety of techniques, among which Stark [39, 40] and optical deceleration [41, 42, 43] are the leading ones. Both these techniques rely on one's ability to orient/align the molecular axis in the laboratory frame. Slow and cold molecules can play a unique role in many *applications*, including spectroscopy, collision dynamics (and coherent control), collective quantum effects, and even in particle physics.

The reliance on special properties of particular molecules has been done away with by the development of techniques that *combine a static electric field with a nonresonant radiative field*. The combined fields give rise to an amplification effect which occurs for any polar molecule, as only an anisotropic polarizability, along with a permanent dipole moment, is required. This is always available in polar molecules. Thus, often a very weak static electric field can convert second-order alignment by a laser into a strong first-order orientation. If the polar molecule is also paramagnetic, combined static electric and magnetic fields yield similar amplification effects [44, 45, 27]. So far, the combined-fields effects have been worked out for linear polar molecules, and corroborated in a number of experiments.

The first experiments which made use of the combined fields where made by the Buck group on linear rare gas molecules [46, 47, 48, 49]. The HXeI molecules were produced by the photolysis of HI embedded in the outer shell of large Xe_n clusters. For a standard photodissociation experiments it would be impossible to distinguish between H atoms from HI and HXeI. Since the polarizability and dipole moment of HI are small compared

to HXeI the combined fields give rise to a highly asymmetric spatial distribution of the product H atoms from HXeI.

In the experiments performed by the group of Sakai [50, 51, 52], the main aim was to verify the effects of molecular orientation in the combined fields. OCS, a molecule with a much smaller dipole moment compared to HXeI, was rotationally cooled in a pulsed seeded supersonic expansion. The first acceleration stage of a time-of-flight mass spectrometer was used to provide the electrostatic field. The molecules were irradiated within the fields by a ND:YAG laser radiation at 1064nm and a pulse length of 12ns. At the peak of the laser pulse a femtosecond laser pulse was used to ionize the OCS molecules, which undergo a Coulomb explosion. The orientation of the fragments was determined from the time-of-flight distribution.

1.3 This thesis

The aim of this thesis was to explore the amplification effect of the combined fields on molecular orientation of symmetric top molecules.

In chapter 2, the basic principles and concepts used throughout this thesis are introduced. First orientation and alignment are defined. Then the symmetric and asymmetric top molecules in the rigid-rotor approximation are described. The interactions of the molecular rotor with electrostatic and nonresonant laser fields are described in section 2.3. The main focus is on symmetric tops, although some links to asymmetric tops are made.

Chapter 3 gives an introduction into the numerical and computational methods.

The detailed analysis of the amplification effect that combined electrostatic and nonresonant radiative fields have on *symmetric top* molecules is given in chapter 4. The analysis draws on previous work of Friedrich and Herschbach on linear molecules [26, 53] as well as on the work of Kim and Felker, who have treated symmetric top molecules in pure nonresonant radiative fields [54]. All possible symmetry combinations of the inertia tensor and the polarizabilty are considered. Both collinear and perpendicular fields are considered.

First the Hamiltonian (in reduced, dimensionless form) for a symmetric top in the combined electrostatic and linearly polarized nonresonant radiative fields is derived and all assumptions made are described. The matrix elements of the Hamiltonian matrix in the symmetric top basis set are calculated and their symmetry properties are discussed. The regime is considered, when the radiative field stays on long enough for the system to develop adiabatically. This makes it possible to introduce adiabatic labelling of the states

in the combined fields, sort them out systematically, and define their directional characteristics, such as orientation and alignment cosines.

In Section 4.2, an effective potential is introduced that makes it possible to regard the molecular dynamics in the combined fields in terms of a 1-D motion. The effective potential is an invaluable tool for making sense of some of the computational results obtained by solving the eigenproblem in question numerically.

In Section 4.3 the results proper are presented. First, the correlation diagrams are constructed between the field free states of a symmetric top and the harmonic librator, which obtains at high fields. The effect of the laser field on the orientation of symmetric tops is described, which has not been done before. Then we turn to the combined fields, and consider collinear fields and perpendicular fields in turn. It is where we discuss the details of the two major mechanisms responsible for the amplification of the orientation by the combined fields.

Section 4.4 discusses the possibilities of applying the combined fields to a swatch of molecules (representing the symmetry combinations of the polarizability and inertia tensors) and of making use of the orientation achieved in a selection of applications.

The main conclusions of the present work are summarized in Chapter 5.

2 Theoretical Principles

This chapter gives a brief introduction to the topic of molecular orientation and alignment. This is followed by a review of the main concepts and approximations necessary for treating orientation and alignment of molecules in combined electrostatic and non-resonant radiative fields. These include the rigid rotor approximation, the interactions of the rotor with external fields, the time-reversal symmetry, and the Hellman-Feynman theorem.

2.1 Orientation and alignment

In the absence of external fields, a molecule rotates freely, with a *random* spatial distribution of the molecular axes, $\mathbf{z}$, or rotational angular momenta, $\boldsymbol{J}$. The directional properties of molecules in spectroscopic or collisional experiments are thus averaged out, and the directional information is lost.

In order to describe the anisotropic distribution of a vector property $\mathbf{V}$ (such as $\mathbf{z}$ or $\mathbf{J}$), a two-vector correlation is used, the *direction-direction correlation* [55] between the vector $\mathbf{V}$ and a reference axis $\mathbf{A}$ of cylindrical symmetry. The azimuthal angle φ of $\mathbf{V}$ about $\mathbf{A}$ is then uniformly distributed, see Fig. 2.1, and the polar angle θ between $\mathbf{A}$ and $\mathbf{V}$ is the observable quantity specifying the two-vector correlation.

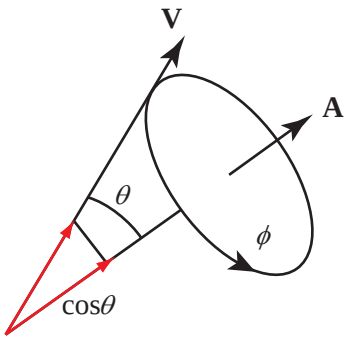

Figure 2.1: Illustration of the direction-direction correlation between a vector $\mathbf{V}$ and a reference axis of cylindrical symmetry $\mathbf{A}$.

Let $n(\theta)$ be the probability distribution of θ or, equivalently, of $\cos\theta$. Such a cylindrically symmetric distribution can be expanded in terms of Legendre polynomials, $P_m(\cos\theta)$, which represent a complete basis set on the interval $(-1, 1)$.

The Legendre series expansion for the spatial distribution reads

$$n(\cos\theta) = \sum_{n=0}^{\infty} a_n P_n(\cos\theta) \tag{2.1}$$

with a_n the Legendre moments. Using the orthogonality relation

$$\int_{-1}^{1} P_m(x) P_n(x) dx = \frac{2}{2m+1}\delta_{mn} \tag{2.2}$$

the Legendre moments are obtained,

$$a_m = \frac{2m+1}{2} \int_{-1}^{1} P_m(\cos\theta) n(\cos\theta) d\theta \tag{2.3}$$

The anisotropy of the distribution of the vector $\mathbf{V}$ is said to exhibit *orientation* or *alignment* if the distribution is *symmetric* or *asymmetric* with respect to the plane perpendicular to the $\mathbf{A}$-direction, respectively. Hence in the case of alignment, only even Legendre moments are nonzero. In the case of orientation, odd moments are nonzero. The monopole term a_0 is proportional to the population, and is usually taken as unity. In most experiments only the first two moments are accessible.

Thus the orientation of a single molecule is characterized by the first Legendre moment

$$a_1 = \frac{3}{2} \langle \cos\theta \rangle \tag{2.4}$$

while the alignment by the second:

$$a_2 = \frac{5}{4} \left\langle 3\cos^2\theta - 1 \right\rangle = \frac{15}{4} \left\langle \cos^2\theta \right\rangle - \frac{5}{4} \tag{2.5}$$

The directional properties of a single molecule (or, more accurately, a single molecular state) are thus given by the expectation values $\langle \cos\theta \rangle$ and $\left\langle \cos^2\theta \right\rangle$ of $\cos\theta$ and $\cos^2\theta$. The directionality of an ensemble of molecules is characterized by the respective ensemble averages $\langle\langle \cos\theta \rangle\rangle$ or $\left\langle\left\langle \cos^2\theta \right\rangle\right\rangle$.

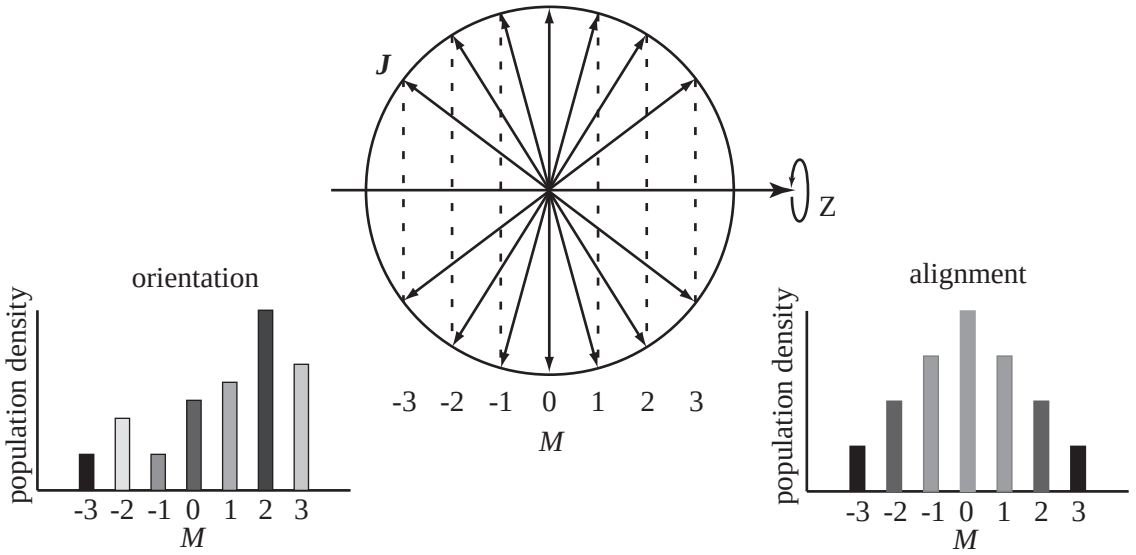

Figure 2.2: Illustration of orientation and alignment of an angular momentum vector. $\boldsymbol{J} = 3$ and has the projection M on the space-fixed axis. If the population varies with the magnitude of M, but not the sign, J is aligned while for a variation with the sign of M, $\boldsymbol{J}$ becomes oriented.

We note that in the case of angular momentum (which has a projection M on the space-fixed axis Z, see Fig. 2.2), an ensemble exhibits alignment of $\boldsymbol{J}$, if the distribution of $|M|$ versus $|M'|$ is nonuniform and states with $+M$ and $-M$ are equally populated. In the case of orientation of $\boldsymbol{J}$, at least some states that differ in the sign of M must be unequally populated.

The notion of orientation pertains to objects that can be thought of as a single-headed arrows, such as electric dipoles. The dipole preferentially points in the direction of the field, which defines the Z-axis, see Fig. 2.3. The notion of alignment pertains to double-headed arrows, which are exemplified by induced dipoles.

In what follows, we'll consider orientation and alignment of the molecular axis, i.e., $\mathbf{V} \equiv \mathbf{z}$. The question arises as to how to create states in which the molecular axis is oriented or aligned. We'll start our considerations with axis orientation.

Polar molecules possess a body-fixed electric dipole moment, $\boldsymbol{\mu}_z$, which is a true vector, and thus the ultimate example of a single-headed arrow. As the name suggests, it's fixed to the molecular frame and thus can be used to specify the orientation of the molecule. However, since the orienting electric field is fixed in the laboratory frame (it defines the laboratory, space-fixed axis, Z), a projection of the body-fixed dipole on the space-fixed frame needs to be considered. Such a projection is called the space-fixed dipole moment, $\boldsymbol{\mu}_Z$, and is given by $\mu_Z = \mu_z \cos\theta$, which can be rewritten in terms of the expectation

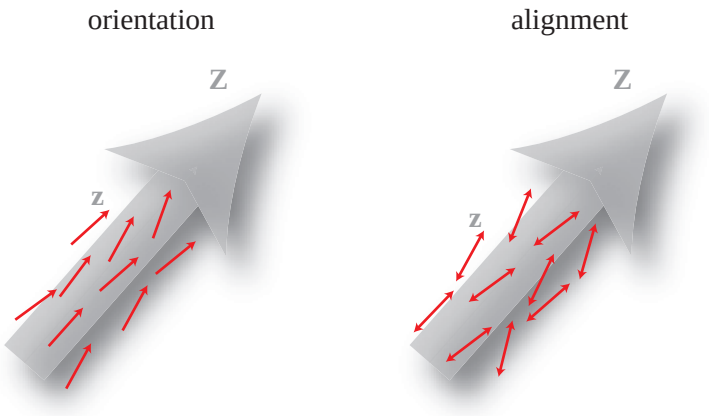

Figure 2.3: Illustration of orientation and alignment. Orientation corresponds to single-headed arrows, such as electric dipoles in an electrostatic field, while alignment corresponds to double-headed arrows, such as the induced electric dipoles in ac electric field.

values as

$$\langle \mu_Z \rangle = \langle \mu_z \rangle \langle \cos\theta \rangle \tag{2.6}$$

But the expectation value of the space-fixed dipole moment in a state of definite parity must be zero [56, 57]. All symmetric top rotor states, see Section 2.2, have a definite parity (i.e., their eigenfunctions remain unchanged or change their sign on reflection at the origin). The vanishing of the space-fixed dipole moment in a state of definite parity follows from the anticommutator between the parity operator, P, and the space-fixed electric dipole moment. Since $\boldsymbol{\mu}_Z$ is a true vector, it reverses its direction when acted upon by P

$$P\boldsymbol{\mu}_Z = -\boldsymbol{\mu}_Z P \quad \text{or} \quad \boldsymbol{\mu}_Z = -P^+\boldsymbol{\mu}_Z P \tag{2.7}$$

The expectation value of a state of definite parity $|\psi_+\rangle$ becomes

$$\langle \psi_+|\boldsymbol{\mu}_Z|\psi_+\rangle = -\left\langle \psi_+|P^+\boldsymbol{\mu}_Z P|\psi_+\right\rangle = -\left\langle \psi_+P^+|\boldsymbol{\mu}_Z|P\psi_+\right\rangle = -\langle \psi_+|\boldsymbol{\mu}_Z|\psi_+\rangle \tag{2.8}$$

which is only possible if

$$\langle \psi_+|\boldsymbol{\mu}_Z|\psi_+\rangle = 0 \tag{2.9}$$

By the same token, the electric dipole operator couples states of opposite parity. Coupling states of opposite parity creates states of indefinite parity, whose orientation is no longer limited by the parity selection rule.

Hence the ability to create oriented states amounts to the ability of coupling (close-lying) states of opposite parity. There are two kinds of close lying states of opposite parity amenable to coupling:

- K-states in polar symmetric tops or equivalent (create precessing states)
- J-states in any polar molecule (create pendular states)
  - polar molecules subject to electrostatic fields
  - polar (and polarizable) molecules subject to combined electrostatic and radiative fields
  - polar and paramagnetic molecules subject to combined static and electric and magnetic fields

For $K > 0$, the levels of a symmetric top occur as nearly degenerate K-doublets whose members have opposite parities. The splitting is due to higher-order distortion coupling, spin-rotation as well as spin-spin interaction [58]. The splitting is on the order of $0.1 - 1$ GHz, which corresponds to an electric field strength of 100 V/cm for a dipole moment of 1 Debye. In an electric field that couples the members of a K-doublet, the body-fixed dipole moment for states with $J, K, M \neq 0$ precesses about Z and so does not average out in first order. Hence such *precessing states* are inherently oriented, with

$$\langle \cos\theta \rangle = \frac{KM}{J(J+1)} \tag{2.10}$$

In all other states (i.e., for $KM = 0$), the dipole moment and hence the orientation is averaged out to first order by molecular rotation.

Another method for creating oriented states relies on the coupling of neighboring J-states that have opposite parities. The molecular rotation is thus transformed into a pendular motion, and the molecular axis librates about the field direction (such a system is a quantum incarnation of the pendulum), see Subsection 2.3.1.

For $KM = 0$ the induced-dipole interaction couples states with the same parity and therefore one can only align the molecular axis. However for $KM \neq 0$, states of opposite parity are coupled by the induced dipole interaction, which can thus create oriented states (see Subsection 2.3.2).

2.2 Rotational states of molecules

A molecule is a quantum rotor which, like the classical rotor, is well approximated by the rigid-rotor model. The rotational Hamiltonian of a molecule can be derived from the full nonrelativistic Hamiltonian by invoking the Born-Oppenheimer separation of the nuclear and electronic degrees of freedom, see e.g. [59].

The nuclei of a molecule form a structure determined by the electronic state of the electronic subsystem. This structure can rotate, vibrate or undergo translation in space. These motions are in fact coupled, but the rigid-rotor approximation assumes that they are not. It thus represents the lowest-order approximation of molecular rotation.

The coordinates suitable for describing the rigid-body rotation are the Euler angles [56]. These can be used to connect the body- and space-fixed frames. The body-fixed frame serves to describe the internal structure of the molecule whereas the space-fixed (laboratory) frame is used to take into account the external fields acting on the molecule.

The three Euler angles (θ, φ, χ) specify the orientation of the molecule-fixed coordinate system xyz with respect to the space-fixed system XYZ, see Fig. 2.4. Let both frames have a common origin, located at the center of mass of the molecule. Three successive rotations transform XYZ into xyz

1. a counterclockwise rotation φ about Z, which carries the Y-axis into the lines of notes N (intersection of the XY and xy plane)
2. a counterclockwise rotation by θ about the lines of nodes N, which carries the Z into z-axis
3. a counterclockwise rotation by χ about z, which carries the line of nodes into the y-axis

A vector $\mathbf{r} = (x_1, x_2, x_3)$ in the molecule fixed system is carried by the unitary transformation $\mathbf{\Phi}$ into the space-fixed system $\mathbf{R} = \mathbf{\Phi r}$, where $\mathbf{\Phi}$ is the direction cosine matrix.

$$\mathbf{\Phi} = \begin{pmatrix} \cos\varphi\cos\theta\cos\chi - \sin\varphi\sin\chi & -\cos\varphi\cos\theta\sin\chi - \sin\varphi\cos\chi & \cos\varphi\sin\theta \\ \sin\varphi\cos\theta\cos\chi + \cos\varphi\sin\chi & -\sin\varphi\cos\theta\sin\chi + \cos\varphi\cos\chi & \sin\varphi\sin\theta \\ -\sin\theta\cos\chi & \sin\theta\sin\chi & \cos\theta \end{pmatrix} \tag{2.11}$$

In the molecule-fixed xyz axis system, the matrix elements of the inertia tensor are given by

$$I_{\alpha\alpha} = \sum_i m_i \left(\beta_i^2 - \gamma_i^2\right) \qquad I_{\alpha\beta} = -\sum_i m_i \alpha_i \beta_i \tag{2.12}$$

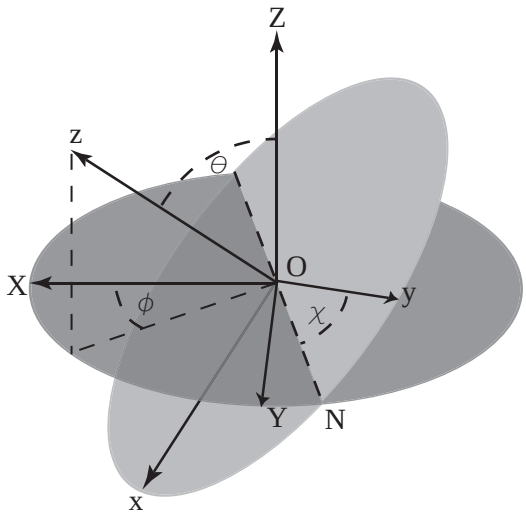

Figure 2.4: Illustration of the two different coordinate frames occurring in molecules, the space-fixed frame XYZ and the body-fixed frame xyz. The Euler angles θ, φ and χ specify the relative orientation with respect to each other.

where $\alpha\beta\gamma$ is a permutation of xyz. It is possible to orient xyz such, that the off-diagonal elements of the inertia tensor vanish. This corresponds to a matrix diagonalisation. The diagonal elements become the *principal moments of inertia*, which are sorted by increasing energy $I_{aa} \leq I_{bb} \leq I_{cc}$. The corresponding axes are labeled by abc and are said to form a *principal axes system.*

In the principal-axes system the rigid-rotor Hamiltonian becomes

$$\mathcal{H}_r = AJ_a^2 + BJ_b^2 + CJ_c^2 \tag{2.13}$$

where J_a, J_b and J_c are the components of the angular momentum operator $\boldsymbol{J}$. The rotational constants (in units of energy) are

$$A = \frac{\hbar^2}{2I_{aa}} \qquad B = \frac{\hbar^2}{2I_{bb}} \qquad C = \frac{\hbar^2}{2I_{cc}} \tag{2.14}$$

Hence the rotational constants are related to one another by the inequality $A \geq B \geq C$. Depending on the moments of inertia or equivalently, the rotational constants, five different types of molecules are distinguished.

$I_{aa} = 0, I_{bb} = I_{cc}$	linear	CO
$I_{aa} = I_{bb} = I_{cc}$	spherical top	CCl_4
$I_{aa} < I_{bb} = I_{cc}$	prolate symmetric top	CH_3Cl
$I_{aa} = I_{bb} < I_{cc}$	oblate symmetric top	$CHCl_3$
$I_{aa} < I_{bb} < I_{cc}$	asymmetric top	CH_2Cl_2

In order to identify the principle axis system abc with the body-fixed coordinates xyz, three different representations exist for right-handed coordinate systems.

	Representation		
Body-fixed Coordinates	I^r	II^r	III^r
x	b	c	a
y	c	a	b
z	a	b	c

2.2.1 Symmetric top molecules

Symmetric top molecules possess a threefold or higher rotation axis, as a result of which two of their rotational constants are equal to one another. Depending on the relation between the two unequal rotational constants, the symmetric top is either prolate ($A > B = C$) or oblate ($A = B > C$). The symmetry axis is also a principle axis of inertia; the z axis is identified with it and referred to as the *figure axis*. For a prolate and oblate molecule, the I^r and III^r representation is used, respectively. Taking $\boldsymbol{J}^2 = J_x^2 + J_y^2 + J_z^2$, the rotational Hamiltonians for a prolate and oblate symmetric top simplify to

$$\mathcal{H}_r^{\text{prolate}} = B\boldsymbol{J}^2 + (A - B)\, J_z^2 \qquad \mathcal{H}_r^{\text{oblate}} = B\boldsymbol{J}^2 + (C - B)\, J_z^2 \tag{2.15}$$

The representations of the angular momentum operator $\boldsymbol{J}$ are different in the space-fixed and molecule-fixed coordinate systems [56, 59]. Since the components of both representations J_z and J_Z commute with one another $[J_z, J_Z] = 0$ and also commute with $\boldsymbol{J}^2$, one can find eigenfunctions $\left|\boldsymbol{J}^2, J_z, J_Z\right\rangle$ which are simultaneously eigenfunctions of $\boldsymbol{J}^2$, J_z and J_Z. The other components, J_x and J_y are constructed using the raising and lowering operators in the body-fixed system $J^{\pm} = J_x \pm iJ_y$. Introducing the quantum numbers J, K and M, the matrix elements are

$$\boldsymbol{J}^2 \left|JKM\right\rangle = J(J+1) \left|JKM\right\rangle \tag{2.16a}$$

$$J_Z \left|JKM\right\rangle = M \left|JKM\right\rangle \tag{2.16b}$$

$$J_z \left|JKM\right\rangle = K \left|JKM\right\rangle \tag{2.16c}$$

$$J^{\pm} \left|JKM\right\rangle = \left[J(J+1) - K(K \mp 1)\right]^{1/2} \left|JK \mp 1M\right\rangle, \tag{2.16d}$$

where M is the projection of the angular momentum $\boldsymbol{J}$ on the space-fixed Z-axis and K on the molecule-fixed z-axis, see Fig. 2.5.[1] In the xyz-system the components of the angular

[1] The typically occurring $\hbar$ prefactors are already included in the rotational constants

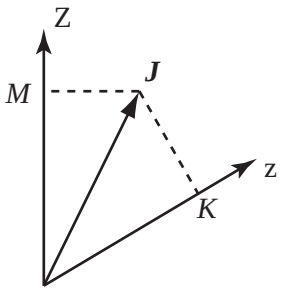

Figure 2.5: Projections M and K of the angular momentum $\hat{\mathbf{J}}$ on the space-fixed Z-axis and molecule-fixed z-axis, correspondingly.

momentum operator become:

$$J_x = -i\cos\chi\left[\cot\theta\frac{\partial}{\partial\chi} - \frac{1}{\sin\theta}\frac{\partial}{\partial\varphi}\right] - i\sin\chi\frac{\partial}{\partial\theta} \tag{2.17a}$$

$$J_y = i\sin\chi\left[\cot\frac{\partial}{\partial\chi} - \frac{1}{\sin\theta}\frac{\partial}{\partial\varphi}\right] - i\cos\chi\frac{\partial}{\partial\varphi} - i\cos\chi\frac{\partial}{\partial\theta} \tag{2.17b}$$

$$J_z = -i\frac{\partial}{\partial\chi} \tag{2.17c}$$

Taking 2.15 and 2.17, the differential equation for the symmetric top is obtained

$$\left[B\left(\frac{1}{\sin\theta}\frac{\partial}{\partial\theta}\left(\sin\theta\frac{\partial}{\partial\theta}\right) + \frac{1}{sin^2\theta}\left(\frac{\partial^2}{\partial\varphi^2} + \frac{\partial^2}{\partial\chi^2} - 2\cos\theta\frac{\partial^2}{\partial\varphi\partial\chi}\right)\right) + A\frac{\partial^2}{\partial\chi^2}\right]\Psi = E\Psi \tag{2.18}$$

This Schrödinger equation has been solved, independently, by Reiche [60] and by Kronig and Rabi [61]. The solution in standard form can be found for example in [62], see Appendix A.

Nevertheless, it is not necessary to deal with these complicated forms, since the wave functions can also be represented in terms of Rotation matrices (or Wigner D-functions) D^J_{MK} [56]:

$$|JKM\rangle = \left[\frac{2J+1}{8\pi^2}\right]^{1/2} D^{J*}_{MK}(\varphi,\theta,\chi) = (-1)^{M-K}\left[\frac{2J+1}{8\pi^2}\right]^{1/2} D^{J}_{-M-K}(\varphi,\theta,\chi) \tag{2.19}$$

These are the products of two phase factors and the $d^J_{MK}(\theta)$ functions, which can be expressed in terms of Jacobi polynomials

$$D^J_{MK}(\varphi,\theta,\chi) = e^{-iM\varphi}d^J_{MK}(\theta)e^{-iK\chi} \tag{2.20}$$

Although the calculation of the $d^J_{MK}(\theta)$ is also rather involved, this representation is much more useful. The calculation of the matrix elements leads to products of the Wigner 3j-symbols. The properties of the 3j-symbols (see Appendix C) are used to evaluate the matrix elements of the Hamiltonian, without explicit integration.

For linear molecules or symmetric tops with $K = 0$, the rotational wave functions reduce to spherical harmonics.

2.2.2 Asymmetric top molecules

For an *asymmetric top molecule*, all three principal moments of inertia are different from one other. In the I^r representation, which is used for near-prolate asymmetric molecules, the rotational Hamiltonian becomes

$$\begin{aligned}\mathcal{H}_r &= AJ_x^2 + BJ_y^2 + CJ_z^2 \\ &= \frac{1}{2}(B+C)\,\boldsymbol{J}^2 + \left[A - \frac{1}{2}(B+C)\right] J_z^2 + \frac{1}{4}(B-C)\left[J^{+2} + J^{-2}\right]\end{aligned} \tag{2.21}$$

The projection of the angular momentum $\boldsymbol{J}$ on any axis of the molecule is no longer constant and K ceases to be a good quantum number. The only remaining good quantum numbers are J and M. The eigenfunctions are linear combinations of the symmetric top wave functions

$$\Psi_{JM}(\varphi,\theta,\chi) = \sum_K A_K \,|JKM\rangle \tag{2.22}$$

Inserting this eigenfunction into the rotor Hamiltonian leads to a $(2J+1)$ by $(2J+1)$ matrix. The eigenenergies are the roots of the secular determinant

$$|\mathcal{H}_{K'K} - E\delta_{K'K}| = 0 \tag{2.23}$$

with

$$\mathcal{H}_{K'K} = \langle JK'M|\mathcal{H}_r|JKM\rangle \tag{2.24}$$

A simplification can be achieved when the symmetry of the inertia ellipsoid is considered. A rotation by 180° about any of the principle axes $R^{\pi}_{a,b,c}$ leaves the ellipsoid unchanged [63]. These twofold rotations together with the identity operation form the D_2 point group also called the Vierergruppe [64]. The rotational Hamiltonian has, of course, the same D_2 symmetry.

Using a symmetrized basis set constructed from the symmetric top wave functions (the so called Wang functions) yields four different blocks and simplifies the secular determinant

$$|JKMs\rangle = \frac{1}{\sqrt{2}}\left[|JKM\rangle + (-1)^s\,|J-KM\rangle\right] \quad \text{for } K \neq 0 \text{ and } s = 0, 1 \tag{2.25}$$

$$|J0M0\rangle = |J0M\rangle \tag{2.26}$$

In the unsymmetrized basis set there are $(2J+1)$ different K values for a given J. The symmetrized basis set separates the matrix into four different blocks each belonging to one of the symmetry species of the D_2 group. The blocks are labeled by the E or O for even or odd K-values and $+$ and $-$ for $s = 0$ and $s = 1$.

2.3 Molecular interactions with fields

Throughout this thesis, we consider *polar* molecules, i.e., molecules which possess a body-fixed permanent electric dipole moment. Examples include heteronuclear diatomics or symmetric and asymmetric top molecules. In contrast, nonpolar molecules, exemplified by homonuclear diatomics or spherical top molecules, have zero body-fixed electric dipole moments. However, all molecules are polarizable, i.e., when subject to an electric field, their electronic subsystem undergoes a spatial distortion, resulting in an induced body-fixed dipole moment, $\mu_{ind} = \boldsymbol{\alpha}\mathcal{E}$, where $\boldsymbol{\alpha}$ is the polarizability tensor and $\mathcal{E}$ is the electric field strength (i.e., the magnitude of the electric field vector). The next dipole term, to be included at higher fields, is proportional to the hyperpolarizability.

The electric dipole moment can interact with an external electric field, which acts as a potential V that perturbs the field-free rotational Hamiltonian, $\mathcal{H}_r$, cf. eq. (2.15). While the permanent dipole potential, V_μ, is proportional to the electric field strength, $\mathcal{E}$, the induced-dipole potential, V_α, is proportional to the square of the electric field, $\mathcal{E}^2$. Therefore, the induced-dipole interaction can be brought about by an (oscillating) radiative field, since the sign of the electric-field vector does not matter. Note that the permanent dipole interaction with an oscillating field averages out to zero.

2.3.1 Interaction of a static electric field with the body-fixed electric dipole moment of a molecule: permanent dipole interaction

By a permanent dipole interaction we mean the interaction of an electrostatic field with the body-fixed permanent dipole moment, $\boldsymbol{\mu}$, of a molecule. The body-fixed electric dipole

moment of a linear molecule is directed along the molecular axis. For a symmetric top, the dipole moment points along the figure axis. In either case, it has also a fixed sense with respect to the molecular frame (a single-headed arrow). Hence the only nonzero component of the dipole is μ_z. With the help of the direction cosine matrix the component is transformed into the space-fixed frame, i.e., $\mu_Z = \mu_z \cos\theta$. The space-fixed frame is defined by the electric field $\boldsymbol{\mathcal{E}} = (0, 0, \mathcal{E})$. As a result, the permanent dipole potential is given by

$$V_\mu = -\boldsymbol{\mu} \cdot \boldsymbol{\mathcal{E}} = -\mu_z \mathcal{E}_Z \cos\theta \tag{2.27}$$

The matrix elements $\langle J'K'M'|\cos\theta|JKM\rangle$ of the $\cos\theta$ operator yield the selection rules $M = M'$, $K = K'$ and $J = J', J' \pm 1$. The elements are:

$$\langle JKM|V_\mu|JKM\rangle = -\mu_z \mathcal{E}_Z \langle JKM|\cos\theta|JKM\rangle = -\mu_z \mathcal{E}_Z \frac{KM}{J(J+1)} \tag{2.28}$$

$$\langle JKM|V_\mu|J+1KM\rangle = -\frac{\mu_z \mathcal{E}_Z}{J+1} \sqrt{\frac{[(J+1)^2 - K^2][(J+1)^2 - M^2]}{(2J+1)(2J+3)}} \tag{2.29}$$

Due to the mixing of different J states, the Hamilton matrix $[\mathcal{H}_r + V_\mu]_{J'J}$ includes nonzero off-diagonal elements. Thus the eigenstates are obtained by the diagonalization of the Hamiltonian matrix.

For weak electric fields, the mixing of different J states is small and the diagonal matrix elements, eq. (2.28), dominate the behavior. If K and M are nonzero, the first-order Stark effect results. The first-order Stark effect removes the M degeneracy of the field-free levels. The Stark energy $E - E_0$ (with E_0 and E the eigenenergy of a state under field free conditions and in the field) becomes

$$E - E_0 = -\mu_z \mathcal{E}_Z \frac{MK}{J(J+1)} \tag{2.30}$$

and so the splitting between the $2J + 1$ states increases linearly with $\mathcal{E}_Z$, K and M. From eq. (2.30) it follows that the eigenenergies for states with $MK > 0$ decrease with increasing field strength. In an inhomogeneous field such a molecule will seek regions of maximum field strength, where its eigenenergy is minimal. Therefore these states were dubbed *high-field-seeking* (hfs). The eigenenergy of states with $MK < 0$ increases with increasing field strength. In an inhomogeneous field, they seek regions of minimal field strength and were dubbed *low-field-seeking* (lfs).

For larger electric fields the coupling of the rotational levels increases and the off-diagonal matrix elements, eq. (2.29), become dominant. This leads to higher order Stark-shifts. The interaction can become so strong that the molecule no longer rotates freely but librates

instead about the electric field direction. Such states are called pendular states [3, 4]. All pendular states are high-field-seeking and strongly oriented.

For an asymmetric top, the dipole moment is not restricted to lie along one of the principle axis. It may have components along any or all of the principle axes $\boldsymbol{\mu} = (\mu_x, \mu_y, \mu_z)$. For an electric field along Z, the space-fixed dipole moment becomes

$$\mu_Z = -\sin\theta\cos\chi\mu_x + \sin\theta\sin\chi\mu_y + \cos\theta\mu_z \tag{2.31}$$

The selection rules become more involved for this case. Bulthuis *et al.* published a series of articles where the orientation of the molecular axis in an electrostatic field was considered for an asymmetric top with the dipole moment along one of the principle axis on inertia [7] and for an arbitrary direction of the dipole moment [8].

2.3.2 Interaction of a radiative field with the anisotropic polarizability of a molecule: induced dipole interaction

The field strength that can be achieved by focusing pulsed laser radiation is quite high ($10^{12} - 10^{14}\mathrm{W/cm^2}$ for 10ns pulses). As a result, the induced dipole interaction in such a field can become significant or even dominant. However, not arbitrarily strong fields can be applied - the intensity must be held below the off-resonance ionization threshold.

The dynamic polarizability tensor occurring in the optically induced dipole moment $\boldsymbol{\mu} = \boldsymbol{\alpha}\boldsymbol{\mathcal{E}}$ for molecules in the vibrational state v and the electronic state ξ in the lab system $\rho = X, Y, Z$ is quite involved, see [65]. It depends on the vibrational and electronic state, the components of the dipole moment operator μ_ρ, the transition frequencies between different vibrational and electronic states $\nu_{v'\xi',v\xi}$, and also the different widths of the levels. The polarizability tensor simplifies considerably for frequencies far detuned from all vibronic resonances and negligible widths of the levels.

$$\alpha^{v\xi}_{\rho\rho'} = \sum_{v'\xi'} \frac{\nu_{v'\xi',v\xi}}{\pi(\nu^2_{v',\xi',v\xi} - \nu^2)} \left\langle v\xi|\mu_\rho|v'\xi'\right\rangle \left\langle v'\xi'|\mu_{\rho'}|v\xi\right\rangle, \tag{2.32}$$

where ν is the frequency of the time dependent electric field, $\boldsymbol{\mathcal{E}}(t) = \boldsymbol{\epsilon}(X, Y, Z, t)\cos(2\pi\nu t)$. Note that the nonresonant polarizability is real. For sufficiently low frequencies $\nu \ll \nu_{v'\xi',v\xi}$, it converges to the dc polarizability.

The center of a laser beam with a Gaussian intensity distribution which propagates along the X axis and is polarized along the Z axis can be approximated by a plane-wave radiation. The pulse has the maximum amplitude $\mathcal{E}_0$ and the shape is characterized by the

envelope function $g(t)$ such that

$$\boldsymbol{\mathcal{E}}^2(t) \equiv \mathcal{E}_Z^2(t) = g(t)\mathcal{E}_0^2 \cos^2(\omega t) \equiv \varepsilon^2(t)\cos^2(\omega t) \tag{2.33}$$

The fast-oscillating part of the time-dependence, $\cos^2(\omega t)$, can be replaced by its average value of $\frac{1}{2}$, obtained by the rotating-wave approximation [65]. The induced-dipole interaction for such a radiation becomes [18, 36]

$$V_\alpha = -\frac{1}{4}\sum_{\rho,\rho'} \varepsilon_\rho \alpha_{\rho\rho'} \varepsilon_{\rho'} \tag{2.34}$$

and only depends on the dc polarizabilities and the pulse shape function of the radiative field.

Similarly to the inertia tensor, the polarizability tensor can be diagonalized in the body-fixed frame, with principal polarizability components α_{xx}, α_{yy}, and α_{zz}. The body-fixed polarizability $\boldsymbol{\alpha}^{\mathrm{mol}}$ is related to the space-fixed polarizability by the transformation

$$\boldsymbol{\alpha}^{\mathrm{lab}} = \boldsymbol{\Phi}^{-1}\boldsymbol{\alpha}^{\mathrm{mol}}\boldsymbol{\Phi} \tag{2.35}$$

with Φ the direction cosine matrix.

For an asymmetric top molecule, the induced-dipole interaction becomes

$$V_\alpha = -\frac{1}{4}\varepsilon^2 \left[\alpha_{zz}\cos^2\theta + \sin^2\theta(\alpha_{xx}\cos^2\varphi + \alpha_{yy}\sin^2\varphi)\right] \tag{2.36}$$

This simplifies for a linear or symmetric top, which have $\alpha_{zz} = \alpha_{||}$ and $\alpha_{xx} = \alpha_{yy} = \alpha_\perp$. As a result,

$$V_\alpha = -\frac{1}{4}\varepsilon^2[(\alpha_{||} - \alpha_\perp)\cos^2\theta + \alpha_\perp] \tag{2.37}$$

The polarizability interaction has been used to align diatomic, symmetric and asymmetric top molecules in linearly or elliptically polarized laser fields. For a recent review of these methods see ref. [36]. All these methods are based on the coupling of states of the same parity, since the $\cos^2\theta$ operator mixes states with same J or states differing by $\Delta J = 2$. However, in the case of symmetric and asymmetric tops also opposite-parity states differing by $\Delta J = 1$ become mixed - the consequences of which are further explored in this thesis.

The effect of different pulse shape functions has been investigated by Ortigoso *et al.* [66] (see also [67]) for linear molecules. In their computational study, the reduced time-

dependant Schrödinger equation

$$i\frac{\hbar}{B}\frac{\partial\Psi(t)}{\partial t} = \frac{\mathcal{H}(t)}{B}\Psi(t) \tag{2.38}$$

shows that the interaction with the radiative field is clocked by the the reduced time, $\hbar/B$. Three different cases have been found. The limiting cases are the short pulse regime with pulse duration $\tau \leq \hbar/B$ and the long pulse regime with pulse duration $\tau \geq 10\hbar/B$. In the long pulse limit, the adiabatic behavior prevails, i.e. the alignment follows the pulse shape function $g(t)$ as if the radiative field were static; it is present only when the pulse is on. In the short pulse regime, the adiabatic behavior breaks down and the alignment does not immediately follow the pulse shape function. The maximum alignment is attained after the center of the laser pulse has passed. The wave function maintains the character of a coherent rotational wave packet. This results in quasiperiodic recurrences of the alignment at later times. In the intermediate range of pulse duration, a blend of the behavior in the two limiting cases is observed.

2.3.3 Combined electrostatic and linearly polarized radiative fields at a tilt angle

In order to determine the combined action of an electrostatic field with a nonresonant radiative field on a polar and polarizable molecule, it is necessary to express the angular variables of one interaction potential in terms of the angular variables of the other potential.

The spherical harmonics addition theorem [68]

$$P_\ell(\cos\gamma) = \frac{4\pi}{2\ell+1}\sum_{\ell=-m}^{m}(-1)^m Y_\ell^m(\theta_b,\varphi_b)Y_\ell^{-m}(\theta_c,\varphi_c) \tag{2.39}$$

simplifies for $\ell = 1$ to

$$\cos\gamma = \cos\theta_b\cos\theta_c + \sin\theta_b\sin\theta_c\cos\Delta\varphi \tag{2.40}$$

The angles are defined in relation to three different points. Point A is located on the z-axis and points $B(\theta_b,\varphi_b)$ and $C(\theta_c,\varphi_c)$ have an arbitrary position in space. The angle γ is spanned by the vectors $\overline{OB}$ and $\overline{OC}$, see left panel of Fig. 2.6. The axes of the molecule-fixed and space-fixed systems are labeled by xyz and XYZ, respectively. The vector $\overline{OA}$ defines the direction of the figure axis or the body-fixed electric dipole moment, while the other two vectors represent the field directions.

In the lab frame, equation (2.40) holds when the angles are replaced in the following

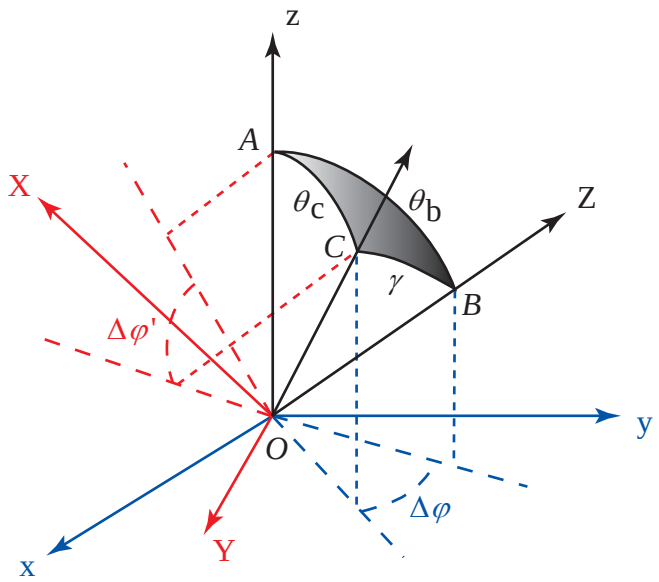

Figure 2.6: Illustration of the coordinate transformation necessary to describe the mutually tilted field case. In the molecular system xyz, with point A on the z-axis, the two fields are depicted by the vectors from the origin O to the points B and C. The polar angles from the z-axis are θ_b and θ_c. The angle spanned by $\overline{OB}$ and $\overline{OC}$ is γ. The points B and C have the blue projections on the xy-plane. They enclose the dihedral angle $\Delta\varphi = \varphi_b - \varphi_c$. Going to the space-fixed system XYZ which is defined by vector $\overline{OB}$ makes θ_b and γ to the polar angles, while θ_c is spanned by $\overline{OA}$ and $\overline{OC}$. The projections on the space-fixed XY-plane are shown in red. The dihedral angle becomes $\Delta\varphi'$.

manner

$$\gamma \to \theta_c' \qquad \theta_c \to \gamma' \qquad \Delta\varphi \to \Delta\varphi' \tag{2.41}$$

with $\theta_c' = \theta_c$ and $\gamma' = \gamma$. Equation (2.40) becomes:

$$\cos\theta_b = \cos\gamma\cos\theta_c + \sin\gamma\sin\theta_c\cos\Delta\varphi' \tag{2.42}$$

2.4 Time-reversal Symmetry

The time-reversal symmetry [64] appears in many physical problems. The time-reversal operator, T, takes $\Psi(t)$ into $\Psi^*(-t)$. This reverses velocities, $\mathbf{v} \to -\mathbf{v}$, linear and angular momenta, $\mathbf{p} \to -\mathbf{p}$ and $\boldsymbol{\ell} \to -\boldsymbol{\ell}$, but leaves positions invariant, $\mathbf{r} \to \mathbf{r}$.

The time-reversal operator is anti-unitary, like the operator of complex conjugation, $\mathcal{K}$.

An anti-unitary operator is also anti-linear $T(c\Psi) = c^*(T\Psi)$ and conserves the magnitude of the scalar product$|(T\psi, T\phi)| = |(\psi, \phi)|$.

The product of a unitary and an anti-unitary operator is anti-unitary, while the product of two anti-unitary operators is unitary. The product of the time-reversal T and complex conjugation $\mathcal{K}$ operators is a unitary operator U, $T\mathcal{K} = U$. An application of $\mathcal{K}$ to this identity yields $T = U\mathcal{K}$, since $\mathcal{K}^2 = 1$. This is the general form of T.

The time-reversal symmetry is responsible for some extra degeneracies of a system, although it does not introduce any new labels beyond those already provided by the rotation symmetry group. This is because two irreducible representations that are connected by the time-reversal symmetry have always equal energy levels, and so can be considered as being degenerate. The two representations are called separable degenerate [69].

2.5 Hellman-Feynman Theorem

For problems which cannot be solved analytically matrix diagonalization is often applied. In order to avoid the calculation of the eigenvectors to determine the expectation values, the Hellman-Feynman theorem [70] can be used.

This is possible when the Hamiltonian depends on a parameter λ, which can be thought of as expressing the strengths of a perturbation $V = \lambda\Xi$.

For the Schrödinger equation in the form

$$\mathcal{H}\left|n\right\rangle = E_n\left|n\right\rangle \tag{2.43}$$

with $E_n = \langle n\left|\mathcal{H}\right|n\rangle$, $\langle n \mid m\rangle = \delta_{nm}$ and $\mathcal{H}_0$ the part of the Hamiltonian $\mathcal{H}$ which does not depend on λ.

The derivative of the eigenenergy with respect to the parameter λ yields the expectation value,

$$\begin{aligned}\frac{\partial E_n}{\partial\lambda} &= \frac{\partial}{\partial\lambda}\langle n\left|\mathcal{H}\right|n\rangle = \left\langle \frac{\partial n}{\partial\lambda}\middle|\,\mathcal{H}\,\middle| n\right\rangle + \left\langle n\middle|\frac{\partial\mathcal{H}}{\partial\lambda}\middle| n\right\rangle + \left\langle n\middle|\,\mathcal{H}\,\middle|\frac{\partial n}{\partial\lambda}\right\rangle \\ &= E_n\left\langle \frac{\partial n}{\partial\lambda}\middle| n\right\rangle + \left\langle n\middle|\frac{\partial\mathcal{H}}{\partial\lambda}\middle| n\right\rangle + E_n\left\langle n\middle|\frac{\partial n}{\partial\lambda}\right\rangle = \left\langle n\middle|\frac{\partial\mathcal{H}}{\partial\lambda}\middle| n\right\rangle + E_n\frac{\partial}{\partial\lambda}\langle n \mid n\rangle \\ &= \left\langle n\middle|\frac{\partial\mathcal{H}}{\partial\lambda}\middle| n\right\rangle = -\langle n\left|\Xi\right|n\rangle = -\langle\Xi\rangle\end{aligned} \tag{2.44}$$

In order to compute an expectation value of Ξ, one needs only the eigenvalues for two adjacent field strengths. Nevertheless care needs to be taken of the step width. If it is too large or too small, the results may differ substantially from the expectation values calculated from wavefunctions.

3 Behind the scenes - the numerical and computational methods used

In this chapter, we give a short introduction to the numerical and computational methods used in this thesis. These include a description of the block structure of the Hamiltonian matrix and its diagonalization; an overview of efficient diagonalization methods and the software packages implementing the computer code; a description of computational methods used, such as parallelization. Since the problem under study abounds in avoided and genuine crossings, an efficient sorting method for the eigenproperties had to be developed and implemented. Its description concludes the chapter.

3.1 Symmetry considerations in numerical computations

The Schödinger equation for the system considered in this thesis is analytically solvable only in the low- and high-field limits. In the general case, it has to be solved numerically, for which we use the matrix method. We first calculate analytically the elements of the Hamiltonian matrix, in the basis set of the unperturbed, free-rotor wave functions. Subsequently, we construct the Hamiltonian matrix, which we then diagonalize, in order to find its eigenproperties, i.e., the eigenvalues and eigenvectors.

It is not necessary to deal with the whole Hamilton matrix at once, since it consists of different blocks, each of which is characterized by a value of the good quantum number(s).

$$\begin{pmatrix} a_{11} & a_{12} & 0 & 0 & 0 & \cdots \\ a_{21} & a_{22} & 0 & 0 & 0 & \cdots \\ 0 & 0 & b_{33} & b_{34} & b_{35} & \cdots \\ 0 & 0 & b_{43} & b_{44} & b_{45} & \cdots \\ 0 & 0 & b_{53} & b_{54} & b_{55} & \cdots \\ \vdots & \vdots & \vdots & \vdots & \vdots & \ddots \end{pmatrix} \tag{3.1}$$

Each of the blocks can be handled separately, since there is no coupling (interaction) among the blocks. This improves considerably the speed of the diagonalization of the

entire Hamiltonian matrix.

3.2 Matrix diagonalization

A general description of matrix diagonalization can be found in a number of sources, e.g., in ref. [71]. Here we give a brief outline of the procedure and a description of some of the diagonalization algorithms. A more detailed account of the algorithms can be found in ref. [72].

The diagonalization of a matrix $\mathbf{A}$ amounts to solving the eigenvalue problem:

$$\mathbf{A}\mathbf{x}_\lambda = \lambda\mathbf{x}_\lambda \qquad \text{with } \mathbf{x}_\lambda \neq 0, \tag{3.2}$$

where λ is the eigenvalue of $\mathbf{A}$ and $\mathbf{x}_\lambda$ is the corresponding eigenvector. Solving the eigenvalue problem amounts, in turn, to finding the roots of the characteristic polynomial

$$p_{\mathbf{A}}(\lambda) \equiv \det(\lambda\mathbf{I} - \mathbf{A}) \tag{3.3}$$

with $\mathbf{I}$ the unit matrix. Since there are no explicit formulae for finding the roots of a high-degree polynomial, say n, and every serious manipulation of a matrix requires on the order of n^3 steps, it is not feasible to solve the characteristic equation in a single sweep.

Instead, the diagonalization methods separate the problem into two parts. Firstly, one reduces the matrix $\mathbf{A}$ by a similarity transformation to a special matrix, typically a tridiagonal matrix or a Hessenberg matrix. To these methods belong, e.g., the Jacobi plane rotation method, the Givens or Householder reduction, and many more [72]. The efficiency of the methods depends strongly on the domain ($\mathbb{R}$ or $\mathbb{C}$), the symmetry of the matrix, and the number of zeroes the matrix contains. Secondly, one solves the simpler characteristic equation for the special matrix. This can be accomplished by a number of methods, e.g. the LR, QR or Cholesky separations based, respectively, on a second separation in lower (**L**eft) and upper (**R**ight) triangular matrices or **Q**uadratic matrices [72].

We note that for larger dimensions of the Hamiltonian matrix, of a rank of several thousand, the time required for diagonalization may become impractically long.

Two different kinds of matrices occur for the symmetric top molecules in the combined fields, depending on whether the fields are collinear or mutually tilted, see Fig. 3.1. For the collinear case, the Hamiltonian matrix can be reduced to a block matrix, with each block characterized by a value of M and K. It is easy to transform the blocks to a

tridiagonal form, since only a secondary diagonal must be eliminated. An advanced Givens transformation would do this, but the matrices are rather small (up to 50 by 50), and therefore it is not essential to use the most efficient method. For the tilted fields, additional matrix elements occur and the rank of the Hamiltonian matrix increases to, typically, several hundred. Moreover, since M is no longer a good quantum number, there are fewer blocks, each characterized by a value of K. In any case, the Hamiltonian matrix remains to be a symmetric one.

$$\begin{pmatrix}
x & x & (x) & 0 & 0 & 0 & 0 & 0 \\
x & x & x & (x) & 0 & 0 & 0 & 0 \\
(x) & x & x & x & (x) & 0 & 0 & 0 \\
0 & (x) & x & x & x & (x) & 0 & 0 \\
0 & 0 & (x) & x & x & x & (x) & 0 \\
0 & 0 & 0 & (x) & x & x & x & (x) \\
0 & 0 & 0 & 0 & (x) & x & x & x \\
0 & 0 & 0 & 0 & 0 & (x) & x & x
\end{pmatrix}
\qquad
\begin{pmatrix}
x & x & 0 & x & x & x & 0 & 0 & 0 & 0 & x & 0 & 0 & 0 & 0 \\
x & x & x & 0 & x & x & x & 0 & 0 & 0 & 0 & x & 0 & 0 & 0 \\
0 & x & x & 0 & 0 & x & x & x & 0 & 0 & 0 & 0 & x & 0 & 0 \\
x & 0 & 0 & x & x & 0 & 0 & 0 & x & x & x & 0 & 0 & 0 & 0 \\
x & x & 0 & x & x & x & 0 & 0 & 0 & x & x & x & 0 & 0 & 0 \\
x & x & x & 0 & x & x & x & 0 & 0 & 0 & x & x & x & 0 & 0 \\
0 & x & x & 0 & 0 & x & x & x & 0 & 0 & 0 & x & x & x & 0 \\
0 & 0 & x & 0 & 0 & 0 & x & x & 0 & 0 & 0 & 0 & x & x & x \\
0 & 0 & 0 & x & 0 & 0 & 0 & 0 & x & x & 0 & 0 & 0 & 0 & 0 \\
0 & 0 & 0 & x & x & 0 & 0 & 0 & x & x & x & 0 & 0 & 0 & 0 \\
x & 0 & 0 & x & x & x & 0 & 0 & 0 & x & x & x & 0 & 0 & 0 \\
0 & x & 0 & 0 & x & x & x & 0 & 0 & 0 & x & x & x & 0 & 0 \\
0 & 0 & x & 0 & 0 & x & x & x & 0 & 0 & 0 & x & x & x & 0 \\
0 & 0 & 0 & 0 & 0 & 0 & x & x & 0 & 0 & 0 & 0 & x & x & x \\
0 & 0 & 0 & 0 & 0 & 0 & 0 & x & 0 & 0 & 0 & 0 & 0 & x & x
\end{pmatrix}$$

Figure 3.1: Examples for the two different kinds of matrices which occur in the calculations (after the separation). The left figure exemplifies the collinear case. The elimination of the elements in the brackets reduces it to the tridiagonal form. The matrix on the right exemplifies the case of tilted fields, with a more complex structure.

In our programs written in C++, we used the GSL package,[1] which contains a function to evaluate the 3j-symbols and offers the required data types. It also contains a function to find the eigenvalues. For larger dimensions, we used a package which contains more efficient functions. The Linear Algebra PACKage (LAPACK)[2] provides efficient algorithms for all types of matrices. The algorithms are well tested and sometimes even adjusted for a special processor architecture. All calculations are performed on a cluster of eight SUN V40z servers, each with four AMD 875 dual core processors, connected via InfiniBand. For these processors the manufacturer (AMD - Advanced Micro Devices), provides a special library called ACML (AMD Core Math Library),[3] which includes all LAPACK functions.

Some of the computations had to be parallelized in order to increase the speed. The ScaLAPACK[4] package contains functions which parallelize the calculation of the eigenvalues/eigenvectors. Although the diagonalization process is very time consuming, the

[1] GNU Scientific Library: www.gnu.org/software/gsl
[2] www.netlib.org/lapack/
[3] AMD Core Math Library: http://developer.amd.com/acml.jsp
[4] Scalable LAPACK: www.netlib.org/scalapack/

major problem is the large density of points necessary for many of the calculations, to preclude missing avoided crossings. In order to achieve optimal performance, *all* steps would have to be parallelized (from matrix creation, to finding the eigenproperties, to sorting and further processing and saving of the data). After each step a synchronization would be necessary since the results obtained on different processors are interdependent. This would be feasible but perhaps not quite worthy of the effort. The amount of messages that would have to be sent among the different processors would also slow the computation.

Therefore, we used a different approach instead. We divided the computation between (i) a root processor, responsible for sorting of the eigenproperties, the calculation of the orientation and alignment cosines, and the data storage, and (ii) auxilliary processors which only setup the Hamiltonian matrix for a specific field strength (one matrix per field strength) and diagonalize it. The results are sent to the root processor. Unless the data are received by the root processor, the processor does not start a new calculation. The efficiency strongly depends on the timing and on the load on the different processors. Especially if the root processor takes too long to finish a task, the latency for the other processors can become high, because the root processor is not yet able to receive a new message.

For these calculations we used up to four processors. The time consumption decreased almost by a factor of 4, which justified this approach. But in the end, the speed of the computations strongly depends on the dimensions of the matrices and of the eigenvectors used in calculating the directional properties.

3.3 Sorting of eigenvalues

The matrix diagonalization delivers the eigenproperties for a particular field configuration (field strength parameters and the tilt angle). In order to generate the dependence of the eigenproperties and the derived quantities (such as the alignment and orientation cosines) on the field parameters, the eigenproperties for an adjacent field configuration have to be "smoothly" connected. While doing so, a mixture of avoided and genuine crossings has to be considered.

The simplest such case occurs for a two-level system, which is represented by a 2×2 matrix. The eigenstates ϕ_i, with $i = 1, 2$, of the unperturbed Hamiltonian $\mathcal{H}_0$ are changed by the presence of an interaction V. The eigenstates ψ_i of the perturbed Hamiltonian $\mathcal{H} = \mathcal{H}_0 + V$ are hybrids of the ϕ_i:

$$\psi_i = a_1^i \phi_1 + a_2^i \phi_2 \tag{3.4}$$

Replacing the wave function ψ in the complete Schrödinger equation leads to the following set of linear equations with matrix elements $\mathcal{H}_{mn} \equiv \langle \phi_m | \mathcal{H} | \phi_n \rangle$.

$$(\mathcal{H}_{11} - E)\, a_1 + \mathcal{H}_{12} a_2 = 0 \qquad \mathcal{H}_{12} a_1 + (\mathcal{H}_{22} - E)\, a_2 = 0 \tag{3.5}$$

This problem can be reduced to solving the determinantal equation

$$\begin{vmatrix} \mathcal{H}_{11} - E & \mathcal{H}_{12} \\ \mathcal{H}_{21} & \mathcal{H}_{22} - E \end{vmatrix} = 0 \tag{3.6}$$

The eigenvalues are

$$E_{1,2} = \frac{1}{2}\left(\mathcal{H}_{11} + \mathcal{H}_{22}\right) \pm \frac{1}{2}\left[\left(\mathcal{H}_{11} + \mathcal{H}_{22}\right)^2 + 4\left|\mathcal{H}_{12}\right|^2\right]^{1/2} \tag{3.7}$$

Dividing (3.5) by a_1 and/or a_2 leads to the ratio of the two components

$$\frac{a_1}{a_2} = \frac{\mathcal{H}_{12}}{E - \mathcal{H}_{11}} \qquad \frac{a_1}{a_2} = \frac{E - \mathcal{H}_{22}}{\mathcal{H}_{21}} \tag{3.8}$$

Substituting for the energy and using $\tan\beta \equiv 2\mathcal{H}_{12}/\left(\mathcal{H}_{11} - \mathcal{H}_{22}\right)$, the two solutions simplify to

$$\left(\frac{a_1}{a_2}\right)_1 = \cot\frac{\beta}{2} \qquad \left(\frac{a_1}{a_2}\right)_2 = -\tan\frac{\beta}{2} \tag{3.9}$$

This gives the wave functions for the perturbed problem as

$$\begin{pmatrix} \psi_1 \\ \psi_2 \end{pmatrix} = \begin{pmatrix} \cos\frac{\beta}{2} & \sin\frac{\beta}{2} \\ -\sin\frac{\beta}{2} & \cos\frac{\beta}{2} \end{pmatrix} \begin{pmatrix} \phi_1 \\ \phi_2 \end{pmatrix} \tag{3.10}$$

The eigenenergies and the wave functions strongly depend on the ratio of $|\mathcal{H}_{11} - \mathcal{H}_{22}|/|\mathcal{H}_{12}|$. For $\mathcal{H}_{12} = 0$, the states can cross as there is no interaction between the states, see figure 3.2. The parameter β is zero and therefore the wave functions ψ_i are equal to the ones in the absence of the perturbation, ϕ_i. As long as the difference of the diagonal elements exceeds the off-diagonal element, $|\mathcal{H}_{11} - \mathcal{H}_{22}| \gg |\mathcal{H}_{12}|$, β remains small and the wave functions mix only weakly, $\psi_1 \approx \phi_1$ and $\psi_2 \approx \phi_2$. For the other extreme, $|\mathcal{H}_{11} - \mathcal{H}_{22}| \ll |\mathcal{H}_{12}|$, the eigenenergies of the two states remain separated by twice the interaction strength $|\mathcal{H}_{12}|$. The states are seen to repel each other, thus avoiding their crossing. The wave functions become $\psi_1 = \frac{1}{\sqrt{2}}(\phi_1 + \phi_2)$ and $\psi_2 = \frac{1}{\sqrt{2}}(-\phi_1 + \phi_2)$. Since the potential can only couple states with the same values of the good quantum numbers (often referred to as states of 'same symmetry'), our analysis of the two-state problem can be summarized by stating that states with the same symmetry do not cross (the non-crossing rule, [57]). For multi-level systems, more than two states can interact, giving rise to multiple avoided crossings.

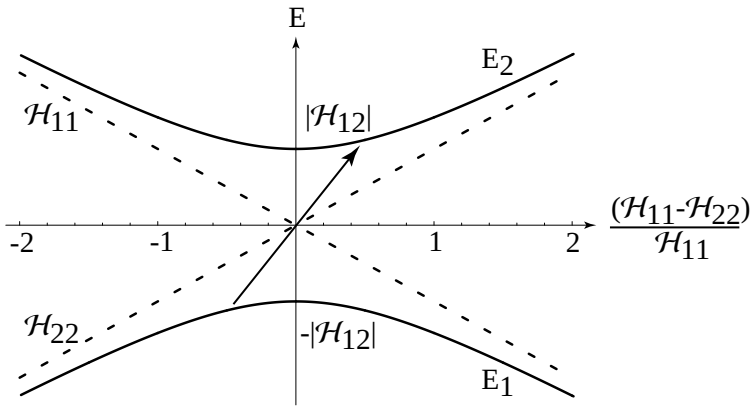

Figure 3.2: Example of avoided (dashed) and genuine (solid) crossings in a two-level system. A non-adiabatic transition is shown by the arrow.

Whether a passage through a crossing will be adiabatic (i.e., the system will emerge in the same state, 1 or 2, in which it entered the crossing) or non-adiabatic (i.e., the system will 'hop' from state 1 to state 2 or vice versa), is determined by the non-adiabatic splitting, ΔE, and the rate at which the system is making the crossing. From the uncertainty principle, it takes a time Δt to distinguish between states 1 and 2 separated by an energy ΔE, $\Delta E \Delta t \sim \hbar$. Only when the interaction time, τ, is shorter than $\Delta t \sim \frac{\hbar}{\Delta E}$ is the probability of a non-adiabatic transition high. Thus, for instance, for $\Delta E \sim B$ (with B the rotational constant of the molecule), the behavior is adiabatic for interaction times (field pulses, τ) such that $\tau \sim \hbar/B$ and non-adiabatic for $\tau \ll \hbar/B$.

Here we consider just the stationary states, i.e. the adiabatic regime.

As for the assignment of the states, there are two kinds of quantities that can be used to keep track of the states as the field parameters vary - the eigenvalues and the eigenvectors. The simplest method is based on sorting all eigenvalues by their ascending or descending order. This can be used if only avoided crossings are present. In the case of genuine crossings the method fails. Since for collinear fields just avoided crossings occur, the method is only adequate for this field configuration.

If there is a mixture of avoided and genuine crossing, it is necessary to use a different method. Since the eigenvalues are differentiable with respect to the fields, one would think that checking for a continuity of their slopes would be enough to keep track of a given state. However, when two states are degenerate or nearly degenerate, the method becomes ambiguous.

Therefore, in order to keep track of the states unambiguously while the field parameters are varied, one needs to rely on the eigenvectors. If $|\Psi_0\rangle$ is the state to be tracked, one has to calculate its overlap $|\langle\Psi_k|\Psi_0\rangle|$ with all the eigenvectors $|\Psi_k\rangle$ that pertain to the

Hamiltonian matrix with the incremented parameters. The state with the largest overlap is then taken as the continuation of Ψ_0. This method has been used for the general problem of tilted fields.

The procedure for calculating the overlaps for a given state Ψ_0 with all the other states Ψ_k can be simplified by eliminating those states which have already been assigned. Another improvement in efficiency is achieved by selecting out only those eigenvectors whose corresponding eigenvalues λ_k lie within a certain range of λ_0. The perturbation theory for matrices provides the tools for implementing this. With the help of the Geršgorin theorem (see [71]) the following corollary can be derived: Let $A \in M_n$ be a normal matrix (such as a Hermitian matrix) with eigenvalues λ_1 , ..., λ_n and let $E \in M_n$. If $\hat{\lambda}$ is an eigenvalue of $A + E$, then there is some eigenvalue λ_i of A for which $\left|\hat{\lambda} - \lambda_i\right| \leq |||E|||_2 = \rho\,(E)$. Here $|||E|||_2$ is the spectral matrix norm of E, which is defined by the maximum of $\sqrt{\lambda}$, where λ is an eigenvalue of E^*E. The overlap integral is then calculated only for those states whose λ_i are within the convergence radius $\rho(E)$.

4 Results and discussion

4.1 Symmetric-top molecules and their interactions with static and radiative electric fields

We consider a symmetric-top molecule which is both *polar* and *polarizable*. The inertia tensor, $\mathbf{I}$, of a symmetric top molecule possesses a three-fold or higher axis of rotation symmetry (the figure axis), and is said to be prolate or oblate, depending on whether the principal moment of inertia about the figure axis is smaller or larger than the remaining two principal moments (which are equal to one another). The principal axes a, b, c of $\mathbf{I}$ are defined such that the principal moments of inertia increase in the order $I_a < I_b < I_c$.

The symmetry of the inertia tensor is reflected in the symmetry of the polarizability tensor, $\boldsymbol{\alpha}$, in that the principal axes of the two tensors are collinear. However, a prolate or oblate inertia tensor does not necessarily imply a prolate or oblate polarizability tensor. Four combinations can be distinguished:

(i.) $\mathbf{I}$ prolate and $\boldsymbol{\alpha}$ prolate, i.e., $I_a < I_b = I_c$ and $\alpha_a < \alpha_b = \alpha_c$ with a the figure axis;

(ii.) $\mathbf{I}$ prolate and $\boldsymbol{\alpha}$ oblate, i.e., $I_a < I_b = I_c$ and $\alpha_a > \alpha_b = \alpha_c$, with a the figure axis;

(iii.) $\mathbf{I}$ oblate and $\boldsymbol{\alpha}$ prolate, i.e., $I_a = I_b < I_c$ and $\alpha_a = \alpha_b > \alpha_c$ with c the figure axis;

(iv.) $\mathbf{I}$ oblate and $\boldsymbol{\alpha}$ oblate, i.e., $I_a = I_b < I_c$ and $\alpha_a = \alpha_b < \alpha_c$, with c the figure axis.

The body-fixed permanent electric dipole moment $\boldsymbol{\mu}$ of a symmetric-top molecule is bound to lie along the molecule's figure axis. The symmetry combinations of $\mathbf{I}$ and $\boldsymbol{\alpha}$ are summarized in Table 4.1 in terms of the rotational constants

$$A \equiv \frac{\hbar^2}{2I_a}; \qquad B \equiv \frac{\hbar^2}{2I_b}; \qquad C \equiv \frac{\hbar^2}{2I_c} \tag{4.1}$$

and polarizability components parallel, $\alpha_{\parallel}$, and perpendicular, $\alpha_{\perp}$, to the figure axis.

The rotational Hamiltonian, $\mathcal{H}_r$, of a symmetric top molecule is given by

$$\mathcal{H}_r = B\boldsymbol{J}^2 + \rho B J_z^2 \tag{4.2}$$

with $\boldsymbol{J}$ the angular momentum operator, J_z its projection on the figure axis z ($z \equiv a$ for prolate and $z \equiv c$ for oblate top), and

$$\rho \equiv \begin{cases} \left(\frac{A}{B} - 1\right) > 0 & \text{for } \mathbf{I} \text{ prolate} \\ \left(\frac{C}{B} - 1\right) < 0 & \text{for } \mathbf{I} \text{ oblate} \end{cases} \tag{4.3}$$

case (i) $\mathbf{I}$ prolate, $\boldsymbol{\alpha}$ prolate	case (ii) $\mathbf{I}$ prolate, $\boldsymbol{\alpha}$ oblate	case (iii) $\mathbf{I}$ oblate, $\boldsymbol{\alpha}$ prolate	case (iv) $\mathbf{I}$ oblate, $\boldsymbol{\alpha}$ oblate
$I_a < I_b = I_c$	$I_a < I_b = I_c$	$I_a = I_b < I_c$	$I_a = I_b < I_c$
$A > B = C$	$A > B = C$	$A = B > C$	$A = B > C$
$\alpha_a < \alpha_b = \alpha_c$	$\alpha_a > \alpha_b = \alpha_c$	$\alpha_a = \alpha_b > \alpha_c$	$\alpha_a = \alpha_b < \alpha_c$
$\alpha_\parallel < \alpha_\perp$	$\alpha_\parallel > \alpha_\perp$	$\alpha_\parallel < \alpha_\perp$	$\alpha_\parallel > \alpha_\perp$

Table 4.1: Symmetry combinations of the inertia and polarizability tensors for a polarizable symmetric top molecule. See text for details.

The symmetric-top molecule is subject to a combination of a *static electric field*, ε_S, with a *nonresonant laser field*, ε_L. The fields ε_S and ε_L can be tilted with respect to one another by an angle, β. We limit our consideration to a pulsed plane wave radiation of frequency ν and time profile $g(t)$ such that

$$\varepsilon_L^2(t) = \frac{8\pi}{c} I g(t) \cos^2(2\pi\nu t) \tag{4.4}$$

where I is the peak laser intensity.[1] We assume the oscillation frequency ν to be far removed from any molecular resonance and much higher than either τ^{-1} (with τ the pulse duration) or the rotational periods. The resulting effective Hamiltonian, $\mathcal{H}(t)$, is thus averaged over the rapid oscillations. This cancels the interaction between μ and ε_L (see Section 2.3 and ref. [73, 74]) and reduces the time dependence of ε_L to that of the time profile,

$$\left\langle \varepsilon_L^2(t) \right\rangle = \frac{4\pi}{c} I g(t) \tag{4.5}$$

Thus the Hamiltonian becomes

$$\mathcal{H}(t) = \mathcal{H}_r + V_\mu + V_\alpha(t) \tag{4.6}$$

[1] The intensity is proportional to the energy density times the velocity of light. It becomes in *SI*-units: $I = \frac{1}{2} c\epsilon_0 |\varepsilon|^2$, with ϵ_0 the vacuum permittivity. In CGS units, which are considered throughout this thesis, ε is replaced by $\varepsilon/\sqrt{4\pi\epsilon_0}$

where the permanent, V_μ, and induced, V_α, dipole potentials are given by

$$V_\mu = -B\omega\cos\theta_S \tag{4.7}$$
$$V_\alpha(t) = -B\Delta\omega(t)\cos^2\theta_L - B\omega_\perp(t) \tag{4.8}$$

with the dimensionless interaction parameters defined as follows

$$\omega \equiv \frac{\mu\varepsilon_S}{B} \tag{4.9a}$$
$$\omega_{||,\perp}(t) = \omega_{||,\perp}g(t) \tag{4.9b}$$
$$\omega_{||,\perp} \equiv \frac{2\pi\alpha_{||,\perp}I}{Bc} \tag{4.9c}$$
$$\Delta\omega \equiv \omega_{||} - \omega_\perp \tag{4.9d}$$
$$\Delta\omega(t) = \omega_{||}(t) - \omega_\perp(t) \equiv \Delta\omega g(t) \tag{4.9e}$$

The time-dependent Schrödinger equation corresponding to Hamiltonian (4.6) can be cast in a dimensionless form

$$i\frac{\hbar}{B}\frac{\partial\psi(t)}{\partial t} = \frac{\mathcal{H}(t)}{B}\psi(t) \tag{4.10}$$

which clocks the time in units of $\hbar/B$, thus defining a "short" and a "long" time for any molecule and pulse duration. In what follows, we limit our consideration to the adiabatic regime, which arises for $\tau \gg \hbar/B$. This is tantamount to $g(t) \to 1$, in which case the Hamiltonian (4.6) can be written as

$$\frac{\mathcal{H}(t)}{B} = \frac{\mathcal{H}_r}{B} - \omega\cos\theta_S - \left(\Delta\omega\cos^2\theta_L + \omega_\perp\right) \tag{4.11}$$

Hence our task is limited to finding the eigenproperties of Hamiltonian (4.11). For $\Delta\omega = \omega = 0$, the eigenproperties become those of a field-free rotor; the eigenfunctions then coincide with the symmetric-top wavefunctions, $|JKM\rangle$, and the eigenvalues become E_{JKM}/B, with K and M the projections of the rotational angular momentum J on the figure and space-fixed axis, respectively. In the high-field limit, $\Delta\omega \to \pm\infty$ and/or $\omega \to \infty$, the range of the polar angle is confined near the quadratic potential minimum, and eq. (4.11) reduces to that for a two-dimensional angular harmonic oscillator (*harmonic librator*), see Section 4.3.1.

If the tilt angle β between the field directions is nonzero, the relation

$$\cos\theta_S = \cos\beta\cos\theta + \sin\beta\sin\theta\cos\varphi \tag{4.12}$$

is employed in Hamiltonian (4.6), with $\theta \equiv \theta_L$ and $\varphi \equiv \varphi_L$, see Figure 4.1.

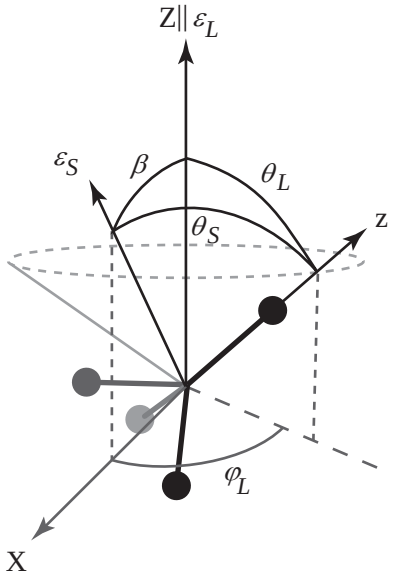

Figure 4.1: Illustration of the angles used in equation (4.12) for substitution for arbitrary field directions.

If the static and radiative fields are *collinear* (i.e., $\beta = 0$ or π), M and K remain good quantum numbers. Note that except when $K = 0$, all states are doubly degenerate. While the permanent dipole interaction V_μ mixes states with $\Delta J = \pm 1$ (which have opposite parities), the induced dipole interaction mixes states with $\Delta J = 0 \wedge \pm 2$ (which have same parities), but, when $MK \neq 0$, also states with $\Delta J = \pm 1$ (which have opposite parities). Thus *either* field has the ability to create *oriented states* of mixed parity.

If the static and radiative fields are *not* collinear (i.e., $\beta \neq 0$ or π), the system no longer possesses cylindrical symmetry. The $\cos\varphi$ operator mixes states which differ by $\Delta M = \pm 1$ and so M ceases to be a good quantum number.

A schematic of the field configurations and molecular dipole moments, permanent and induced, is shown is Figure 4.2.

The elements of the Hamiltonian matrix in the symmetric-top basis set $|JKM\rangle$ possess the following symmetries

$$\left\langle J'KM' \left| \frac{\mathcal{H}}{B} \right| JKM \right\rangle = (-1)^{M'-M} \left\langle J' - K - M' \left| \frac{\mathcal{H}}{B} \right| J - K - M \right\rangle \tag{4.13}$$

$$\left\langle J' - KM' \left| \frac{\mathcal{H}}{B} \right| J - KM \right\rangle = (-1)^{M'-M} \left\langle J'K - M' \left| \frac{\mathcal{H}}{B} \right| JK - M \right\rangle \tag{4.14}$$

Since the Hamiltonian has the same diagonal elements for the two symmetry representations belonging to $+K$ and $-K$, it follows that they are connected by a unitary transformation, U. On the other hand, complex conjugation, $\mathcal{K}$, of a symmetric top state yields

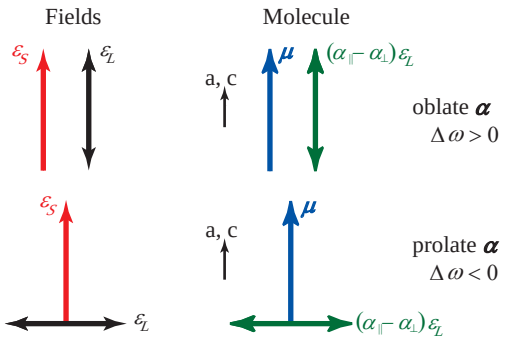

Figure 4.2: Schematic of the configurations of the fields and dipoles. An electrostatic, ε_S, and a linearly polarized radiative, ε_L, field are considered to be either collinear or perpendicular to one another. While the permanent dipole, μ, of a symmetric top molecule is always along the figure axis (a or c for a prolate or oblate tensor of inertia), the induced dipole moment, $(\alpha_{||} - \alpha_\perp)\varepsilon_L$, is directed predominantly along the figure axis for an oblate anisotropy of the polarizability tensor, $\alpha_{||} > \alpha_\perp$, and perpendicular to it for a prolate polarizability, $\alpha_{||} < \alpha_\perp$. See Table 4.1 and text.

$$\mathcal{K}\,|JKM\rangle = (-1)^{M-K}\,|J-K-M\rangle \tag{4.15}$$

and so we see from eqs. (4.13) and (4.14) that the $+K$ and $-K$ representations are related by the combined operation $U\mathcal{K}$, which amounts to time reversal. The two representations have the same eigenenergies and are separable degenerate [69]. We note that the $+K$ and $-K$ representations are connected by time-reversal both in the absence and presence of an electric field (see also ref. [64]); the time reversal of a given matrix element is effected by a multiplication by $(-1)^{M'-M}$. The symmetry properties, eqs. (4.13) and (4.14), are taken advantage of when setting up the Hamiltonian matrix. In what follows, we concentrate on the case of collinear (i.e., $\beta = 0$ or π) and perpendicular fields (i.e., $\beta = \pi/2$).

We label the states in the field by the good quantum number K and the nominal symbols $\tilde{J}$ and $\tilde{M}$ which designate the values of the quantum numbers J and M of the free-rotor state that adiabatically correlates with the state at $\Delta\omega \neq 0$ and/or $\omega > 0$, $J \to \tilde{J}$ and $M \to \tilde{M}$. We condense our notation by taking K to be nonnegative, but keep in mind that each state with $K \neq 0$ is doubly degenerate, on account of the $+K$ and $-K$ symmetry representation. For collinear fields, $\tilde{M} = M$.

In the *tilted fields*, the adiabatic label of a state depends on the order in which the parameters ω, $\Delta\omega$ and β are turned on, see Subsection 4.3.4. As a result, we distinguish among $\left|\tilde{J}, K, \tilde{M}; \omega, \Delta\omega, \beta\right\rangle$, $\left|\tilde{J}, K, \tilde{M}; \Delta\omega, \omega, \beta\right\rangle$, $\left|\tilde{J}, K, \tilde{M}; \omega, \beta, \Delta\omega\right\rangle$, and $\left|\tilde{J}, K, \tilde{M}; \Delta\omega, \beta, \omega\right\rangle$

states, or $\left|\tilde{J}, K, \tilde{M}; \{p\}\right\rangle$ for short, with $\{p\}$ any one of the parameter sets ω, $\Delta\omega$, β or $\Delta\omega$, ω, β or ω, β, $\Delta\omega$ or $\Delta\omega$, β, ω.

The $|\tilde{J}, K, \tilde{M}; \{p\}\rangle$ states are recognized as coherent linear superpositions of the field-free symmetric-top states,

$$\left|\tilde{J}, K, \tilde{M}; \{p\}\right\rangle = \sum_{J,M} a_{JM}^{\tilde{J}K\tilde{M}} \, |JKM\rangle \tag{4.16}$$

with $a_{JM}^{\tilde{J}K\tilde{M}}$ the expansion coefficients. For a given state, these depend solely on $\{p\}$,

$$a_{JM}^{\tilde{J}K\tilde{M}} = a_{JM}^{\tilde{J}K\tilde{M}}\left(\{p\}\right) \tag{4.17}$$

The orientation and the alignment are given by the direction-direction (two-vector) correlation [55] between the dipole moment (permanent or induced) and the field vector (ε_S or ε_L). A direction-direction correlation is characterized by a single angle, here by the polar angle θ_S (for the orientation of the permanent dipole with respect to ε_S) or θ_L (for the alignment of the induced dipole with respect to ε_L). The distribution in either θ_S or θ_L can be described in terms of a series in Legendre polynomials and characterized by Legendre moments. The first odd Legendre moment of the distribution in θ_S is related to the expectation value of $\cos\theta_S$, the *orientation cosine*,

$$\begin{aligned}
\langle\cos\theta_S\rangle \equiv & \sum_{J'M'}\sum_{JM} a_{J'M'}^{\tilde{J}K\tilde{M}*} a_{JM}^{\tilde{J}K\tilde{M}} (2J+1)^{\frac{1}{2}}(2J'+1)^{\frac{1}{2}}(-1)^{M-K}
\begin{pmatrix} J & 1 & J' \\ -K & 0 & K \end{pmatrix} \\
& \times \left[\cos\beta \begin{pmatrix} J & 1 & J' \\ -M & 0 & M' \end{pmatrix} + \sin\beta\sqrt{\frac{1}{2}}\left(\begin{pmatrix} J & 1 & J' \\ -M & -1 & M' \end{pmatrix} - \begin{pmatrix} J & 1 & J' \\ -M & 1 & M' \end{pmatrix}\right)\right] \\
= & \left\langle \tilde{J}, K, \tilde{M}; \{p\}\right| \cos\theta_S \left|\tilde{J}, K, \tilde{M}; \{p\}\right\rangle
\end{aligned} \tag{4.18}$$

and the first even Legendre moment of the distribution in θ_L to the expectation value of $\cos^2\theta_L$, the *alignment cosine*,

$$\begin{aligned}
\left\langle\cos^2\theta_L\right\rangle \equiv & \sum_{J'M}\sum_{J} a_{J'M}^{\tilde{J}K\tilde{M}*} a_{JM}^{\tilde{J}K\tilde{M}} \left[\delta_{JJ'}\frac{1}{3} + \frac{2}{3}(2J+1)^{\frac{1}{2}}(2J'+1)^{\frac{1}{2}}(-1)^{M-K}\right. \\
& \left. \times \begin{pmatrix} J & 2 & J' \\ -M & 0 & M \end{pmatrix}\begin{pmatrix} J & 2 & J' \\ -K & 0 & K \end{pmatrix}\right] \\
= & \left\langle \tilde{J}, K, \tilde{M}; \{p\}\right| \cos^2\theta_L \left|\tilde{J}, K, \tilde{M}; \{p\}\right\rangle
\end{aligned} \tag{4.19}$$

The states with same $|K|$ and same MK have both the same energy,

$$E\left(\tilde{J},+K,\tilde{M};\{p\}\right)=E\left(\tilde{J},-K,-\tilde{M};\{p\}\right) \tag{4.20}$$

and the same directional properties, as follows from the Hellmann-Feynman theorem

$$\langle\cos\theta_S\rangle=-\frac{\partial\left(\frac{E}{B}\right)}{\partial\omega} \tag{4.21}$$

and

$$\langle\cos^2\theta_L\rangle=-\frac{\partial\left(\frac{E}{B}+\omega_\perp\right)}{\partial\Delta\omega} \tag{4.22}$$

The angular amplitudes of the permanent and induced dipoles are given, respectively, by

$$\theta_{S,0}=\arccos\langle\cos\theta_S\rangle \tag{4.23}$$

and

$$\theta_{L,0}=\arccos[\langle\cos^2\theta_S\rangle]^{\frac{1}{2}} \tag{4.24}$$

To use the Hellman-Feynman theorem to calculate the expectation values, it would be necessary to calculate the energies as a function of ω and $\Delta\omega$. The label switching derail this calculation. Therefore all expectation values are calculated by equations (4.18) and (4.19). The results have been checked for agreement with the results obtained by the Hellman-Feynman theorem. Applying the Hellman-Feynman theorem is even worse, since care must be taken, for an accurate step width. Sometimes very weak changes of the fields strength are necessary to change the behavior dramatically. Due to the wide application of the Hellman-Feynman theorem in literature, always both expectation values are shown. This allows a qualitatively comparison of the expectation values, obtained from the wave-functions, with the eigenenergies. But the main focus of this thesis is on the orientation cosine.

The elements of the Hamiltonian matrix, evaluated in the symmetric-top basis set, are listed in Appendix B. The dimension of the Hamiltonian matrix determines the accuracy of the eigenproperties computed by diagonalization. The dimension of the matrix for the collinear case is given as $J_{\max}+1-\max(|K|,|M|)$, with J ranging between $\max(|K|,|M|)$ and $J_{\max}$. For the states and field strengths considered here, a 12×12 matrix yields an improvement of less than 0.1% of E/B over a 11×11 matrix. But the convergence depends strongly on the state considered. For the perpendicular case the dimension of the matrix is $(J_{max}+1)^2-K^2$ with J ranging between $|K|$ and J_{max} and M between

$-J$ and J. Convergence within 0.1% can be achieved for the states considered with $J_{max} = 10$.

The $\left|\tilde{J}, K, \tilde{M}; \{p\}\right\rangle$ states are not only labeled but also identified in our computations by way of their adiabatic correlation with the field-free states. For the collinear case, it is sufficient to sort the eigenenergies by increasing energy since all crossings in one block of the full Hamiltonian matrix, specified by K and M, are avoided. For tilted fields, the states undergo numerous crossings, genuine as well as avoided. Therefore the identification algorithm described in Section 3.3 is used, which is based on a gradual perturbation of the field free symmetric-top states. Rather than comparing the eigenenergies, it compares the wavefunctions, which are deemed to belong to the same state when their coefficients evolve continuously through a crossing as a function of the parameters $\{p\}$. For perpendicular fields, a correlation with the case of collinear fields is used in addition, in order to keep track of which state is which.

4.2 Effective potential

In order to obtain the most probable spatial distribution (geometry), wavefunctions, such as

$$\left|\tilde{J}, K, \tilde{M}; \{p\}\right\rangle = \Xi_{\tilde{J},K,\tilde{M};\{p\}}(\theta, \varphi) \equiv \Xi(\theta, \varphi) \tag{4.25}$$

obtained by solving the Schrödinger equation in curvilinear coordinates, need to be properly spatially weighted by a non-unit Jacobian factor, here $\sin\theta$. Alternatively, a wavefunction,

$$|\Phi|^2 = |\Xi|^2 \sin\theta \tag{4.26}$$

with a *unit Jacobian* can be constructed which gives the most probable geometry directly; such a wavefunction is an eigenfunction of a Hamiltonian

$$\frac{\mathcal{H}'}{B} = -\frac{d^2}{d\theta^2} + U \tag{4.27}$$

where U is an effective potential. eq. (4.27) shows that Φ corresponds to the solution of a 1-D Schrödinger equation for the curvilinear coordinate θ and for the effective potential U. Since Φ can only take significant values within the range demarcated by U, one can glean the geometry from the effective potential and the eigenenergy. In this way, one can gain insight into the qualitative features of the eigenproblem without the need to find the eigenfunctions explicitly. Conversely, one can use the concept

of the effective potential to organize the solutions and to interpret them in geometrical terms.

For collinear fields, the effective potential takes the form (see Appendix D):

$$U = \left[\frac{M^2 - \frac{1}{4}}{\sin^2\theta} - \frac{1}{4}\right] - \rho K^2 + \frac{K^2 - 2MK\cos\theta}{\sin^2\theta} - \omega\cos\theta - \left(\Delta\omega\cos^2\theta + \omega_\perp\right) \quad (4.28)$$

Its first term, symmetric about $\theta = \pi/2$, arises due to the centrifugal effects and, for $|M| > 0$, provides a repulsive contribution competing with the permanent (fourth term) and induced (fifth term) interactions. For $|K| > 0$, the second term just uniformly shifts the potential, either down when $\rho > 0$ (prolate top), or up when $\rho < 0$ (oblate top). The third term provides a contribution which is *asymmetric* with respect to $\theta = \pi/2$ for *precessing states*, i.e., states with $MK \neq 0$. It is this term which is responsible for the first-order Stark effect in symmetric tops and for the inherent orientation their precessing states possess. The fourth term, due to the permanent dipole interaction, is asymmetric with respect to $\theta = \pi/2$ for any state, and accounts for all higher-order Stark effects. The fifth, induced-dipole term, is symmetric about $\theta = \pi/2$. However, it gives rise to a single well for $\boldsymbol{\alpha}$ prolate ($\alpha_\parallel < \alpha_\perp$) and a double-well for $\boldsymbol{\alpha}$ oblate ($\alpha_\parallel > \alpha_\perp$). This is of key importance in determining the energy level structure and the directionality of the states bound by the wells.

4.3 Behavior of the eigenstates

4.3.1 Correlation diagrams

In the strong-field limit, a symmetric top molecule becomes a harmonic librator whose eigenproperties can be obtained in closed form. The eigenenergies in the harmonic-librator limit are listed in Tables 4.2 and 4.3 and used in constructing the correlation diagrams between the field-free and the harmonic librator limits, shown in Figures 4.3 (for the permanent dipole interaction, $\omega \to \infty$) and 4.4 (for the prolate, $\Delta\omega \to -\infty$, and oblate, $\Delta\omega \to \infty$, induced-dipole interaction).

The correlation diagram for the permanent dipole interaction, Fig. 4.3, reveals that states with $K = 0$ split into $\tilde{J} + 1$ doublets, each with the same value of $|M|$. The other states, on the other hand, split into $\tilde{J} + |K|$ at least doubly degenerate states, each of which is characterized by a value of $|K + M|$ for a given $\tilde{J}$. For $|K| < \tilde{J}$ some states are more than doubly degenerate. In the harmonic librator limit, the levels are *infinitely degenerate* and are separated by an energy difference of $(2\omega)^{1/2}$.

$\omega \to \infty$
$\frac{E_{N,K,M}}{B} = \rho K^2 + N(2\omega)^{\frac{1}{2}} + KM + \frac{1}{8}\left[3(K-M)^2 - 3 - N^2\right] - \omega$ $N = 2\tilde{J} - \lvert K+M\rvert + 1$

Table 4.2: Eigenenergies for the permanent dipole interaction in the harmonic librator limit. See [75].

The correlation diagrams for the induced dipole interaction reveal that states with $\tilde{J} < |M| + |K|$ (shown by black lines in Fig. 4.4) for $\boldsymbol{\alpha}$ oblate and *all* states for $\boldsymbol{\alpha}$ prolate which have same $|MK|$ form *degenerate doublets*. In contradistinction, states with $\tilde{J} \geq |M| + |K|$ (shown by red and green lines in Fig. 4.4 for $K = 0$ and $K \neq 0$, respectively) bound by V_α oblate occur as *tunneling doublets*. This behavior reflects a crucial difference between the $\boldsymbol{\alpha}$ prolate and $\boldsymbol{\alpha}$ oblate case, namely that the induced-dipole potential, V_α, is a double well potential for $\boldsymbol{\alpha}$ oblate and a single-well potential for $\boldsymbol{\alpha}$ prolate.

The members of a given tunneling doublet have same values of KM and $|K|$, but $\tilde{J}$'s that differ by ± 1. The tunneling splitting between the members of a given tunneling doublet decreases with increasing $\Delta\omega$ as $\exp(a - b\Delta\omega^{1/2})$, with $a, b \geq 0$, rendering a tunneling doublet quasi-degenerate at a sufficiently large field strength. In the harmonic

$\boldsymbol{\alpha}$ prolate: $\Delta\omega \to -\infty$	$\boldsymbol{\alpha}$ oblate: $\Delta\omega \to \infty$
$\frac{E_{N,K,M}}{B} = \rho K^2 +$ $+(2N+1)(-\Delta\omega)^{\frac{1}{2}} + M^2 + K^2 -$ $-\frac{1}{4}(2N^2+2N+3) - \omega_\perp$	$\frac{E_{N^\pm,K,M}}{B} = \rho K^2 +$ $+2(N^\pm+1)(\Delta\omega)^{\frac{1}{2}} + \frac{M^2}{2} + \frac{K^2}{2} - \frac{(N^\pm+1)^2}{2} -$ $-\Delta\omega - \omega_\perp - \frac{1}{2}$
$N = \tilde{J} - \lvert M\rvert$ for $\lvert M\rvert \geq \lvert K\rvert$ $N = \tilde{J} - \lvert K\rvert$ for $\lvert M\rvert < \lvert K\rvert$	for $\tilde{J} < \lvert M\rvert + \lvert K\rvert$ $N^\pm = 2\tilde{J} - \lvert K\rvert - \lvert M\rvert$ for $KM \gtrless 0$
	for $\tilde{J} \geq \lvert M\rvert + \lvert K\rvert$ $N^\pm = \tilde{J} - 1$ for $KM \gtrless 0$ when $\tilde{J} - \lvert K+M\rvert$ is odd $N^\pm = \tilde{J}$ for $KM \gtrless 0$ when $\tilde{J} - \lvert K+M\rvert$ is even
	for K or $M = 0$ $N^- = \tilde{J} - 1$ when $\tilde{J} - \lvert M\rvert$ or $\tilde{J} - \lvert K\rvert$ is odd $N^+ = \tilde{J}$ when $\tilde{J} - \lvert M\rvert$ or $\tilde{J} - \lvert K\rvert$ is even

Table 4.3: Eigenenergies for the induced dipole interaction in the harmonic librator limit. See also [54].

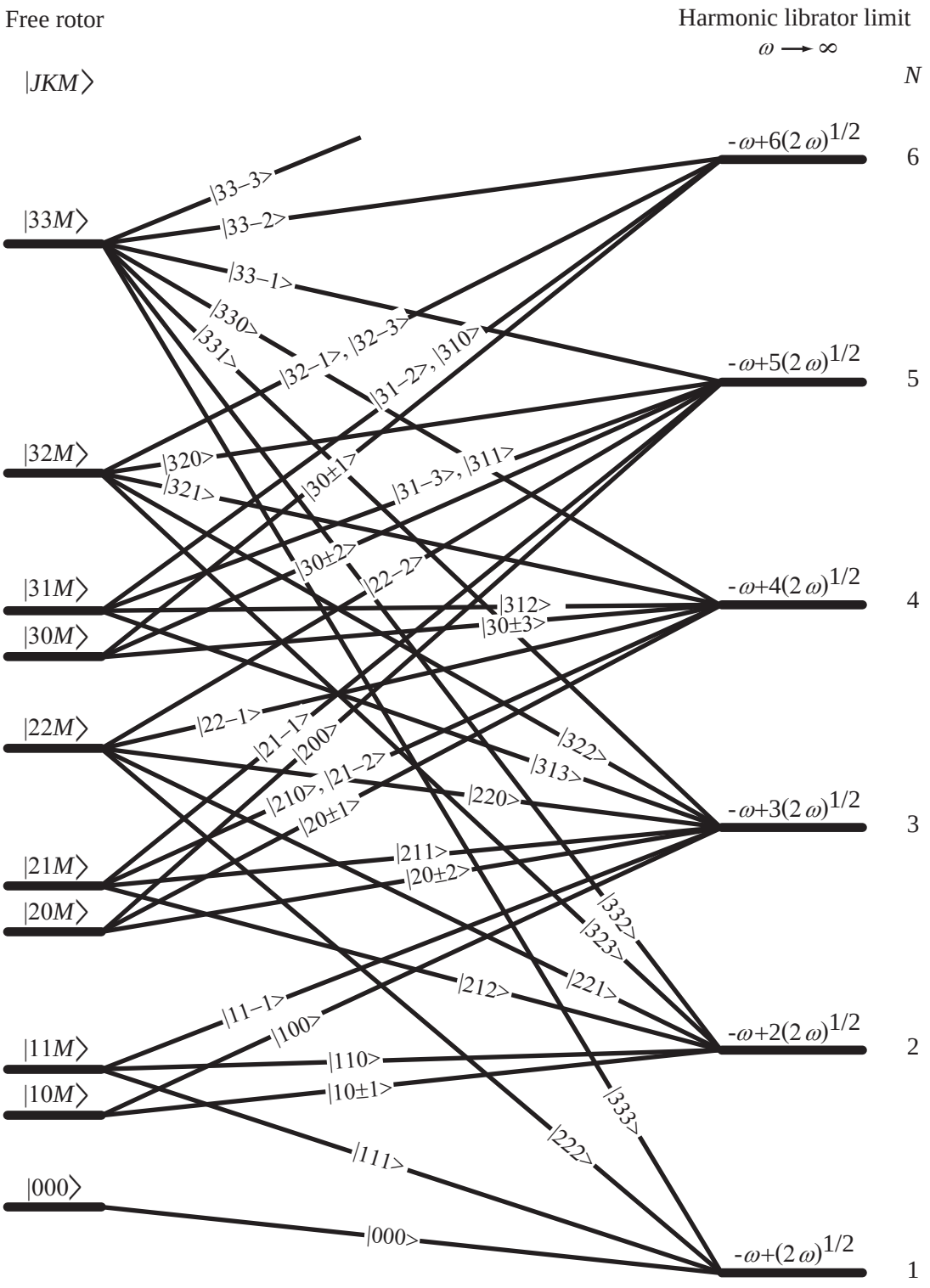

Figure 4.3: Correlation diagram, for the permanent dipole interaction, between the field-free ($\omega \rightarrow 0$) symmetric-top states $|JKM\rangle$ and the harmonic librator states $|N\rangle$ obtained in the high-field limit ($\omega \rightarrow \infty$), see also [75]. At intermediate fields, the states are labeled by $\left|\tilde{J}KM\right\rangle$.

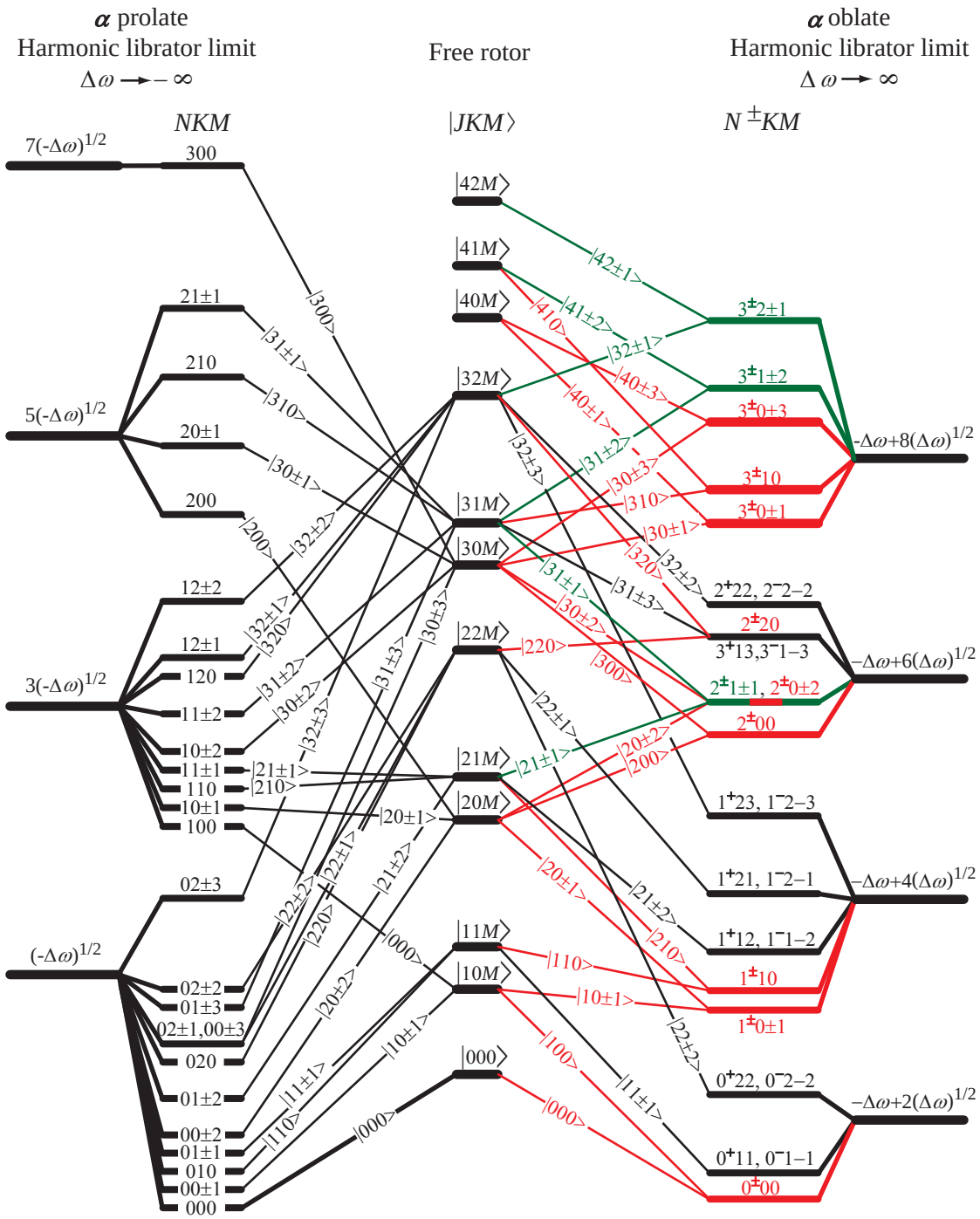

Figure 4.4: Correlation diagram, for the induced-dipole interaction, between the field-free ($\Delta\omega \rightarrow 0$) symmetric-top states $|JKM\rangle$ (center) and the harmonic librator states $|NKM\rangle$ obtained in the high-field limit for the prolate, $\Delta\omega \rightarrow -\infty$ (on the left), and oblate, $\Delta\omega \rightarrow \infty$ (on the right) case. The harmonic librator states are labeled by the librator quantum number N and the projection quantum numbers K and M. At intermediate fields, the states are labeled by $\left|\tilde{J}KM\right\rangle$. States that form tunneling doublets (only for $\Delta\omega \rightarrow \infty$) have $\tilde{J} \geq |K| + |M|$ and are shown in color: red for doublets with $KM = 0$, green for doublets with $K, M \neq 0$. Members of the degenerate doublets have $\tilde{J} < |K| + |M|$ and are shown in black. See text for details.

librator limit, the quasi-degenerate members of a given tunneling doublet coincide with the N^+ and N^- states, see Table 4.3. The N^+ and N^- states with $N^+ = N^-$ for $\tilde{J} < |M| + |K|$ always pertain to the same $\tilde{J}$ but different KM and so are precluded from forming tunneling doublets as they *do not* interact. In the α prolate case, the formation of any tunneling doublets is barred by the absence of a double well. Note that in both the prolate and oblate case, the harmonic librator levels are *infinitely degenerate* and their spacing is equal to $2|\Delta\omega|^{1/2}$.

The correlation diagrams of Figs. 4.3 and 4.4 reveal another key difference between the permanent and induced dipole interactions, namely the ordering of levels pertaining to the same $\tilde{J}$. The energies of the levels due to V_μ increase with increasing $|K + M|$. For V_α prolate, they decrease with increasing $|M|$ for levels with $|M| \geq |K|$ while states with $|M| \leq |K|$ have the same asymptote. The energy level pattern becomes even more complex for V_α oblate. There are $|K| + 1$ asymptotes. If $|K| = \tilde{J}$, the energy decreases with increasing $|M|$, while for $|K| < \tilde{J}$ it only decreases for levels with $|M| + |K| \geq \tilde{J}$. All other levels connect alternately to the asymptotes with $N^{(\pm)} = \tilde{J}$ or $\tilde{J} - 1$. This leads to a tangle of crossings, avoided or not, once the two interactions are combined, as will be exemplified below.

4.3.2 Collinear fields

Figures 4.5 and 4.6 display the dependence of the eigenenergies, panels (a)-(c), orientation cosines, panels (d)-(f), and alignment cosines, panels (g)-(i), of the states with $0 < \tilde{J} \leq 3$, $-1 \leq MK \leq 1$, and $K = 1$ on the dimensionless parameters ω and $\Delta\omega$ that characterize the permanent and induced dipole interactions. These states were chosen as examples since they well represent the behavior of a symmetric top in the combined fields. The two figures show the dependence on $\Delta\omega$ for fixed values of ω and vice versa. Note that negative values of $\Delta\omega$ correspond to $\boldsymbol{\alpha}$ prolate and positive values to $\boldsymbol{\alpha}$ oblate. The plots were constructed for $\mathbf{I}$ prolate with $A/B = 2$ but, apart from a constant shift, the curves shown are identical with those for $\mathbf{I}$ oblate. Thus Figs. 4.5 and 4.6 represent the entire spectrum of possibilities as classified in Table 4.1.

The left panels of Figs. 4.5 and 4.6 show the eigenenergies and the orientation and alignment cosines for the cases of pure permanent and pure induced dipole interactions, respectively. For an angle

$$\gamma \equiv \arccos \frac{KM}{J(J+1)} \tag{4.29}$$

such that $0 < \gamma < \pi/2$, the *pure permanent dipole interaction*, $\omega > 0$ and $\Delta\omega = 0$, panels (a), (d), (g) of Fig. 4.5, produces states whose eigenenergies decrease with increasing field strength (i.e., the states are *high-field seeking*) at all values of ω and their orientation

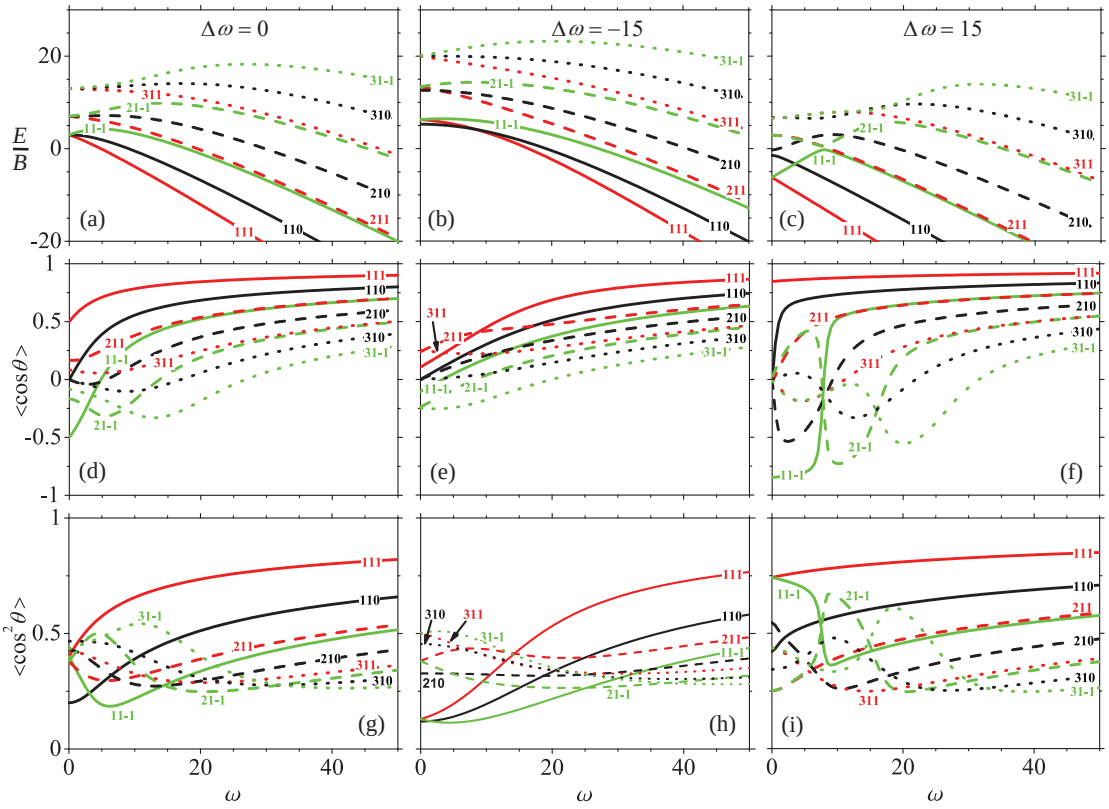

Figure 4.5: Dependence, in collinear fields, of the eigenenergies, panels (a)-(c), orientation cosines, panels (d)-(f), and alignment cosines, panels (g)-(i), of the states with $0 < \tilde{J} \leq 3$, $-1 \leq MK \leq 1$, and $K = 1$ on the dimensionless parameter ω (which characterizes the permanent dipole interaction with the electrostatic field) for fixed values of the parameter $\Delta\omega$ (which characterizes the induced-dipole interaction with the radiative field; $\Delta\omega < 0$ for prolate polarizability anisotropy, $\Delta\omega > 0$ for oblate polarizability anisotropy). The states are labeled by $|\tilde{J}KM\rangle$. Note that panels (a), (d), and (g) pertain to the permanent dipole interaction alone. See text.

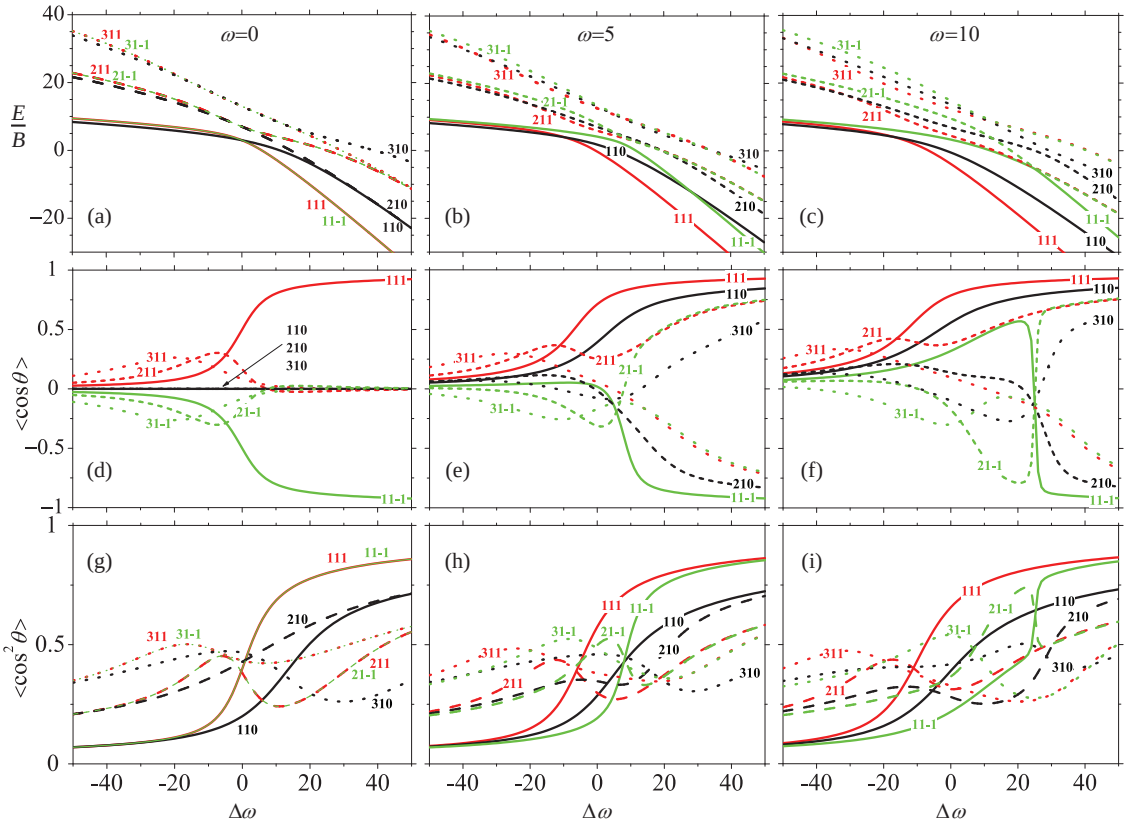

Figure 4.6: Dependence, in collinear fields, of the eigenenergies, panels (a)-(c), orientation cosines, panels (d)-(f), and alignment cosines, panels (g)-(i), of the states with $0 < \tilde{J} \leq 3$, $-1 \leq MK \leq 1$, and $K = 1$ on the dimensionless parameter $\Delta\omega$ (which characterizes the induced-dipole interaction with the radiative field; $\Delta\omega < 0$ for prolate polarizability anisotropy, $\Delta\omega > 0$ for oblate polarizability anisotropy) for fixed values of the parameter ω (which characterizes the permanent dipole interaction with the radiative field). The states are labeled by $|\tilde{J}KM\rangle$. Note that panels (a), (d), and (g) pertain to the induced-dipole interaction alone. See text.

cosines are positive, which signifies that the body-fixed dipole moment is oriented along ε_S (*right-way orientation*). For states with $\pi/2 < \gamma < \pi$, the eigenenergies first increase with ω (i.e., the states are *low-field seeking*) and the body-fixed dipole is oriented oppositely with respect to the direction of the static field ε_S (the so called *wrong-way orientation*). For states with $K = 0$, the angle γ becomes the tilt angle of the angular momentum vector with respect to the field direction, which, for $J > 0$, is given by

$$\gamma_0 \equiv \arccos \frac{|M|}{[J(J+1)]^{\frac{1}{2}}} \tag{4.30}$$

At small ω, states with $\gamma_0 > 3^{-1/2}$ are low-field seeking and exhibit the wrong-way orientation, while states with $\gamma_0 < 3^{-1/2}$ are high-field seeking and right-way oriented.

At large-enough values of ω, all states, including those with $K = 0$, become high-field seeking and exhibit right-way orientation. In any case, the dipole has the lowest energy when oriented along the field. Since the asymmetric effective potential (4.28) disfavors angles near 180°, and increasingly so with increasing KM, the eigenenergies for a given $\tilde{J}$ decrease with increasing KM. The ordering of the levels pertaining to the same $\tilde{J}$ is then such that states with higher KM are always lower in energy.

The eigenenergies and orientation and alignment cosines for a *pure induced-dipole interaction*, $\omega = 0$ and $|\Delta\omega| > 0$, are shown in panels (a), (d), and (g) of Fig. 4.6. The eigenenergies are given by

$$\frac{E}{B} = \frac{\langle \mathcal{H} \rangle}{B} = J(J+1) + \rho K^2 - \Delta\omega \langle \cos^2\theta \rangle - \omega_\perp, \tag{4.31}$$

cf. eqs. (4.2) and (4.11). However, Figs. 4.5 and 4.6 only show $E/B + \omega_\perp \equiv \lambda$, which increase with increasing laser intensity for $\boldsymbol{\alpha}$ prolate and decrease for $\boldsymbol{\alpha}$ oblate. Note that both prolate and oblate eigenergies, eq. (4.31), decrease with increasing laser intensity, and so all states created by a pure induced-dipole interaction are high-field seeking as a result. Note that

$$\left\langle \cos^2\theta \right\rangle = -\frac{\partial\lambda}{\partial\Delta\omega} \tag{4.32}$$

and thus the alignment cosines are given by the negative slopes of the curves shown in Fig. 4.6.

In panels (d) and (g) one can see that only the precessing states are oriented, and that their orientation shows a dependence on the $\Delta\omega$ parameter which qualitatively differs for $\boldsymbol{\alpha}$ oblate and $\boldsymbol{\alpha}$ prolate: for $\Delta\omega > 0$, the orientation is enhanced for states with $\tilde{J} < |M| + |K|$ and suppressed for states with $\tilde{J} \geq |M| + |K|$, while for $\Delta\omega < 0$ it tends to be suppressed by the radiative field for all states. This behavior follows readily from the form of the effective potential, eq. (4.28), as shown in Figure 4.7. For the prolate case

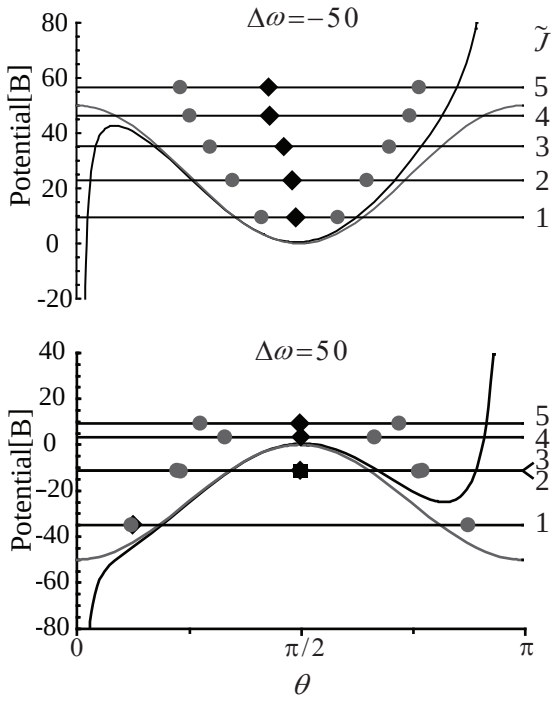

Figure 4.7: Effective potential, U, for $KM = 1$ and $K = 1$ along with the eigenenergies of states with $\tilde{J} = 1, 2, ..., 5$ (horizontal lines) and their alignment (diamonds) and orientation (circles) amplitudes $\theta_{L,0}$ and $\theta_{S,0}$. The grey line shows the induced-dipole potential, V_α. See eqs. (4.28), (4.23), (4.24) and text.

($\Delta\omega < 0$), the potential becomes increasingly centered at $\theta \to \pi/2$ with increasing field strength, and therefore tends to force the body-fixed electric dipole (and thus the figure axis) into a direction perpendicular to the field. On the other hand, for the oblate case ($\Delta\omega > 0$), the effective potential provides, respectively, a forward ($\theta \to 0$) and a backward ($\theta \to \pi$) well for the N^+ and N^- states of a tunneling doublet (for $\tilde{J} \geq |M| + |K|$) or of a degenerate doublet (for $\tilde{J} < |M| + |K|$). However, only for the degenerate-doublet states does the increasing field strength result in an enhanced orientation at $\varepsilon_S = 0$. This distinction is captured by the effective potential, Fig. 4.7, whose asymmetric forward (for $MK > 0$) or backward ($MK < 0$) well lures in the $\tilde{J} < |M| + |K|$ states. The $\tilde{J} \geq |M| + |K|$ states become significantly bound by the V_α oblate potential at $\Delta\omega$ values large enough to make them feel the double well, which makes the two opposite orientations nearly equiprobable.

Figure 4.8 shows the dependence of the J-state parity mixing on the $\Delta\omega$ parameter at $\omega = 0$ (panel (a)) and $\omega = 10$ (panel (b)). The mixing is captured by a parameter

$$\xi \equiv \sum_{J=2n+1} \left(a_{JM}^{\tilde{J}K\tilde{M}} \right)^2 \tag{4.33}$$

with n an integer. In the absence of even-odd J mixing, $\xi = 0$ for $\tilde{J}$ even and $\xi = 1$ for $\tilde{J}$ odd; for a "perfect" J -parity mixing, $\xi = \frac{1}{2}$ for either $\tilde{J}$ even or odd. We see that for the sampling of states shown, the non-precessing states become parity mixed only when $\omega > 0$. However, all precessing states are J-parity mixed as long as $\Delta\omega \neq 0$.

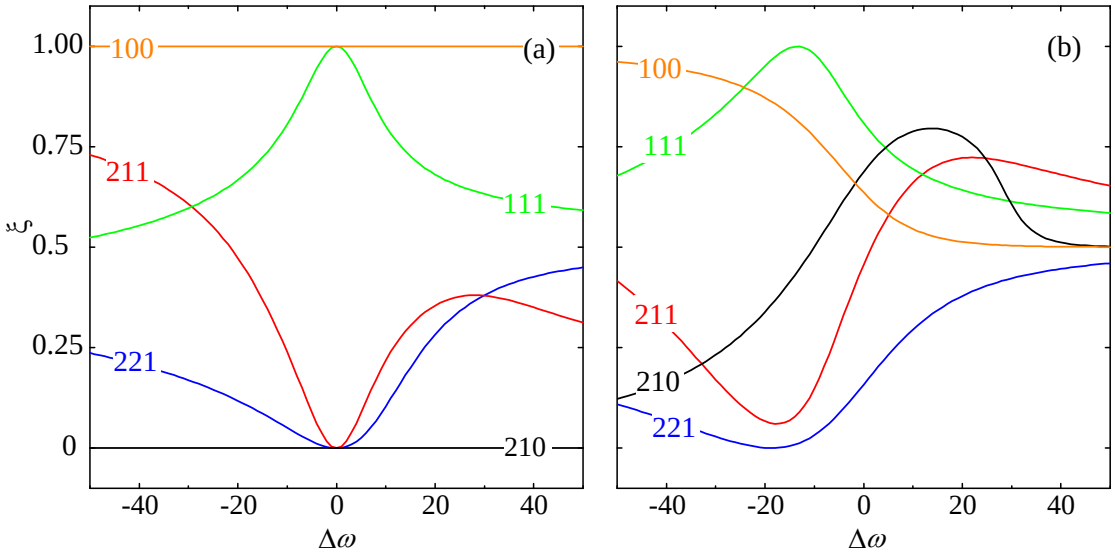

Figure 4.8: Dependence of the J-parity mixing parameter ξ on the $\Delta\omega$ parameter at $\omega = 0$ (panel (a)) and $\omega = 10$ (panel (b)). Note that the better the J-parity mixing the closer is the ξ parameter to $\frac{1}{2}$. See text.

The eigenenergies as well as eigenfunctions in the harmonic librator limit for both the prolate and oblate polarizability interactions have been found previously by Kim and Felker [54], and we made use of the former in constructing the correlation diagram in Fig. 4.4. We note that in the prolate case, the eigenenergies and alignment cosines, as calculated from Kim and Felker's eigenfunctions, agree with our numerical calculations for the states considered within 4% already at $\Delta\omega = -50$. The prolate harmonic librator eigenfunctions render, however, the orientation cosines as equal to zero, which they are generally not at any finite value of $\Delta\omega$.

For the $\boldsymbol{\alpha}$ oblate case, the eigenenergies in the harmonic librator limit agree with those obtained numerically for the states considered within 5% at $\Delta\omega = 50$. The orientation and alignment cosines can be obtained only for sufficiently strong fields otherwise the numerical integration fails. For $\Delta\omega \approx 350$ the alignment cosines for all states shown are available. The difference between the numerical results and the results obtained from the analytic eigenfunctions (even for those states for which the alignment cosine is available for smaller $\Delta\omega$) is less then 3%. We note that for $\tilde{J} < |M| + |K|$, only one eigenfunction exists, pertaining either to N^+ for $KM > 0$ or to N^- for $KM < 0$, cf. Table 4.3. This eigenfunction is strongly directional, lending a nearly perfect right-way orientation to an N^+ state and a nearly perfect wrong-way orientation to an N^- state. These eigenfunctions pertain to the degenerate doublets. The analytically and numerically calculated orientation cosines agree within 0.01% for $\Delta\omega = 100$. For $\tilde{J} \geq |M| + |K|$ (including the cases when either $K = 0$ or $M = 0$) both the N^+ and N^- analytic solutions exist, cf. Table 4.3, and pertain to

the tunneling doublets. The degeneracy of the doublets in the $\Delta\omega \to +\infty$ limit precludes using the analytic eigenfunctions in calculating the orientation cosines. In contrast to the numerical results, the analytic solution predicts a strong orientation, which in fact is not present, as shown in Fig. 4.7. The linear combination of the analytic eigenfunctions f^+ and f^- - which is also a solution - given as $f_{1,2} = 1/\sqrt{2}(f^+ \pm f^-)$, does not exhibit any orientation, just alignment.

The above behavior of symmetric-top molecules as a function of $\Delta\omega$ at $\omega = 0$ sets the stage for what happens once the static field is turned on and so $\omega > 0$. For $\Delta\omega > 0$, the combined electrostatic and radiative fields act *synergistically*, making *all states sharply oriented*. For $\Delta\omega < 0$, the orientation either remains nearly zero (for states with $KM = 0$) or tends to vanish (for states with $KM \neq 0$) with increasing $|\Delta\omega|$.

The synergistic action of the combined fields arises in two different ways, depending on whether $\tilde{J} < |M| + |K|$ or $\tilde{J} \geq |M| + |K|$.

For $\tilde{J} \geq |M| + |K|$, the orientation is due to a coupling of the members of the tunneling doublets (e.g., the $|2, 1, 1\rangle$ and $|3, 1, 1\rangle$ states) by the permanent dipole interaction. The tunneling doublets occur, and hence this mechanism is in place, for $\Delta\omega > 0$. The coupling of the tunneling-doublet members by the permanent dipole interaction is the more effective the smaller is the level splitting between the doublet members (which correlate with the N^+ and N^- in the harmonic librator limit). Since the levels of a tunneling doublet can be drawn arbitrarily close to one another by the induced dipole interaction, the coupling of its members by even a weak static field can be quite effective, resulting in a strong orientation of both states. The wrong-way orientation of the upper members of the tunneling doublets can be converted into a right-way orientation. Such a conversion takes place at sufficiently large ω where the permanent dipole interaction prevails over the induced dipole interaction. As noted in previous work [53], the coupling of the tunneling doublets by V_μ also arises for the non-precessing states, in which case one can speak of a *pseudo-first-order Stark effect* in the combined fields. The precessing states show in addition the well known first-order Stark effect in the electrostatic field alone, which relies on the coupling of states with the same $|K|$ and does not involve any hybridization of J.

As noted above, the $\tilde{J} < |M| + |K|$ states are strongly oriented by the induced-dipole interaction alone. Since the members of a degenerate doublet that correlate with the N^+ and N^- states (e.g., the $|1, 1, 1\rangle$ and $|1, 1, -1\rangle$ states) have *different* values of KM, adding an electrostatic field does not lead to their coupling, as collinear V_μ and V_α can only mix states with same KM. However, the static field skews the effective potential U, eq. (4.28), that enhances the orientation of the right-way oriented states (N^+) and, at sufficiently high ω, reverses the orientation of the initially wrong-way oriented states (N^-), see below.

The molecular-axis orientation by which the synergism of the static and radiative fields for $\boldsymbol{\alpha}$ oblate manifests itself can be best seen in Fig. 4.5f and interpreted with the help of the effective potential, Figures 4.9 and 4.10. Figs. 4.6d,e,f provide additional cuts through the same $(\omega, \Delta\omega)$ parameter space. Conspicuously, all states, for $\boldsymbol{\alpha}$ oblate, become right-way oriented at a sufficiently large ω, cf. Fig. 4.5f. However, some of the states either become (e.g., $|2,1,0\rangle$) or are (e.g., $|1,1,-1\rangle$) wrong-way oriented first. As ω increases, the $|2,1,-1\rangle$ state is even seen to become right-way oriented, then wrong-way oriented, and finally right way oriented again. This behavior is a consequence of the different types of coupling that the states in question are subjected to. We'll discuss them in turn.

The $|2,1,0\rangle$ state is the upper member of a tunneling doublet whose lower member is the $|1,1,0\rangle$ state, cf. Fig. 4.4. At $\omega = 0$, the $|1,1,0\rangle$ and $|2,1,0\rangle$ states are not oriented, as is the case for any states with $KM = 0$. However, the value of $\Delta\omega = 15$ is large enough to push the levels into a quasi-degeneracy, see Fig. 4.6a, in which case the static field can easily couple them. But at $\omega \ll \Delta\omega$, such a coupling results in localizing the wavefunctions of the $|1,1,0\rangle$ and $|2,1,0\rangle$ pair in the forward and backward wells, respectively, of the effective potential U, which, for $\omega \ll \Delta\omega$, are mainly due to the polarizability interaction. As ω becomes comparable to $\Delta\omega$, the effective potential becomes skewed. The forward well grows deeper at the expense of the backward well and the wrong-way oriented $|2,1,0\rangle$ state is flushed out into the forward well as a result, thus acquiring the right-way orientation. The blue effective potentials and wavefunctions in the middle panels of Figs. 4.9 and 4.10 detail this behavior. We note that the lower and upper member of a given tunneling doublet is always right- and wrong-way oriented, respectively, at $\omega \ll \Delta\omega$. This is because the coupling by V_μ makes the states to repel each other, whereby the upper level is pushed upward and the lower level downward. The noted orientation of the two states then immediately follows from the Hellmann-Feynman theorem.

The $|1,1,-1\rangle$ state has $\tilde{J} < |M| + |K|$ and thus, in the radiative field alone, is a member of a degenerate doublet, along with the $|1,1,1\rangle$ state, cf. the blue effective potentials and wavefunctions in the upper left and right panels of Fig. 4.9. While the $|1,1,1\rangle$ state is always right way oriented, the $|1,1,-1\rangle$ state is wrong-way oriented even at $\omega = 0$ thanks to the asymmetry of the effective potential due to its angle-dependent third term, proportional to KM, cf. eq. (4.28). An increase in ω removes the degeneracy of the doublet and causes the wrong-way oriented $|1,1,-1\rangle$ state to have a higher energy than the right-way oriented $|1,1,1\rangle$ state. As ω increases, V_μ deepens the forward well and, as a result, the wavefunction of the $|1,1,-1\rangle$ state rolls over into it, thus making the state right-way oriented.

The $|2,1,-1\rangle$ state exhibits an even more intricate behavior. Instead of a wrong-way orientation at low ω, enhanced by the radiative field, the state becomes right way oriented first,

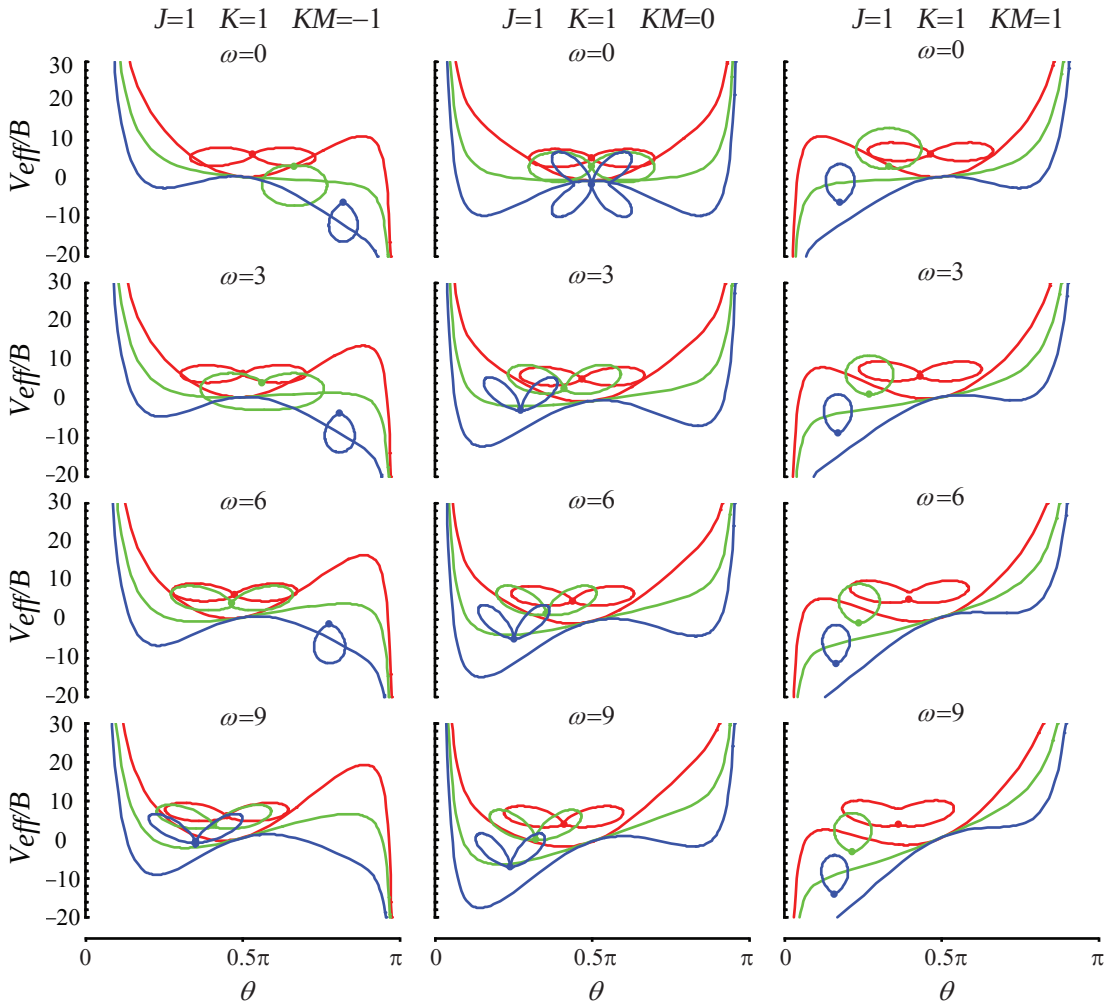

Figure 4.9: Effective potential, U, for $K = 1$ and $MK = -1$ (left panels), $MK = 0$ (center panels), and $MK = 1$ (right panels) along with the eigenenergies and orientation amplitudes (shown by dots) and squares of the wavefunctions for states with $\tilde{J} = 1$. The columns are comprised of panels pertaining to increasing values of ω. Red curves correspond to $\Delta\omega = -15$, green curves to $\Delta\omega = 0$, and blue curves to $\Delta\omega = 15$. See text.

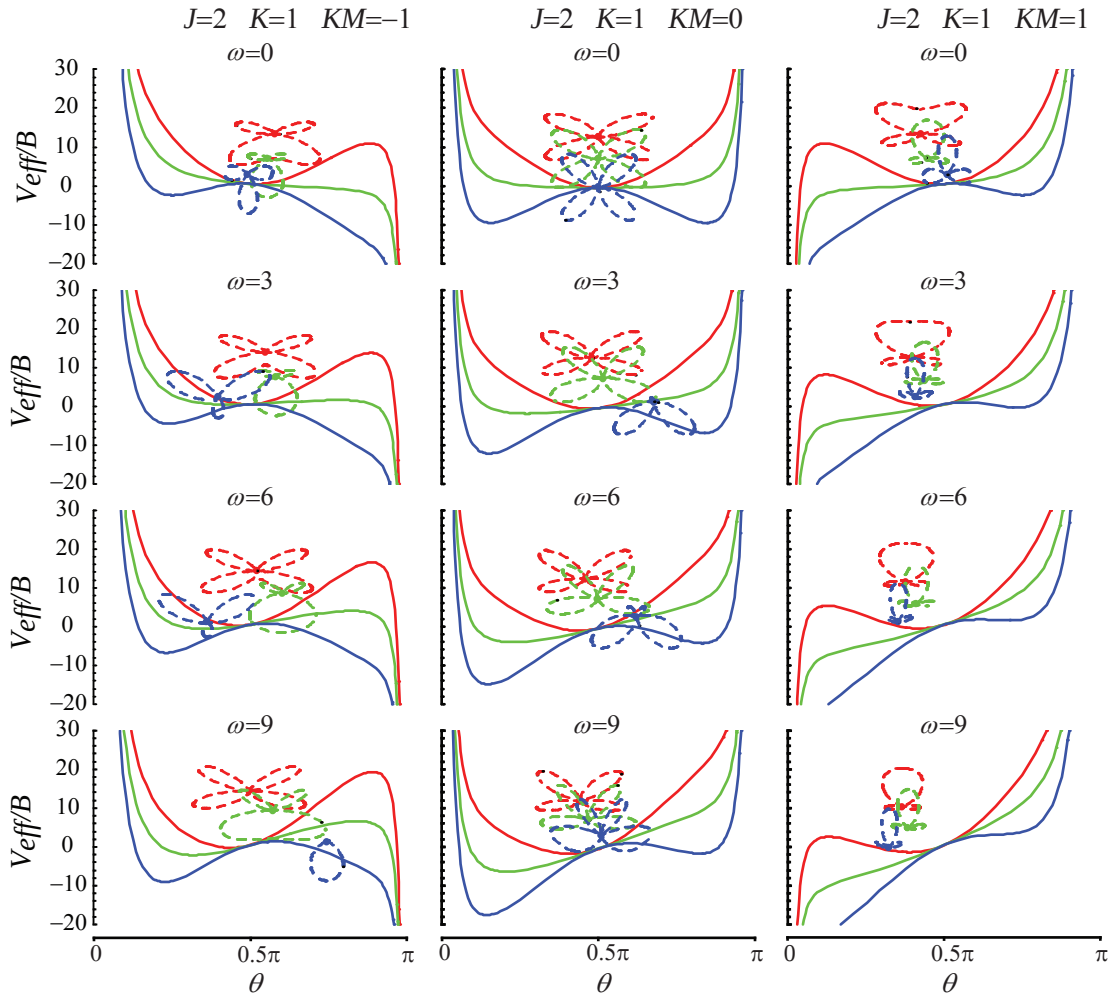

Figure 4.10: Effective potential, U, for $K = 1$ and $MK = -1$ (left panels), $MK = 0$ (center panels), and $MK = 1$ (right panels) along with the eigenenergies and orientation amplitudes (shown by dots) and squares of the wavefunctions for states with $\tilde{J} = 2$. The columns are comprised of panels pertaining to increasing values of ω. Red curves correspond to $\Delta\omega = -15$, green curves to $\Delta\omega = 0$, and blue curves to $\Delta\omega = 15$. See text.

due to an avoided crossing with the $|1,1,-1\rangle$ state (whose behavior, sketched above, is, of course, also affected by the same avoided crossing). This is followed, at increasing ω, by a "native" wrong-way orientation that, at $\omega \gtrsim 20$, is reversed by virtue of the deepening forward well of the effective potential, which confines the state.

We note that the tangle of level crossings seen in Figs. 4.5 and 4.6 that complicate the directional properties of symmetric tops in the combined fields is caused by the reversed ordering of the energy levels due to the permanent and induced dipole interactions: as the static and radiative fields are cranked up, the levels "comb" through one another.

4.3.3 Perpendicular fields

For a tilt angle $\beta \neq 0$ or π between the static, ε_S, and radiative, ε_L, fields, the combined-fields problem loses its cylindrical symmetry and M ceases to be a good quantum number. This greatly contributes to the complexity of the energy level structure and the directional properties of the states produced. At the same time, the M-dependent effective potential, eq. (4.28), so useful for understanding the directionality of the states produced by the collinear fields, cannot be applied to the case of perpendicular fields, as M is not defined.

Figures 4.11 and 4.12 show the dependence of the eigenenergies and of the orientation and alignment cosines on the field strength parameters ω and $\Delta\omega$ for a similar set of states as in Figs. 4.5 and 4.6 for the collinear fields.

Figs. 4.12c and d capture well the main patterns of the behavior. For $\boldsymbol{\alpha}$ prolate, the interaction with the radiative field ε_L aligns the body-fixed electric dipole $\boldsymbol{\mu}$ along the perpendicular static field ε_S, cf. Fig. 4.2. For $\boldsymbol{\alpha}$ oblate, ε_L aligns $\boldsymbol{\mu}$ perpendicular to ε_S. As a result, in perpendicular fields, $\boldsymbol{\alpha}$ prolate yields a strong orientation whereas $\boldsymbol{\alpha}$ oblate a vanishing one. This is the inverse of the situation in collinear fields. However, since V_α prolate is a single-well potential, the levels lack the patterns found for collinear fields for V_α oblate. Due to the multitude of avoided crossings, the states often switch between the right and wrong-way orientation, even over tiny ranges of the interaction parameters. Therefore, a much finer control of the parameters is needed in the case of perpendicular fields in order to preordain a certain orientation. For $\boldsymbol{\alpha}$ oblate, the coupling of the different states is weak, and the avoided crossings that abound in the parallel case, Fig. 4.6, are almost absent, Fig. 4.12.

The states are essentially all high-field seeking in the radiative field for $\Delta\omega > 0$ and low-field seeking for $\Delta\omega < 0$. This reflects the repulsive and attractive character of the polarizability interaction in the prolate and oblate case, respectively. In the oblate case, the states shown are essentially high-field seeking in the static field. This means that for $\Delta\omega > 0$,

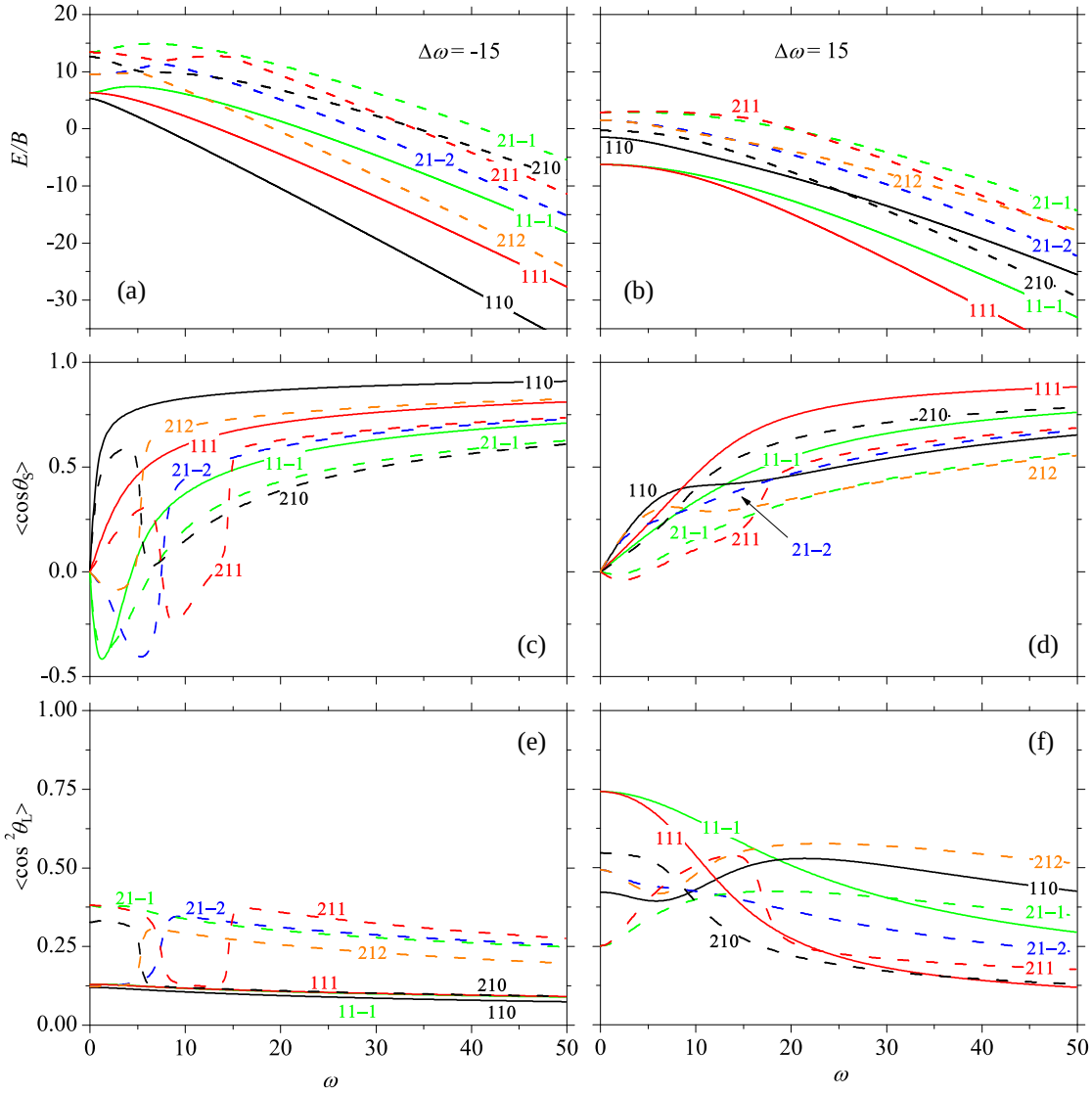

Figure 4.11: Dependence, in perpendicular fields, of the eigenenergies, panels (a)-(b), orientation cosines, panels(c)-(d), and alignment cosines, panels (e)-(f), of the states with $0 < \tilde{J} \leq 3$, $-1 \leq MK \leq 1$, and $K = 1$ on the dimensionless parameter ω (that characterizes the permanent dipole interaction with the electrostatic field) for fixed values of the parameter $\Delta\omega$ (that characterizes the induced-dipole interaction with the radiative field; $\Delta\omega < 0$ for prolate polarizability anisotropy, $\Delta\omega > 0$ for oblate polarizability anisotropy). The states are labeled by $|\tilde{J}KM\rangle$. The orientation cosines $\langle\cos\theta_S\rangle$ are calculated with respect to the electrostatic field and the alignment cosines $\langle\cos^2\theta_L\rangle$ with respect to the laser field. See text.

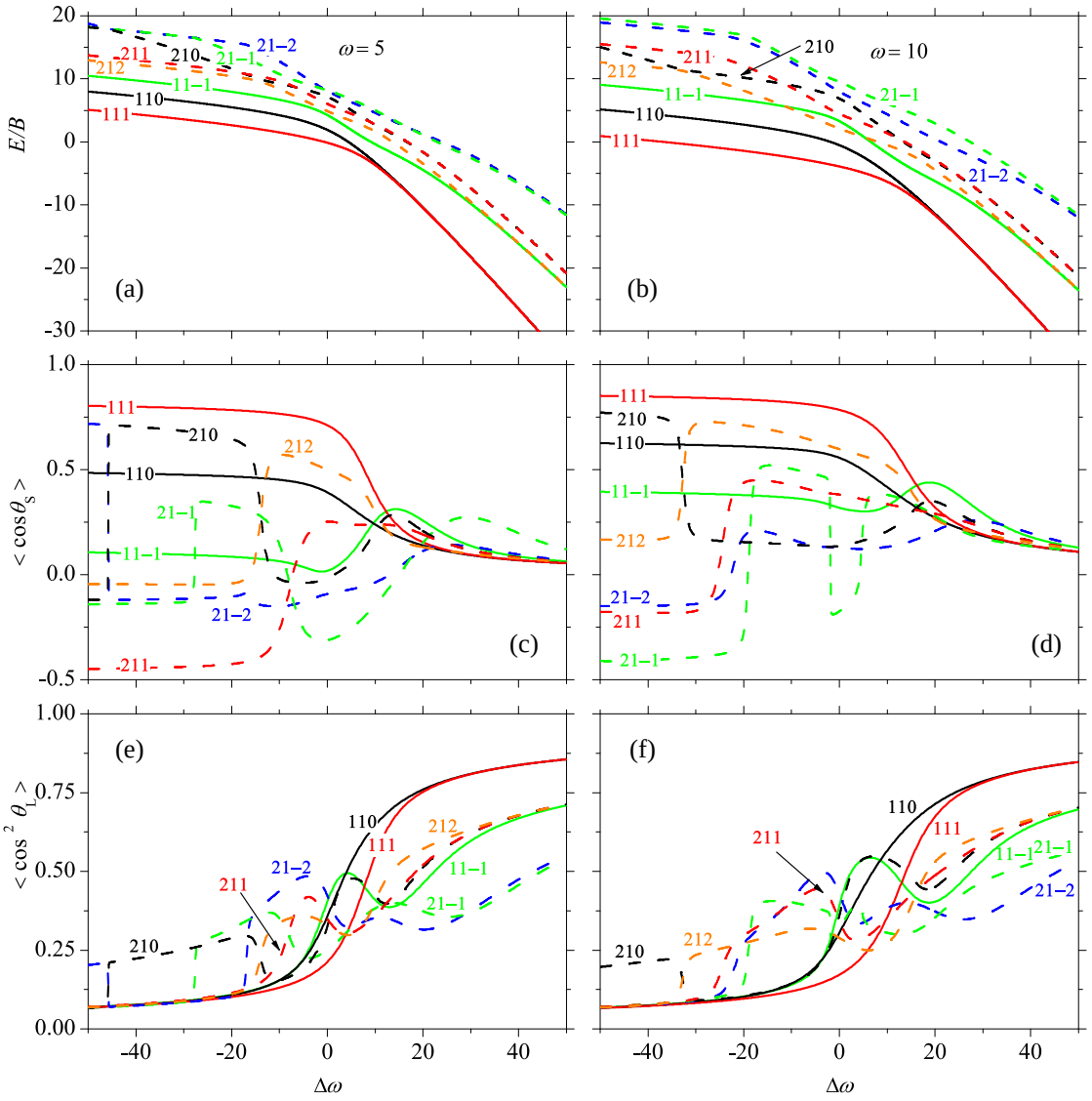

Figure 4.12: Dependence, in perpendicular fields, of the eigenenergies, panels (a)-(b), orientation cosines, panels(c)-(d), and alignment cosines, panels (e)-(f), of the states with $0 < \tilde{J} \leq 3$, $-1 \leq MK \leq 1$, and $K = 1$ on the dimensionless parameter $\Delta\omega$ (that characterizes the induced-dipole interaction with the radiative field; $\Delta\omega < 0$ for prolate polarizability anisotropy, $\Delta\omega > 0$ for oblate polarizability anisotropy) for fixed values of the parameter ω (that characterizes the permanent-dipole interaction with the electrostatic field). The states are labeled by $|\tilde{J}KM\rangle$. The orientation cosines $\langle\cos\theta_S\rangle$ are calculated with respect to the electrostatic field and the alignment cosines $\langle\cos^2\theta_L\rangle$ with respect to the laser field. See text.

much of the wrong-way orientation seen, e.g., in Fig. 4.5d,f, can be eliminated, see Fig. 4.11d. Unfortunately, the elimination of the wrong-way orientation happens at the expense of the magnitude of the orientation, which remains small.

Depending on the relative strength of the two fields, the effects of one can dominate those of the other. This contrasts with the behavior in the collinear fields where even a tiny admixture of the static field can dramatically change the behavior of the states due to the radiative field (such as the coupling of the tunneling doublets).

A detailed comparison of the effect the two fields have on a given state is complicated by the dependence of the state label on the sequence in which the parameters ω, $\Delta\omega$ and β are varied. This behavior is further analyzed in the next section. Here we give a sampling of the effects of the fields on certain states.

As the dependence of the orientation cosine on the ω parameter indicates, see Fig. 4.11c, the largest orientation for a prolate polarizability is attained for the $|1,1,0\rangle$ state. Other states, such as the $|1,1,-1\rangle$ state, become right-way oriented only for sufficiently large field strengths. At ω large, the orientation of all states becomes substantially greater than what is achievable with collinear fields, cf. Fig. 4.5e. But for the oblate polarizability, the states behave similarly and no state is found to exhibit a unique behavior.

On the other hand, in dependence on $\Delta\omega$, Fig. 4.12, the $|1,1,1\rangle$ state - instead of the $|1,1,0\rangle$ state - shows the strongest right-way orientation over most of the range presented. This is an example of the sequence dependence of the state label. The $|2,1,-1\rangle$ state exhibits the most dramatic changes. It has three rather sharp turn-around points, where the direction of the dipole moment changes. Another example of the sequence dependance of the label is the $|2,1,1\rangle$ state in Fig. 4.11c which is wrong-way oriented at $\omega \approx 10$. In Figure 4.12d, not even one of the states shown is wrong-way oriented for $\Delta\omega \approx -20$ to 0.

When $\Delta\omega \gg \omega$ quasi-degenerate states are formed, similar to the tunneling doublets. However, the electrostatic field is not able to couple them as a result of which the states are only aligned.

4.3.4 'Label switching'

Generally, the label of a given state in the tilted fields depends on the sequence in which the fields are switched on and the tilt angle spanned by them is varied. Figure 4.13 shows the evolution of the states with $\tilde{J} = 1$, $K = 1$ and $\tilde{M} = -1, 0, 1$ for three different sequences leading to a crossing points in figures 4.11 and 4.12 at $\omega = 10$, $\Delta\omega = -15$ and $\beta = \pi/2$. The three sequences are:

1. Parameter ω is turned to a value of 10; then the laser field is switched on to a value of $\Delta\omega = -5 \cdot 10^{-5}$; then the tilting of the fields is carried out to $\beta = \pi/2$; finally $\Delta\omega$ is raised in steps of $5 \cdot 10^{-5}$ up to -15. The states are labeled as $\left|\tilde{J}, K, \tilde{M}; \omega, \beta, \Delta\omega\right\rangle$.

2. Parameter $\Delta\omega$ is turned up to a value of -15; $\omega = 5 \cdot 10^{-5}$; the fields are tilted to $\beta = \pi/2$; ω is raised (in steps of $5 \cdot 10^{-5}$) to the value of 10. The states are labeled as $\left|\tilde{J}, K, \tilde{M}; \Delta\omega, \beta, \omega\right\rangle$.

3. Parameter $\Delta\omega$ is turned up to -15 and ω up to 10; then the fields are tilted to $\beta = \pi/2$. The states are labeled as $\left|\tilde{J}, K, \tilde{M}; \Delta\omega, \omega, \beta\right\rangle$, but the results obtained are identical to $\left|\tilde{J}, K, \tilde{M}; \omega, \Delta\omega, \beta\right\rangle$.

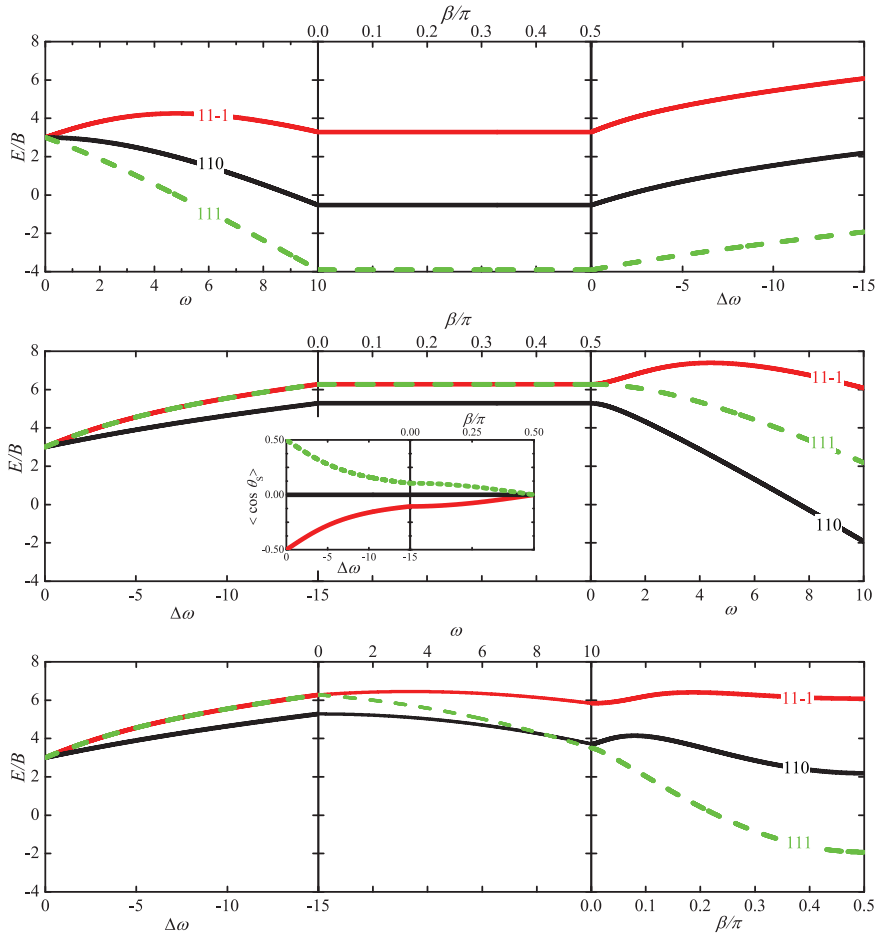

Figure 4.13: Comparison of the evolution of states for different path through the parameter space. From top to bottom these are: $\left|\tilde{J}K\tilde{M}; \omega, \beta, \Delta\omega\right\rangle$, $\left|\tilde{J}K\tilde{M}; \Delta\omega, \beta, \omega\right\rangle$ and $\left|\tilde{J}K\tilde{M}; \Delta\omega, \omega, \beta\right\rangle$. In the middle panel the $|\tilde{1}1\tilde{0}\rangle$ state is interchanged with the $|\tilde{1}1\tilde{-1}\rangle$ state in the other two panels. We dub this effect 'label switching.'

As one can see, there are no discontinuities for any of the calculations that might suggest that we lost track of a given state. However, when we compare the three calculations, we end up with different labels adiabatic for the same state at the crossing point. The $|\tilde{1}, 1, \tilde{0}\rangle$ and the $|\tilde{1}, 1, \tilde{-1}\rangle$ change their labels for sequence 2 compared to 1 and 3. For sequence 1 and 2, no genuine crossings are seen. Therefore, it is impossible that the tracking procedure jumped an avoided crossing. In the left panel, when only a single field is considered, each of the states shown is treated in a different calculation. The same is the case for the middle panel of the third sequence, because the fields are still parallel and M is a good quantum number. Each of the states belongs to a different block of the Hamiltonian matrix. In all other panels, the whole matrix is considered. In the middle panel of sequence 2, the two $M = \pm 1$ states look degenerate, but they are not. Due to the very weak electric field, which is necessary to give a meaning to the field tilting, a small splitting is present. The wavefunctions and thus the orientation (see inset in Fig. 4.13) is different for these two states.

To our knowledge this phenomenon, which we dub *label switching*, has not been described before. Label switching occurs not only between states with the same $\tilde{J}$ and different $\tilde{M}$ but also between different $\tilde{J}$'s. We think two different mechanism are responsible for label switching:

- symmetry breaking
- chaotic behavior of the underlying classical system and the concomitant singularities of the the classical phase space

The first mechanism is a very simple one, which 'always' occurs when one analyzes representations of systems with different symmetries in the parameter space.

Consider a system which depends on two different parameters, a and b. For $b = 0$, let the system be symmetric, but for $b \neq 0$ let *every* symmetry be broken. Notice that in our case ω and β play the respective roles of a and b for fixed $\Delta\omega$. Consider now two states whose energies are, for $a = 0 = b$, $E_1 < E_2$. If a is changed and $b = 0$, both states belong to a different representation of their symmetry group, which means they belong to different blocks. These states can cross. After the crossing, E_1 becomes larger then E_2. If now b is changed, the states belong to the same block and cannot cross anymore. E_1 remains always larger than E_2. For the reverse sequence of switching of the fields, the initial order of energies, $E_1 < E_2$, remains in place since all crossings are avoided [76].

This simple picture considers avoided crossings only when the symmetry is broken. But in our case, there seems to be a hidden symmetry left, which prevents the system to possess solely avoided crossings. For sufficiently high densities (small step sizes) of points in the parameter space, one would expect to make the avoided crossings visible. Instead, many

of the crossings tested have been found to be genuine. The genuine crossings come about as a consequence of the complexity of the Hamiltonian matrix. In the case of collinear fields, only the two off-diagonals are nonzero and the diagonal entries increase from left to right. Therefore there is an off-diagonal matrix element between neighboring states. For an arbitrary field configuration, the matrices are much larger and the entries on the diagonal are no longer sorted by increasing energy. Two states can be very close in energy, but do not necessarily share an off-diagonal element. Therefore, they do not interact and thus may cross. A more suitable basis set would reproduce such a 'hidden symmetry'. An example for a better choice of basis set for the perpendicular fields would be a linear combination of the symmetric top functions $|JKMs\rangle = 1/\sqrt{2}\,[|JKM\rangle + (-1)^s\,|JK-M\rangle]$ with $s = 0, 1$, similar to the symmetrized basis set for asymmetric top molecules. This is the case since $+M$ and $-M$ states are equally involved in the hybrids. But this new basis set would cause problems for the parallel case. From this consideration we infer that 'label switching' is due not just to symmetry breaking.

Another problem arises when one considers closed paths in parameter space, such as those in Figure 4.14. We reduce the 3D parameter space (ω, $\Delta\omega$, β) to two dimensions, i.e. we vary only two of the three parameters, keeping the third fixed. For an arbitrary starting point, we sort all energies in ascending order. Then we follow the evolution of the states along a closed path. When we reach the end point, we compare the energies with their starting values. As long as only $\Delta\omega$ and β are varied, the energies at the beginning and at the end agree with each other for all cases that we tested. But for all other combinations, there are states which do not fall on themselves. The most disagreements are found for the ω-β curves, which are also present in the ω-$\Delta\omega$ plots. For a fixed value of $\beta \neq 0$, the symmetry does not change and one would not expect such a behavior. This leads us to the conclusion that not only the tilting process and therefore the symmetry breaking is responsible for the label switching. The presence of the electric field seems to be playing a major role.

Over recent years, the simultaneous use of classical and quantum mechanics in analyzing qualitative features of quantum systems found a wide application, e.g., in the describtion of rotation or vibration of molecules, e.g. [77], or atoms in fields [78]. The concurrent analysis of a problem by classical, semi-classical and quantum mechanics enable a further insight into the quantum mechanical system.

One of the systems considered was the classical analog of a rigid rotor. Diatomic (linear) molecules have been investigated by Arango *et al.* in electrostatic and tilted pulsed non-resonant laser fields both classically and quantum mechanically [79, 80]. These authors found that the quantum lattice (see below) is perturbed at an energy range where classical chaos sets in. In the tilted fields j and m, the analogs of the quantum numbers J and M, are no longer conserved and the system is nonintegrable. Therefore it can exhibit chaos

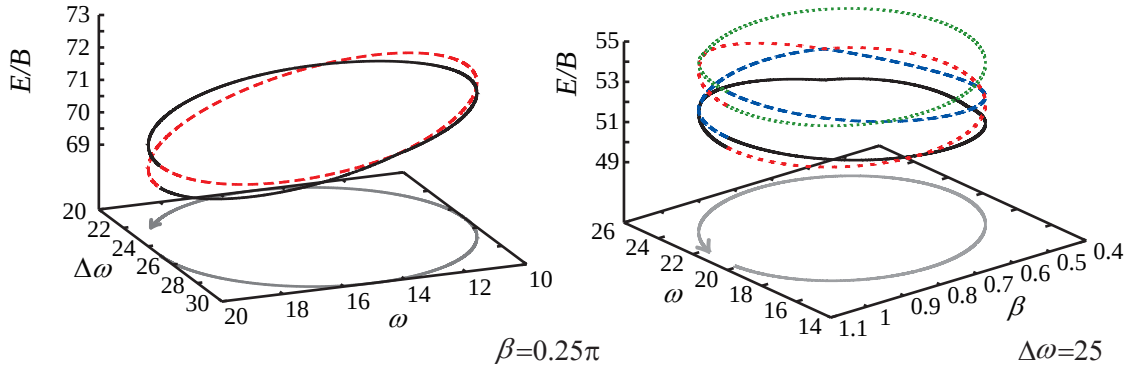

Figure 4.14: Two closed curves in the parameter space. After one revolution the labels for the states differ. These curves have been calculated with 100000, 500000 and 1000000 points, with the same results. In the left panel only, the tilt angle and therefore the symmetry is changed.

and shows a "downright botanical" complexity [80]. But already in the single electric field, where the system is integrable, it shows a 'strange' behavior.

Compared to a linear $^1\Sigma$ molecule, the symmetric top introduces an additional integral of motion, as encapsulated in the quantum number K. But qualitative results of the 'simpler' case can be used to interpret the 'more complex' system.

The linear rotor in the combined tilted fields has also been checked for the effect of 'label switching,' by considering closed curves in parameter space and it *does* indeed exhibit label switching. But due to the slightly different kind of interaction with the radiative field, namely $\Delta J = 0, 2$, not all calculations can be done for this case. In the single radiative field it would be necessary to separate the blocks further to lift the degeneracy in the blocks and obtain the 'real' eigenvectors. Therefore we consider only the symmetric top case.

Arango *et al.* [79] and Kozin and Roberts [81] have shown that the diatomic and the symmetric top in the single electric field exhibit classical and quantum *monodromy* [82]. Monodromy is not yet well understood in physics and its consequences are unknown, see e.g. [83]. It was introduced into physics by Duistermaat in 1980 for the classical spherical pendulum [84] and later for its quantum analog [85].

The diatomic in an electric field is a realization of the spherical pendulum, while the symmetric top is a Lagrange top, which shows a somewhat different kind of monodromy. Monodromy in classical integrable systems is a obstruction to the existence of global action-angle variables (i.e. constants of motion). Their lack is a necessary condition for chaos.

In quantum mechanics, monodromy reveals itself as a defect in the discrete lattice of states. Following reference [85], one plots the energies of the states as a function of one of the quantum numbers and obtains a discrete grid of points, each belonging to a certain state. Between adjacent grid points one can define a cell. This cell is transported within the grid by moving each corner in the same direction to the next point of the lattice. The system is said to exhibit monodromy if on a closed path around a critical point the cell changes its shape.

Parallel transport of a lattice cell is shown in Fig. 4.15 for the symmetric top in an electric field. The perturbation in such a system is a critical point, as shown in ref. [81], which also provides a detailed explanation in terms of a comparison with classical mechanics. Such a comparison is useful for explaining the forbidden regions and the perturbations of the lattice, since the quantum lattice is an analog of the energy-momentum diagram in classical mechanics.

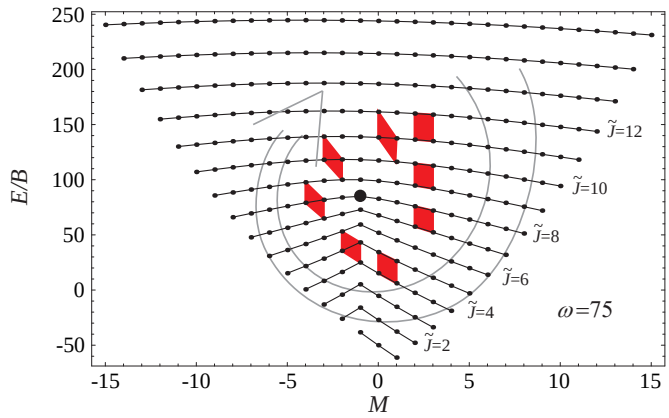

Figure 4.15: Monodromy diagram for a symmetric top molecule with $K = 1$ in an electric field. A cell is marked by two red arrows. After a parallel transport around the perturbation of the lattice, indicated by the thick point, the cell has a different shape, which indicates the presence of monodromy in the system.

The lines of constant $\tilde{J}$ show a characteristic kink and are not smooth at low energies. Such $\tilde{J}$'s cannot serve as global quantum numbers because they should be defined smoothly.

A comparison with classical calculations reveals that the perturbation of the lattice occurs at the same energy as a point of classical relative equilibrium, for which the motion becomes a steady one. It is at the equilibrium where the dipole is oriented oppositely to the electric field. Changing the field strength results in a shift of the relative equilibrium in the lattice and the system undergoes different types of bifurcations, see [81].

The diatomic does not show monodromy in a radiative field. The monodromy diagram looks like the one for an oblate polarizability of a symmetric top, see Figure 4.16b. It nicely reveals the formation of tunneling doublets, but parallel transport does not alter a cell. However, for a prolate polarizability, the system exhibits monodromy, see Figure 4.16a. In the combined fields, the different quantum lattices overlap and both kinds of system exhibit monodromy, see Fig. 4.17.

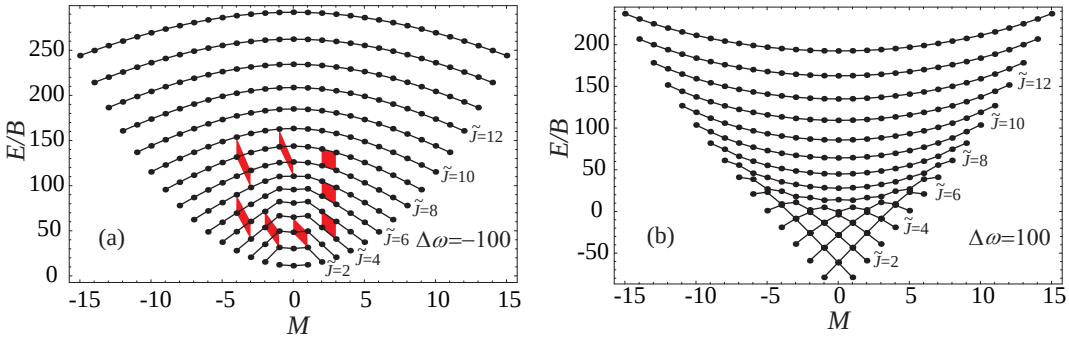

Figure 4.16: Monodromy diagram for $K = 1$ symmetric rotor states in a radiative field for the two types of polarizabilty anisotropy. Only the prolate case exhibits monodromy. See text.

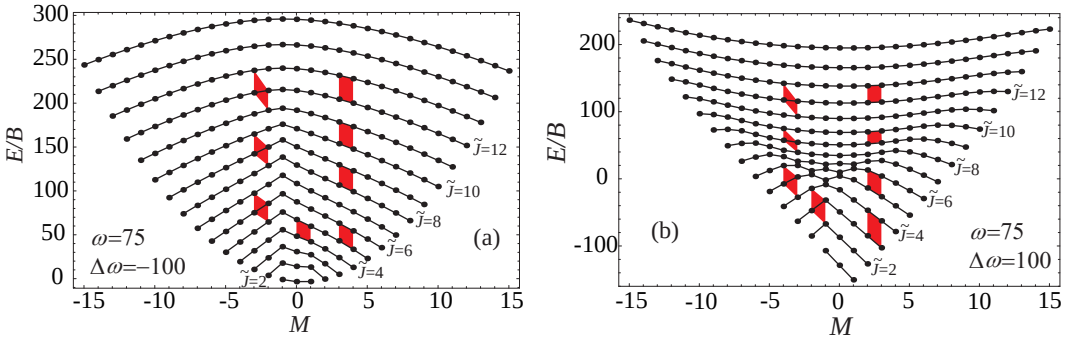

Figure 4.17: Monodromy diagrams for $K = 1$ symmetric rotor states in the combined collinear fields for both kinds of the polarizability anisotropy. Both diagrams exhibit the same type of monodromy.

For tilted fields, M ceases to be a good quantum number and a constant of motion for the classical diatomic and symmetric top. The system becomes nonintegrable. For tilt angles $\beta \sim \pi/4$, the diatomic exhibits extensive classical chaos [79]. Primary periodic orbits which undergo extensive bifurcations serve to organize the global phase space structure. The investigation of nearest-neighbor distributions for the quantum mechanical system gives some hints as to that this system is chaotic. These calculations have been performed for diatomics [79] as well as for symmetric-tops [86, 87].

In the case of tilted fields, the construction of quantum lattices is precluded since M is no longer a good quantum number. It is not clear which projections could be used for the monodromy diagram. K is the only remaining good quantum number, and therefore one would choose it, but it would be necessary to fix M. The equal weight of the $+M$ and $-M$ states in perpendicular fields shows a way out. As already implemented for diatomics [79], the root-mean-square expectation value of M, $\langle M^2 \rangle^{1/2}$, could be used to construct a quantum lattice. For the perpendicular case, the expectation value, $\langle M \rangle$, of M is zero, but $\langle M^2 \rangle^{1/2}$ is nonzero and can be employed in the whole range of tilt angles. Such lattices can be compared with classical results, since the $\langle m^2 \rangle^{1/2}$ is defined in classical calculations, see [79].

The analysis of the quasi-monodromy diagrams is complicated by the dependence on the representation chosen. If the laser field is tilted with respect to the electrostatic field, $\langle M^2 \rangle^{1/2}$ changes (not the energy!). Only $\langle M \rangle$ is well-defined independently of the representation. This must be considered in a concurrent classical calculations.

Figure 4.18 shows quasi-monodromy diagrams for several ratios of the two field strength. Panel (a) reveals for large $\langle M^2 \rangle^{1/2}$ the structure of the unperturbed symmetric top. But the field strengths considered are already sufficient to change the structure for low $\langle M^2 \rangle^{1/2}$ values. The diagrams change dramatically by changing the ratio of the two field strengths. For $|\Delta\omega| > \omega$, varying the intensity of the radiative field preserves the structure, see panels (b),(d) and (c),(e). A classical parallel transport is not possible, but panel (d) seems to consist of two regions with a rather sharp border between them. One region is above $\langle M^2 \rangle^{1/2} > 7$ with small holes in it, the other is formed by low energies and low $\langle M^2 \rangle^{1/2}$ values. By connecting the neighboring $\langle M^2 \rangle^{1/2}$ values, one obtains lines which look concave or convex - possibly a hint for an alteration of the cell. The dense distribution of the states around the border makes a parallel transport difficult if not impossible. For the oblate polarizability, the two regions in panel (e) are separated by a wider boarder. Also the regions with the same type of cell are much more perturbed. If the electric field exceeds the radiative field strength, the structure completely changes. The structure differs markedly for the two types of polarizability anisotropy, even though the electrostatic field alone is supposed to determine the behavior.

Since there are so many changes in the structure of the quasi-monodromy diagrams, it is not feasible to use quantum mechanical calculations in order to obtain further insight into the behavior of the system. The complexity of the structure leads us to the conclusion that the system exhibits monodromy for some paths and not for others. It may be revealing to consider the corresponding classical system, since monodromy is related to singularities of the underlying classical phase space.

In summary, we found that label switching always occurs in tilted fields. Monodromy, however, is present for both collinear and tilted fields. In the collinear case, monodromy

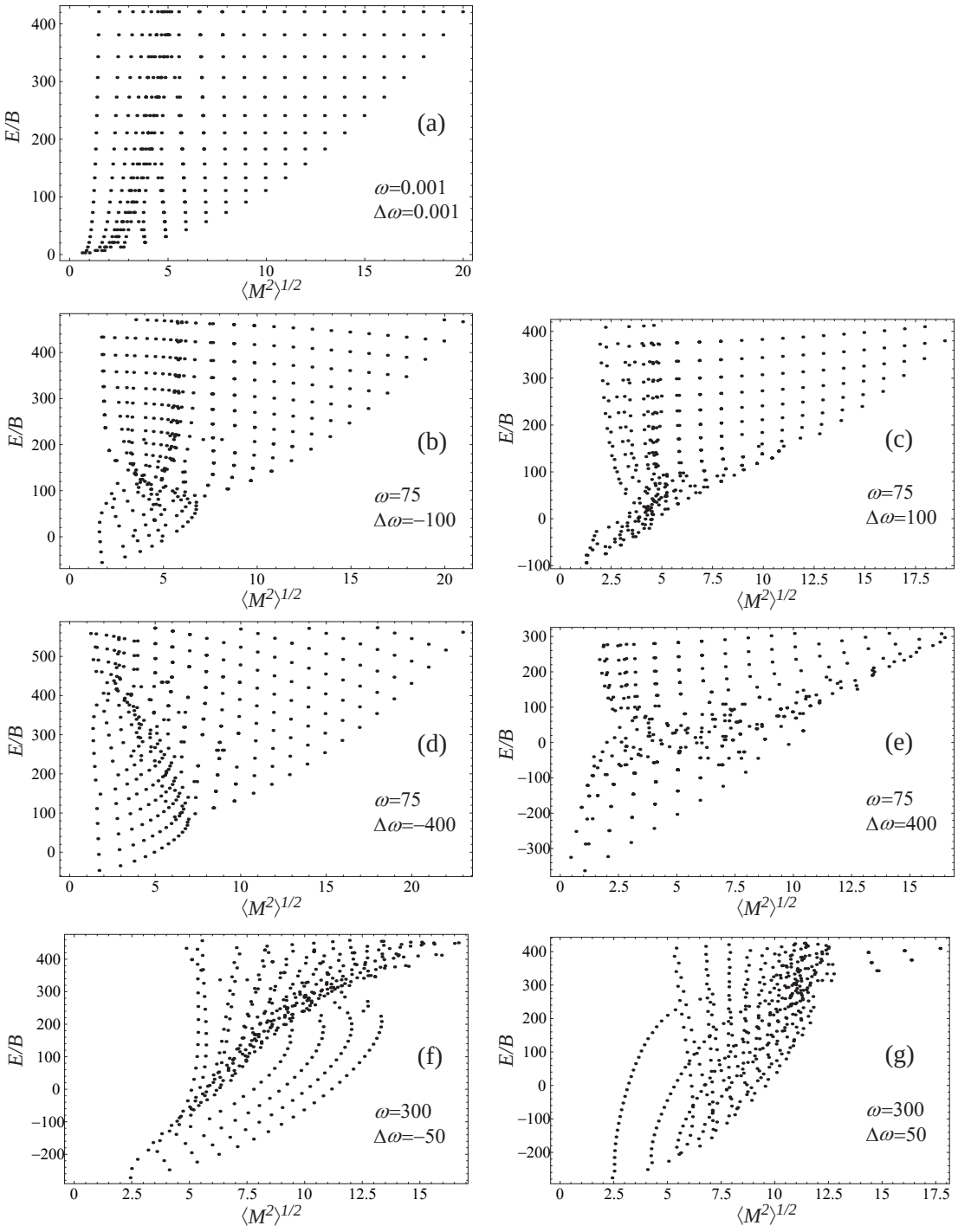

Figure 4.18: Energy vs. $\langle M^2 \rangle^{1/2}$ diagrams for $K = 1$ symmetric rotor states in perpendicular fields for several ratios of $\omega/\Delta\omega$. The structure changes dramatically for the different figures which might be a hint for the change of the type of monodromy. See text.

manifests itself as a focus-focus singularity (i.e., a point perturbation of the lattice); this singularity moves around the lattice as a function of field strength. For the perpendicular case, the quasi-monodromy diagrams suggest that a different type of singularity is present, but our calculations have not revealed which type it is. The general reason for label switching remains obscure. Our calculations suggest that label switching arises in connection with the change of the character of a crossing, from avoided to genuine or vice versa. A possible role of Berry's phase [88] has not been invoked. Whether label switching could be experimentally observed and utilized is not clear at this point. Although we believe that it is not an artefact of the calculations, we cannot exclude this possibility with absolute certainty.

4.4 Examples and applications

Table 4.4 lists a swatch of molecules that fall under the various symmetry combinations of the $\boldsymbol{\alpha}$ and $\mathbf{I}$ tensors, as defined in Table 4.1. The table lists the rotational constants, dipole moments, polarizability anisotropies as well as the values of the interaction parameters ω and $\Delta\omega$ attained, respectively, at a static field strength of 1 kV/cm and a laser intensity of 10^{12} W/cm^2. The conversion factors are also included in the table. While the field strength of the electrostatic field of a kV/cm is easy to obtain (or sometimes even difficult to avoid), a laser intensity of a petawatt per cm^2 is somewhat harder to come by. However, pulsed laser radiation can be easily focused to attain such an intensity, and a nanosecond pulse duration is generally sufficient to ensure adiabaticity of the hybridization process.

We note that the directional properties displayed in Figs. 4.5-4.12 should be attainable for most of the molecules listed in Table 4.4.

The amplification of molecular orientation in the combined fields may find a number of new applications.

In molecule optics [91], a combination of a pulsed nonresonant radiative field with an inhomogeneous electrostatic field can be expected to give rise to temporally controlled, state-specific deflections. In an inhomogeneous static field produced by an electrode microarray [92], and a ns laser pulse of 10^{12} W/cm^2, deflections on the order of a mrad appear feasible for light molecules. Since the synergistic effect of the combined static and radiative fields is only in place when both fields are on, the deflection of the molecules would be triggered by the presence of the ns laser pulse. The sensitivity of the deflection process to the magnitude of the space-fixed electric dipole moment and its direction (right- or wrong-way) would simultaneously enable state-selection.

Molecule	B [MHz]	μ [D]	$\Delta\alpha$ [Å^3]	ω @1 kV/cm	$\Delta\omega$ @10^{12} W/cm^2
Acetonitrile	9199	3.92	1.89	0.22	65.0
Ammonia	298500	1.47	0.24	0.0025	0.24
Benzene-Ar	1113	(0.1)	−6.1	(0.05)	−1735
Bromomethane	9568	1.82	1.95	0.10	64.5
Chloromethane	13293	1.89	1.69	0.07	40.2
Fluoromethane	10349	1.85	0.84	0.09	25.7
Iodomethane	7501	1.64	2.15	0.11	90.7
Trichlormethane	3302	1.04	−2.68	0.16	−257
Trifluoromethane	7501	1.65	−0.18	0.11	−7.60

Table 4.4: Values of parameters ω and $\Delta\omega$ for choice symmetric top molecules whose properties were taken from [89, 90]. The conversion factors are: $\omega = 503.2\ \mu\ [D]\ \varepsilon_S$ [kV/cm]$/B$ [MHz] and $\Delta\omega = 3.1658 \times 10^{-7}\ I$ [W/cm^2] $\Delta\alpha$ [Å^3]$/B$ [MHz]. Numbers in parentheses are order-of-magnitude estimates.

The directional properties of symmetric tops in the combined fields may come handy in the studies of rare-gas molecules of the type found by Buck and Farnik. Some of the species identified by these authors may in fact possess a three-fold or higher axis of rotation symmetry [93].

Drawing on the analogy with previous work on spectral effects in single electrostatic [12, 15, 94] or radiative fields [18], we also note that the combined fields can be expected to dramatically modify the spectra of symmetric top molecules: this is due to a change of both energy levels and the transition dipoles. The latter are dramatically affected by the directionality of the wavefunctions, which give rise to widely varying overlaps. However, detailed simulations of such effects in the combined fields still need to be carried out.

Last but not least, molecules in tilted electrostatic and radiative fields can serve as prototypical systems for the study of quantum chaos. The absence of good quantum numbers and the multitude of unstable equilibria suggest this possibility. Indeed, as pointed out in the work of the Ezra group [79, 80], linear molecules in non-collinear fields exhibit chaotic dynamics. We hope that our present study of symmetric tops in the combined fields will provide an impetus for further work on quantum chaos and monodromy exhibited by such nonintegrable molecular systems.

5 Summary

In our theoretical study of the directional properties of symmetric top molecules in combined electrostatic and nonresonant radiative fields, we saw that collinear (perpendicular) fields force permanent dipoles of molecules with oblate (prolate) polarizability anisotropy into alignment with the static field. We found that the amplification mechanism that produces highly oriented states for linear molecules ($K = 0$) is also in place for precessing states of symmetric tops with $\tilde{J} \geq |K|+|M|$. This mechanism is based on the coupling by a collinear electrostatic field of the tunneling doublet states created by the interaction of the oblate polarizability with a linearly polarized radiative field. The efficacy of this coupling is enhanced by an increased strength, $\Delta\omega > 0$, of the anisotropic polarizability interaction that traps the tunneling doublets it creates deeper in a double-well potential, and draws the members of the doublets closer to one another. Apart from this synergistic effect of the combined fields, there is another effect in place, but for states with $\tilde{J} < |K| + |M|$. Such states occur as exactly degenerate doublets in the radiative field alone, whose both members are strongly but mutually oppositely oriented along the polarization plane of the field. This orientation can be manipulated by adding an electrostatic field, which easily couples the right-way oriented states to its direction, whether this is parallel or perpendicular to the radiative field. At a sufficiently large strength, ω, of the permanent dipole interaction, the wrong-way oriented member of the (no longer) degenerate doublet becomes also right-way oriented. The above patterns of the energy levels are complicated by numerous avoided crossings, themselves unavoidable, due to the opposite ordering of the energy levels for the permanent and induced dipole interaction.

The absence of cylindrical symmetry for perpendicular fields is found to preclude the wrong-way orientation for the oblate polarizability, causing all states to become high-field seeking with respect to the static field. The changes of the system's parameters ω, $\Delta\omega$, and β cause genuine crossings to become avoided and vice versa. This, in turn, causes the eigenstates to follow different adiabatic paths through the parameter space and to end up with adiabatic labels that depend on the paths taken.

The amplification of molecular orientation by the synergistic action of the combined fields may prove useful in molecule optics and in spectroscopy. Monodromy and quantum chaos lurk behind the combined fields effects whose further analysis may thus be expected to shed new light on both.

Appendices

A Symmetric-top wave functions

To solve the prolate symmetric top Schödinger equation, see eq. (2.18), the 'cyclic coordinates' χ and φ are separated from the wavefunction

$$\Psi_{JKM} = \Theta(\theta) e^{-iK\chi} e^{-iM\varphi} \tag{A.1}$$

which simplifies the Schrödinger equation to a one dimensional differential equation in θ:

$$\left[\frac{1}{\sin\theta}\frac{\partial}{\partial\theta}\left(\sin\theta\frac{\partial}{\partial\theta}\right) - M^2\frac{1}{\sin^2\theta} - K^2\left(\frac{\cos^2\theta}{\sin^2\theta} + \frac{A}{B}\right) + 2\frac{\cos\theta}{\sin^2\theta}KM + \frac{E}{B}\right]\Theta(\theta) = 0 \tag{A.2}$$

The ansatz

$$x = \frac{1}{2}(1-\cos\theta) \qquad\qquad \lambda = \frac{E}{B} - \frac{A}{B}K^2 \tag{A.3}$$

reduce it to the hypergeometric differential equation. The solution can be expressed by the hypergeometric functions $F(a,b,c;x)$ or further reduced to the Jacobi polynomials $P_n^{(\alpha,\delta)}(x)$. The whole solution Ψ_{JKM} becomes

$$\Psi_{JKM} = N_{JKM} x^{\frac{1}{2}|K-M|}(1-x)^{\frac{1}{2}|K+M|}\frac{n!}{(\alpha+1)_n}P_n^{(\alpha,\delta)}(1-2x)e^{-iK\chi}e^{-iM\varphi} \tag{A.4}$$

with

$$n = J - \frac{1}{2}|K-M| - \frac{1}{2}|K+M| \qquad \alpha = |K-M| \qquad \delta = |K+M| \tag{A.5}$$

Whereas N_{JKM} is the normalization constant and $(x)_n$ the Pochhammer symbol. For a detailed derivation see [62].

B The matrix elements used

It is expedient to represent the elements of the Hamiltonian matrix in the basis of the symmetric-top wavefunctions, $|JKM\rangle$. These are related to the Wigner D-functions D^J_{MK} via

$$|JKM\rangle = (-1)^{M-K} \left[\frac{2J+1}{8\pi^2}\right]^{1/2} D^J_{-M-K}(\varphi,\theta,\chi) \tag{B.1}$$

The field operators can be expressed in terms of the Legendre polynomials $P_J(\cos\theta)$ and spherical harmonics $Y_{JM}(\theta,\varphi)$, which in turn, are related to the Wigner D-functions by

$$D^J_{M0}(\varphi,\theta,\chi) = \left(\frac{4\pi}{2J+1}\right)^{1/2} Y^*_{JM}(\theta,\varphi) \tag{B.2}$$

$$D^J_{00}(\varphi,\theta,\chi) = P_J(\cos\theta) \tag{B.3}$$

The evaluation of the matrix elements of the Hamiltonian then only requires the application of the 'triple product over Wigner function' theorem,

$$\int D^{J_3}_{M_3K_3}(\mathbf{R}) D^{J_2}_{M_2K_2}(\mathbf{R}) D^{J_1}_{M_1K_1}(\mathbf{R}) d\Omega = 8\pi^2 \begin{pmatrix} J_1 & J_2 & J_3 \\ M_1 & M_2 & M_3 \end{pmatrix} \begin{pmatrix} J_1 & J_2 & J_3 \\ K_1 & K_2 & K_3 \end{pmatrix} \tag{B.4}$$

where $\mathbf{R}$ denotes (φ,θ,χ).

(A) For the collinear case, the matrix elements to be determined are:

$$\begin{aligned} \left\langle J'K'M' \left| \frac{\mathcal{H}}{B} \right| JKM \right\rangle = & \left\langle J'K'M' \left| J(J+1) + \rho K^2 - \omega_\perp \right| JKM \right\rangle \\ & -\omega \left\langle J'K'M' \left| \cos\theta \right| JKM \right\rangle \\ & -\Delta\omega \left\langle J'K'M' \left| \cos^2\theta \right| JKM \right\rangle \end{aligned} \tag{B.5}$$

where

$$\cos\theta = P_1(\cos\theta) = D^1_{00}(\varphi,\theta,\chi) \tag{B.6}$$

$$\cos^2\theta = \frac{1}{3}\left(2P_2(\cos\theta)+1\right) = \frac{1}{3}\left(2D^2_{00}(\varphi,\theta,\chi)+1\right) \tag{B.7}$$

The properties of the 3j-symbols, see Appendix C, preclude interactions between states with different M and K. As a result, states belonging to certain M and K values can be treated in a separate calculation.

$$\begin{aligned}\left\langle J'KM\left|\frac{\mathcal{H}}{B}\right|JKM\right\rangle &= \delta_{JJ'}\left(J(J+1)+\rho K^2-\omega_\perp\right)\\ &-\omega(2J+1)^{1/2}(2J'+1)^{1/2}(-1)^{M-K}\underbrace{\begin{pmatrix}J & 1 & J'\\ -M & 0 & M\end{pmatrix}}_{J'=J,J\pm1}\underbrace{\begin{pmatrix}J & 1 & J'\\ -K & 0 & K\end{pmatrix}}_{J'=J,J\pm1}\\ &-\Delta\omega\frac{2}{3}(2J+1)^{1/2}(2J'+1)^{1/2}(-1)^{M-K}\underbrace{\begin{pmatrix}J & 2 & J'\\ -M & 0 & M\end{pmatrix}}_{J'=J,J\pm1,J\pm2}\underbrace{\begin{pmatrix}J & 2 & J'\\ -K & 0 & K\end{pmatrix}}_{J'=J,J\pm,J\pm2}\end{aligned} \tag{B.8}$$

(B) For the case of tilted fields, the matrix elements can be expressed either in terms of the static field or the laser field. The 'simpler' case is keeping the laser field fixed in space and tilting the electric field relative to it. Then the $\cos\theta$ operator is replaced by:

$$\begin{aligned}\cos\theta_s &= \cos\beta\cos\theta+\sin\beta\sin\theta\cos\varphi\\ &= \cos\beta D^1_{00}+\sin\beta\sqrt{\frac{1}{2}}\left(D^1_{-10}-D^1_{10}\right)\end{aligned} \tag{B.9}$$

Different K states do not mix. The matrix elements are:

$$\begin{aligned}
\left\langle J'KM' \left| \frac{\mathcal{H}}{B} \right| JKM \right\rangle &= \delta_{JJ'}\delta_{MM'}\left(J(J+1)+\rho K^2-\omega_\perp\right) \\
&- \omega\cos\beta(2J+1)^{1/2}(2J'+1)^{1/2}(-1)^{M-K}\underbrace{\begin{pmatrix} J & 1 & J' \\ -M & 0 & M \end{pmatrix}}_{J'=J,J\pm1}\underbrace{\begin{pmatrix} J & 1 & J' \\ -K & 0 & K \end{pmatrix}}_{J'=J,J\pm1} \\
&- \omega(2J+1)^{1/2}(2J'+1)^{1/2}(-1)^{M-K}\sin\beta\sqrt{\frac{1}{2}} \\
&\times\left[\underbrace{\begin{pmatrix} J & 1 & J' \\ -M & -1 & M' \end{pmatrix}}_{J'=J,J\pm1;M'=M+1}\underbrace{\begin{pmatrix} J & 1 & J' \\ -K & 0 & K \end{pmatrix}}_{J'=J,J\pm1} - \underbrace{\begin{pmatrix} J & 1 & J' \\ -M & 1 & M' \end{pmatrix}}_{J'=J,J\pm1;M'=M-1}\underbrace{\begin{pmatrix} J & 1 & J' \\ -K & 0 & K \end{pmatrix}}_{J'=J,J\pm1}\right] \\
&- \Delta\omega(2J+1)^{1/2}(2J'+1)^{1/2}(-1)^{M-K}\underbrace{\begin{pmatrix} J & 2 & J' \\ -M & 0 & M \end{pmatrix}}_{J'=J,J\pm1,J\pm2}\underbrace{\begin{pmatrix} J & 2 & J' \\ -K & 0 & K \end{pmatrix}}_{J'=J,J\pm,J\pm2}
\end{aligned} \tag{B.10}$$

If, on the other hand, the laser field is tilted relative to the fixed static field (see Fig. B.1), the $\cos^2\theta_L$ operator could be written as (with $\varphi \equiv \varphi_S$ and $\theta \equiv \theta_S$):

$$\begin{aligned}
\cos^2\theta_L &= \cos^2\beta\cos^2\theta + 2\sin\beta\cos\beta\sin\theta\cos\theta\cos\varphi + \sin^2\beta\sin^2\theta\cos^2\varphi \\
&= \frac{1}{3} + \frac{2}{3}\cos^2\beta D^2_{00} + 2\sqrt{\frac{1}{6}}\sin\beta\cos\beta\left(D^2_{-10} - D^2_{10}\right) - \frac{1}{3}D^2_{00}\sin^2\beta \\
&\quad + \sqrt{\frac{1}{6}}\sin^2\beta\left(D^2_{-20} + D^2_{20}\right)
\end{aligned} \tag{B.11}$$

The selection rules then become: $J' = J, J\pm1, J\pm2$ and $M' = M, M\pm1, M\pm2$. The equivalence of the two choices of expressing the fields has been numerically checked, but only the first, 'simple' choice, has been used in the calculations.

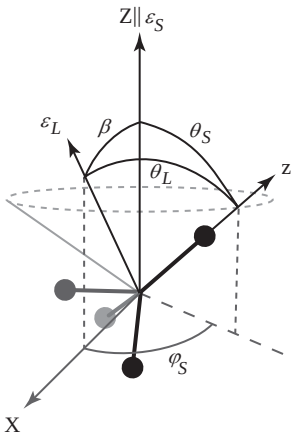

Figure B.1: Illustration of the angles used for substitution for the laser field tilted relative to the electrostatic field.

C Wigner 3j-symbols

C.1 Properties of the 3j-symbols

The 3j-symbols $\begin{pmatrix} j_1 & j_2 & J \\ m_1 & m_2 & -M \end{pmatrix}$ which occur in the calculations involving the coupling of angular momenta are defined for integer and half-integer values and fulfill the following relations [95]:

1. $m_1 \in \{-|j_1|...|j_1|\}$
   $m_2 \in \{-|j_2|...|j_2|\}$
   $M \in \{-|J|...|J|\}$
2. $m_1 + m_2 = M$
3. triangular inequality $|\mathbf{j}_1 - \mathbf{j}_2| \leq \mathbf{J} \leq |\mathbf{j}_1 + \mathbf{j}_2|$
4. Integer perimeter rule $j_1 + j_2 + J \in \mathbb{N}$

The 3j-symbols exhibit various symmetries. An even permutation of the columns leaves the sign unchanged, an odd one changes the sign according to $(-1)^{j_1+j_2+j_3}$.

$$\begin{aligned} \begin{pmatrix} j_1 & j_2 & j_3 \\ m_1 & m_2 & m_3 \end{pmatrix} &= \begin{pmatrix} j_3 & j_1 & j_2 \\ m_3 & m_1 & m_2 \end{pmatrix} = \begin{pmatrix} j_2 & j_3 & j_1 \\ m_2 & m_3 & m_1 \end{pmatrix} \\ &= \begin{pmatrix} j_1 & j_2 & j_3 \\ m_1 & m_2 & m_3 \end{pmatrix} = (-1)^{j_1+j_2+j_3} \begin{pmatrix} j_1 & j_3 & j_2 \\ m_1 & m_3 & m_2 \end{pmatrix} = ... \end{aligned}$$

The same factor is used for a replacement of the second row by its negative.

$$\begin{pmatrix} j_1 & j_2 & j_3 \\ m_1 & m_2 & m_3 \end{pmatrix} = (-1)^{j_1+j_2+j_3} \begin{pmatrix} j_1 & j_2 & j_3 \\ -m_1 & -m_2 & -m_3 \end{pmatrix}$$

C.2 Some important 3j-symbols

The most commonly used 3j-symbols are:

$$
\begin{aligned}
\begin{pmatrix} j & 1 & j \\ m & 0 & -m \end{pmatrix} &= -\frac{(-1)^{j-m}m}{\sqrt{j}\sqrt{1+j}\sqrt{1+2j}} \\
\begin{pmatrix} j+1 & 1 & j \\ m & 0 & -m \end{pmatrix} &= \begin{pmatrix} j & 1 & j+1 \\ m & 0 & -m \end{pmatrix} = -\frac{(-1)^{j+m}\sqrt{1+j-m}\sqrt{1+j+m}}{\sqrt{1+j}\sqrt{1+2j}\sqrt{3+2j}} \\
\begin{pmatrix} j-1 & 1 & j \\ m & 0 & -m \end{pmatrix} &= \begin{pmatrix} j-1 & 1 & j \\ m & 0 & -m \end{pmatrix} = \frac{(-1)^{j+m}\sqrt{j-m}\sqrt{j+m}}{\sqrt{j}\sqrt{-1+2j}\sqrt{1+2j}} \\
\begin{pmatrix} j & 2 & j \\ m & 0 & -m \end{pmatrix} &= -\frac{(-1)^{j+m}(j+j^2-3m^2}{\sqrt{j}\sqrt{1+j}\sqrt{-1+2j}\sqrt{3+2j}} \\
\begin{pmatrix} j+1 & 2 & j \\ m & 0 & -m \end{pmatrix} &= \begin{pmatrix} j & 2 & j+1 \\ m & 0 & -m \end{pmatrix} = \frac{(-1)^{j+m}\sqrt{3}\sqrt{1+j-m}\sqrt{m}\sqrt{1+j+m}}{\sqrt{j}\sqrt{1+j}\sqrt{2+j}\sqrt{1+2j}\sqrt{3+2j}} \\
\begin{pmatrix} j+2 & 2 & j \\ m & 0 & -m \end{pmatrix} &= \begin{pmatrix} j & 2 & j+2 \\ m & 0 & -m \end{pmatrix} \\
&= \frac{(-1)^{j+m}\sqrt{\frac{3}{2}}\sqrt{1+j-m}\sqrt{m}\sqrt{2+j-m}\sqrt{1+j+m}\sqrt{2+j+m}}{\sqrt{1+j}\sqrt{2+j}\sqrt{1+2j}\sqrt{3+2j}\sqrt{5+2j}} \\
\begin{pmatrix} j-1 & 2 & j \\ m & 0 & -m \end{pmatrix} &= \begin{pmatrix} j & 2 & j-1 \\ m & 0 & -m \end{pmatrix} = -\frac{(-1)^{j+m}\sqrt{3}\sqrt{j-m}\sqrt{m}\sqrt{j+m}}{\sqrt{-1+j}\sqrt{j}\sqrt{1+j}\sqrt{-1+2j}\sqrt{1+2j}} \\
\begin{pmatrix} j-2 & 2 & j \\ m & 0 & -m \end{pmatrix} &= \begin{pmatrix} j & 2 & j-2 \\ m & 0 & -m \end{pmatrix} \\
&= \frac{(-1)^{j+m}\sqrt{\frac{3}{2}}\sqrt{-1+j-m}\sqrt{j-m}\sqrt{-1+j+m}\sqrt{j+m}}{\sqrt{-1+j}\sqrt{j}\sqrt{-3+2j}\sqrt{-1+2j}\sqrt{1+2j}} \\
\begin{pmatrix} j & 1 & j \\ m+1 & -1 & -m \end{pmatrix} &= \begin{pmatrix} j & 1 & j \\ m & 1 & -(m+1) \end{pmatrix} = -\frac{(-1)^{j+m}\sqrt{j-m}\sqrt{1+j+m}}{\sqrt{2}\sqrt{j}\sqrt{1+j}\sqrt{1+2j}} \\
\begin{pmatrix} j & 1 & j \\ m & -1 & -(m-1) \end{pmatrix} &= \begin{pmatrix} j & 1 & j \\ m-1 & 1 & -m \end{pmatrix} = \frac{(-1)^{j+m}\sqrt{1+j-m}\sqrt{j+m}}{\sqrt{2}\sqrt{j}\sqrt{1+j}\sqrt{1+2j}} \\
\begin{pmatrix} j+1 & 1 & j \\ m+1 & -1 & -m \end{pmatrix} &= \begin{pmatrix} j & 1 & j+1 \\ m & 1 & -(m+1) \end{pmatrix} = \frac{(-1)^{j+m}\sqrt{1+j+m}\sqrt{2+j+m}}{\sqrt{2}\sqrt{1+j}\sqrt{1+2j}\sqrt{3+2j}} \\
\begin{pmatrix} j & 1 & j+1 \\ m & -1 & -(m-1) \end{pmatrix} &= \begin{pmatrix} j+1 & 1 & j \\ m-1 & 1 & -m \end{pmatrix} = \frac{(-1)^{j+m}\sqrt{1+j-m}\sqrt{2+j-m}}{\sqrt{2}\sqrt{1+j}\sqrt{1+2j}\sqrt{3+2j}} \\
\begin{pmatrix} j-1 & 1 & j \\ m+1 & -1 & -m \end{pmatrix} &= \begin{pmatrix} j & 1 & j-1 \\ m & 1 & -(m+1) \end{pmatrix} = \frac{(-1)^{j+m}\sqrt{-1+j-m}\sqrt{j-+m}}{\sqrt{2}\sqrt{j}\sqrt{-1+2j}\sqrt{1+2j}} \\
\begin{pmatrix} j & 1 & j-1 \\ m & -1 & -(m-1) \end{pmatrix} &= \begin{pmatrix} j-1 & 1 & j \\ m-1 & 1 & -m \end{pmatrix} = \frac{(-1)^{j+m}\sqrt{-1+j-m}\sqrt{j+m}}{\sqrt{2}\sqrt{j}\sqrt{-1+2j}\sqrt{1+2j}}
\end{aligned}
$$

D Derivation of the effective potential

The Schrödinger equation for a symmetric top molecule can be reduced to a one-dimensional differential equation. This is accomplished by replacing the Jacobian that carries a nonuniform spatial weighting by a unit Jacobian such that

$$|\Phi|^2 = |\Psi|^2 \underbrace{\sin\theta}_{\mathcal{J}} \qquad \text{with } \mathcal{J}^{1/2} = \sqrt{\sin\theta} \text{ and } \mathcal{J}^{-1/2} = \frac{1}{\sqrt{\sin\theta}} \tag{D.1}$$

with Ψ the wavefunction obtained by solving the original Schrödinger equation, $\mathcal{J}$ the corresponding Jacobian, and Φ the probability amplitude with a uniform spatial weighting. Hence,

$$\begin{aligned} \langle\Psi|\mathcal{H}|\Psi\rangle &= \left\langle |\Psi|\mathcal{J}^{-1/2}\mathcal{J}^{1/2}\mathcal{H}\mathcal{J}^{-1/2}\mathcal{J}^{1/2}|\Psi\right\rangle \\ &= \left\langle |\Psi\mathcal{J}^{-1/2}|\mathcal{J}^{1/2}\mathcal{H}\mathcal{J}^{-1/2}|\mathcal{J}^{1/2}\Psi\right\rangle \\ &= \langle\Phi|\mathcal{H}'|\Phi\rangle \end{aligned} \tag{D.2}$$

Now it is necessary to determine $\mathcal{H}'$ for the symmetric top. $\mathcal{H}$ is replaced by the differential equation (2.18).

$$\mathcal{H}' = \mathcal{J}^{\frac{1}{2}}\left(-\frac{1}{\sin\theta}\frac{\partial}{\partial\theta}\left(\sin\theta\frac{\partial}{\partial\theta}\right) - \frac{1}{\sin^2\theta}\left(\frac{\partial^2}{\partial^2\varphi} + \frac{\partial^2}{\partial\chi^2} - 2\cos\theta\frac{\partial^2}{\partial\varphi\partial\chi}\right) - \rho\frac{\partial^2}{\partial\chi^2} + V_\mu + V_\alpha\right)\mathcal{J}^{-\frac{1}{2}}$$

Using the solution of the Schrödinger equation $\Psi = e^{-iM\varphi}e^{-iK\chi}\Theta(\theta)$ one obtains:

$$\mathcal{H}' = -\frac{d^2}{d\theta^2} + U \tag{D.3}$$

where U is the effective potential, given by

$$U = \underbrace{\left[\frac{M^2 - \frac{1}{4}}{\sin^2\theta} - \frac{1}{4}\right] + V_\mu + V_\alpha}_{\text{this part is identical to linear rotors}} + \underbrace{\frac{K^2 - 2\cos\theta MK}{\sin^2\theta}}_{\text{symmetric-top anisotropy}} - \underbrace{\rho K^2}_{\text{uniform shift of potential}} \tag{D.4}$$

A detailed description of all the terms can be found in the Section 4.2.

Bibliography

[1] K. H. Kramer and R.B. Bernstein. Focusing And Orientation Of Symmetric-Top Molecules With Electric 6-Pole Field. *J. Chem. Phys.*, 42(2):767–770, 1965.

[2] P. R. Brooks and E. M. Jones. Reactive Scattering Of K Atoms From Oriented CH_3I Molecules. *J. Chem. Phys.*, 45(9):3449–3450, 1966.

[3] H. J. Loesch and A. Remscheid. Brute Force In Molecular Reaction Dynamics - A Novel Technique For Measuring Steric Effects. *J. Chem. Phys.*, 93(7):4779–4790, October 1990.

[4] B. Friedrich and D. R. Herschbach. Spatial Orientation Of Molecules In Strong Electric-Fields And Evidence For Pendular States. *Nature*, 353(6343):412–414, October 1991.

[5] R. D. Levine and R.B. Bernstein. *Molecular Reaction Dynamics and Chemical Reactivity.* Oxford University Press Inc, USA, 1987.

[6] B. Friedrich and D. R. Herschbach. On The Possibility Of Aligning Paramagnetic Molecules Or Ions In A Magnetic-Field. *Z.Phys.D*, 24(1):25–31, August 1992.

[7] J. Bulthuis, J. Moller, and H. J. Loesch. Brute force orientation of asymmetric top molecules. *J. Phys. Chem. A*, 101(41):7684–7690, October 1997.

[8] W. Kong and J. Bulthuis. Orientation of asymmetric top molecules in a uniform electric field: Calculations for species without symmetry axes. *J. Phys. Chem. A*, 104(5):1055–1063, February 2000.

[9] A. Slenczka, B. Friedrich, and D. Herschbach. Pendular Alignment Of Paramagnetic Molecules In Uniform Magnetic-Fields. *Phys. Rev. Lett.*, 72(12):1806–1809, March 1994.

[10] B. Friedrich, D. R. Herschbach, J. M. Rost, H. G. Rubahn, M. Renger, and M. Verbeek. Optical-Spectra Of Spatially Oriented Molecules - ICl In A Strong Electric-Field. *J. Chem. Soc., Faraday Trans.*, 89(10):1539–1549, May 1993.

[11] A. Durand, J. C. Loison, and J. Vigue. Hyperfine-Structure Of Pendular States And The Sign Of The Dipole-Moment Of ICl-A-State. *J. Chem. Phys.*, 101(5):3514–3519, September 1994.

[12] J. M. Rost, J. C. Griffin, B. Friedrich, and D. R. Herschbach. Pendular States And Spectra Of Oriented Linear-Molecules. *Phys. Rev. Lett.*, 68(9):1299–1301, March 1992.

[13] P. A. Block, E. J. Bohac, and R. E. Miller. Spectroscopy Of Pendular States - The Use Of Molecular-Complexes In Achieving Orientation. *Phys. Rev. Lett.*, 68(9):1303–1306, March 1992.

[14] H. J. Loesch. Orientation And Alignment In Reactive Beam Collisions - Recent Progress. *Annu. Rev. Phys. Chem.*, 46:555–594, 1995.

[15] M. Wu, R. J. Bemish, and R. E. Miller. Photodissociation Of Molecules Oriented By Dc Electric-Fields - Determining Photofragment Angular-Distributions. *J. Chem. Phys.*, 101(11):9447–9456, December 1994.

[16] G. Bazalgette, R. White, J. C. Loison, G. Trenec, and J. Vigue. Photodissociation Of ICl Molecules Oriented In An Electric-Field - Direct Determination Of The Sign Of The Dipole-Moment. *Chem. Phys. Lett.*, 244(3-4):195–198, October 1995.

[17] A. Slenczka. Polarization spectroscopy of pendular molecules in the gas phase. *Chem. Eur. J.*, 5(4):1136–1143, April 1999.

[18] B. Friedrich and D. Herschbach. Alignment And Trapping Of Molecules In Intense Laser Fields. *Phys. Rev. Lett.*, 74(23):4623–4626, June 1995.

[19] B. Friedrich and D.R. Herschbach. *Comments At. Mol. Phys*, 32:47, 1995.

[20] B. Friedrich and D. Herschbach. Alignment enhanced spectra of molecules in intense non-resonant laser fields. *Chem. Phys. Lett.*, 262(1-2):41–46, November 1996.

[21] W. S. Kim and P. M. Felker. Ground-state intermolecular spectroscopy and pendular states in benzene-argon. *J. Chem. Phys.*, 107(7):2193–2204, August 1997.

[22] J. J. Larsen, K. Hald, N. Bjerre, H. Stapelfeldt, and T. Seideman. Three dimensional alignment of molecules using elliptically polarized laser fields. *Phys. Rev. Lett.*, 85(12):2470–2473, September 2000.

[23] D. T. Strickland, Y. Beaudoin, P. Dietrich, and P. B. Corkum. Optical Studies Of Inertially Confined Molecular-Iodine Ions. *Phys. Rev. Lett.*, 68(18):2755–2758, May 1992.

[24] T. Seideman. Manipulating external degrees of freedom with intense light: Laser focusing and trapping of molecules. *J. Chem. Phys.*, 106(7):2881–2892, February 1997.

[25] B. Friedrich and D. Herschbach. Spatial Taming And Trapping Of Molecules. *J. Chin. Chem. Soc.*, 42(2):111–117, April 1995.

[26] B. Friedrich and D. Herschbach. Manipulating Molecules via Combined Static and Laser Fields. *J.Phys.Chem.A*, 103:10280–10288, 1999.

[27] B. Friedrich and D. Herschbach. Steric proficiency of polar (2)Sigma molecules in congruent electric and magnetic fields. *Phys. Chem. Chem. Phys.*, 2(4):419–428, 2000.

[28] R. J. Beuhler, R.B. Bernstein, and K. H. Kramer. Observation Of Reactive Asymmetry Of Methyl Iodide . Crossed Beam Study Of Reaction Of Rubidium With Oriented Methyl Iodide Molecules. *J. Am. Chem. Soc.*, 88(22):5331–&, 1966.

[29] D. H. Parker and R. B. Bernstein. Oriented Molecule Beams Via The Electrostatic Hexapole - Preparation, Characterization, And Reactive Scattering. *Annu. Rev. Phys. Chem.*, 40:561–595, 1989.

[30] M. H. Alexander and S. Stolte. Investigation of steric effects in inelastic collisions of NO(X (2)Pi) with Ar. *J. Chem. Phys.*, 112(18):8017–8026, May 2000.

[31] A. Moise, D. H. Parker, and J. J. ter Meulen. State-to-state inelastic scattering of OH by HI: A comparison with OH-HCl and OH-HBr. *J. Chem. Phys.*, 126(12):124302, March 2007. and refs therein.

[32] Special Issue: Imaging Probes of Spectroscopy and Dynamics. *PCCP*, 8(25):2905–3036, 2006.

[33] H. Sato. Photodissociation of simple molecules in the gas phase. *Chem. Rev.*, 101(9):2687–2725, September 2001.

[34] T. P. Rakitzis, A. J. van den Brom, and M. H. M. Janssen. Directional dynamics in the photodissociation of oriented molecules. *Science*, 303(5665):1852–1854, March 2004.

[35] Numerous works on pendular spectroscopy can be found in "List of Publications of Roger E. Miller" J. Phys Chem. A 111, 7248 2007.

[36] H. Stapelfeldt and T. Seideman. Colloquim: Aligning molecules with strong laser pulses. *Rev.Mod.Phys.*, 75(2):543–557, 2003.

[37] A. D. Bandrauk, Y. Fujimura, and R. J. Gordon. *Laser Control and Manipulation of Molecules #821.* An American Chemical Society Publication, 2002.

[38] J. Doyle, B. Friedrich, R. V. Krems, and F. Masnou-Seeuws. Quo vadis, cold molecules? *Eur. Phys. J. D*, 31(2):149–164, November 2004.

[39] J. M. Doyle and B. Friedrich. Chemical physics - Molecules are cool. *Nature*, 401(6755):749–+, October 1999.

[40] H. L. Bethlem and G. Meijer. Production and application of translationally cold molecules. *Int. Rev. Phys. Chem.*, 22(1):73–128, January 2003.

[41] B. Friedrich. Slowing of supersonically cooled atoms and molecules by time-varying nonresonant induced dipole forces. *Phys. Rev. A*, 6102(2):025403, February 2000.

[42] R. Fulton, A. I. Bishop, M. N. Shneider, and P. F. Barker. Controlling the motion of coldmolecules with deep periodic optical potentials. *Nature Physics*, 2(7):465–468, July 2006.

[43] B. Friedrich and G. Meijer. Ultracold physics - Molecules riding waves. *Nature Physics*, 2(7):437–438, July 2006.

[44] B. Friedrich, A. Slenczka, and D. Herschbach. Hybridization Of Rotor States In Parallel Electric And Magnetic-Fields. *Chem. Phys. Lett.*, 221(5-6):333–340, April 1994.

[45] A. Boca and B. Friedrich. Fine structure, alignment, and orientation of (SO)-S-32-O-16 and (OO)-O-16-O-18 molecules in congruent electric and magnetic fields. *J. Chem. Phys.*, 112(8):3609–3619, February 2000.

[46] R. Baumfalk, N. H. Nahler, and U. Buck. Photodissociation of oriented HXeI molecules in the gas phase. *J. Chem. Phys.*, 114(11):4755–4758, March 2001.

[47] H.N. Nahler, R. Baumfalk, and U. Buck. Photodissociation of oriented HXeI molecules generated from $HI - Xe_n$ clusters. *J.Chem.Phys.*, 119(1):224–231, 2003.

[48] B. Friedrich, N. H. Nahler, and U. Buck. The pseudo-first-order Stark effect and the orientation of HXeI molecules. *J. Mod. Opt.*, 50(15-17):2677–2689, October 2003.

[49] V. Poterya, O. Votava, M. Farnik, M. Oncak, P. Slavicek, P. Slavicek, U. Buck, and B. Friedrich. Generation and Orientation of organoxenon molecule $H - Xe - CCH$ in the gas phase. *J. Chem. Phys.*, page 104313, 2008.

[50] S. Minemoto, H. Nanjo, H. Tanji, T. Suzuki, and H. Sakai. Observation of molecular orientation by the combination of electrostatic and nonresonant, pulsed laser fields. *J. Chem. Phys.*, 118(9):4052–4059, March 2003.

[51] H. Sakai, S. Minemoto, H. Nanjo, H. Tanji, and T. Suzuki. Controlling the orientation of polar molecules with combined electrostatic and pulsed, nonresonant laser fields. *Phys. Rev. Lett.*, 90(8):083001, February 2003.

[52] H. Sakai, S. Minemoto, H. Nanjo, H. Tanji, and T. Suzuki. Orientation of polar molecules with combined electrostatic and pulsed, nonresonant laser fields. *Eur. Phys. J. D*, 26(1):33–37, October 2003.

[53] B. Friedrich and D. Herschbach. Enhanced orientation of polar molecules by combined electrostatic and nonresonant induced dipole forces. *J. Chem. Phys.*, 111(14):6157–6160, 1999.

[54] W. Kim and P.M. Felker. Optical-field-induced pendular states and pendular band contours in symmetric tops. *J. Chem. Phys.*, 108(16):6763–6779, 1998.

[55] L.C. Biedenharn and M.E. Rose. Theory of angular correlation of nuclear radiations. *Rev.Mod.Phys.*, 25:729, 1953.

[56] R. Zare. *Angular Momentum: Understanding Spatial Aspects in Chemistry and Physics (Baker Lecture Series).* John Wiley & Sons Inc, 1988.

[57] G. Herzberg. *Molecular Spectra and Molecular Structure: Spectra of Diatomic Molecules.* Krieger Pub Co, 1989.

[58] W. Klemperer, K. K. Lehmann, J. K. G. Watson, and S. C. Wofsy. Can Molecules Have Permanent Electric-Dipole Moments. *J. Phys. Chem.*, 97(10):2413–2416, March 1993.

[59] H. W. Kroto. *Molecular Rotation Spectra.* Dover Publications Inc., 1992.

[60] F. Reiche. Die Quantelung des symmetrischen Kreisels nach Schrödingers Undulationsmechanik. *Zeitschrift für Physik*, 39:444, 1926.

[61] R. de L. Kronig and I.I. Rabi. The symmetrical top in undulatory mechanics. *Phys. Rev.*, 29:262–269, 1927.

[62] C. H. Townes and A. L. Schawlow. *Microwave Spectroscopy.* Dover Publications Inc., 1975.

[63] P.R. Bunker and P. Jensen. *Fundamentals of Molecular Symmetry (Series in Chemical Physics).* Institute of Physics Publishing, 2005.

[64] M. Tinkham. *Group Theory and Quantum Mechanics.* McGraw-Hill Book Company, 1964.

[65] T. Seideman. New means of spatially manipulating molecules with light. *J. Chem. Phys.*, 111(10):4397–4405, September 1999.

[66] J. Ortigoso, M. Rodriguez, M. Gupta, and B. Friedrich. Time evolution of pendular states created by the interaction of molecular polarizability with a pulsed nonresonant laser field. *J. Chem. Phys.*, 110(8):3870–3875, February 1999.

[67] L. Cai, J. Marango, and B. Friedrich. Time-dependent alignment and orientation of molecules in combined electrostatic and pulsed nonresonant laser fields. *Phys. Rev. Lett.*, 86(5):775–778, January 2001.

[68] G.B. Arfken and H.-J. Weber. *Mathematical Methods for Physicists*. Academic Press Inc.,U.S., 1995.

[69] P.R. Bunker and P. Jensen. *Molecular Symmetry & Spectroscopy*. NRC Press (Canada), 1998.

[70] R. P. Feynman. Forces in molecules. *Phys. Rev.*, 56(4):340–343, August 1939.

[71] R.A. Horn and C.R. Johnson. *Matrix Analysis*. Cambridge University Press, 1990.

[72] F.S. Acton. *Numerical Methods that Work (Spectrum)*. The Mathematical Association of America, 1997.

[73] C. M. Dion, A. Keller, O. Atabek, and A. D. Bandrauk. Laser-induced alignment dynamics of HCN: Roles of the permanent dipole moment and the polarizability. *Phys. Rev. A*, 59(2):1382–1391, 1999.

[74] N. E. Henriksen. Molecular alignment and orientation in short pulse laser fields. *Chem. Phys. Lett.*, 312(2-4):196–202, 1999.

[75] A. I. Maergoiz and J. Troe. Weak-Field And Strong-Field Stark Energy-Levels Of Symmetrical-Top Dipolar Molecules. *J. Chem. Phys.*, 99(5):3218–3223, September 1993.

[76] This description is based upon a personal comment by Dimitrii Sadovskki and Boris Zhilinskii. 2008.

[77] M. S. Child, T. Weston, and J. Tennyson. Quantum monodromy in the spectrum of H_2O and other systems: new insight into the level structure of quasi-linear molecules. *Mol. Phys.*, 96(3):371–379, February 1999.

[78] R. H. Cushman and D. A. Sadovskii. Monodromy in the hydrogen atom in crossed fields. *Physica D-Nonlinear Phenomena*, 142(1-2):166–196, August 2000.

[79] C. A. Arango, W. W. Kennerly, and G. S. Ezra. Quantum monodromy for diatomic molecules in combined electrostatic and pulsed nonresonant laser fields. *Chem. Phys. Lett.*, 392(4-6):486–492, July 2004.

[80] C. A. Arango, W. W. Kennerly, and G. S. Ezra. Classical and quantum mechanics of diatomic molecules in tilted fields. *J. Chem. Phys.*, 122(18):184303, May 2005.

[81] I. N. Kozin and R. M. Roberts. Monodromy in the spectrum of a rigid symmetric top molecule in an electric field. *J. Chem. Phys.*, 118(23):10523–10533, June 2003.

[82] D. A. Sadovskii and B. I. Zhilinskii. Quantum monodromy and its generalizations and molecular manifestations. *Mol. Phys.*, 104(16-17):2595–2615, August 2006.

[83] B. Zhilinskii. *Topology in Condensed Matter*, chapter 7 Hamiltonian Monodromy as Lattice Defect, pages 165–186. Springer, 2006.

[84] J. J. Duistermaat. On Global Action-Angle Coordinates. *Commun. Pure Appl. Math*, 33(6):687–706, 1980.

[85] R. Cushman and J. J. Duistermaat. The Quantum-Mechanical Spherical Pendulum. *Bulletin Of The American Mathematical Society*, 19(2):475–479, October 1988.

[86] W.W. Kennerly. *Molecules rotating in electric fields by quantum and semi-quantum mechanics*. PhD thesis, Faculty of the Graduate School of Cornell University, 2005.

[87] C.A. Arango. *Classical and semiclassical mechanics of molecular rotors in tilited fields*. PhD thesis, Faculty of the Graduate School of Cornell University, 2005.

[88] J. W. Zwanziger, M. Koenig, and A. Pines. Berrys Phase. *Annu. Rev. Phys. Chem.*, 41:601–646, 1990.

[89] L. Pogliani. Model with dual indices and complete graphs. The heterogeneous description of the dipole moments and polarizabilities. *New J. Chem.*, 27(6):919–927, 2003.

[90] CrossFire Beilstein database.

[91] B. S. Zhao, S. H. Lee, H. S. Chung, Hwang S., W. K. Kang, B. Friedrich, and D. S. Chung. Separation of a benzene and nitric oxide mixture by a molecule prism. *J. Chem. Phys.*, 119(17):8905–8909, November 2003.

[92] S. A. Schulz, H. L. Bethlem, J. van Veldhoven, J. Kupper, H. Conrad, and G. Meijer. Microstructured switchable mirror for polar molecules. *Phys. Rev. Lett.*, 93(2):020406, July 2004.

[93] U. Buck and M. Farnik. Oriented xenon hydride molecules in the gas phase. *Int. Rev. Phys. Chem.*, 25(4):583–612, October 2006.

[94] D. T. Moore, L. Oudejans, and R. E. Miller. Pendular state spectroscopy of an asymmetric top: Parallel and perpendicular bands of acetylene-HF. *J. Chem. Phys.*, 110(1):197–208, January 1999.

[95] Weisstein, Eric W. “Wigner 3j-Symbol.“From MathWorld–A Wolfram Web Resource. http://mathworld.wolfram.com/Wigner3j-Symbol.html.

Acknowledgements

Over the past year, I have performed research for my diploma thesis at the Molecular Physics Department of the Fritz-Haber-Institut. This work would not have been accomplished without the assistance of many people.

I would like to thank Gerard Meijer for giving me the opportunity to work on my diploma thesis in his department.

I am grateful to my supervisor Bretislav Friedrich, who taught me a great deal about cold molecules and manipulating them with fields. I would especially like to thank him for providing me with a lot of freedom to explore my own ideas. His anecdotes about the history of science were always quite fascinating.

I am grateful Thomas Möller from the Technical University for supporting this thesis project.

A special thanks goes to Jochen Küpper, who helped me a lot in getting the computer programs running. The problems with the libraries would not have been solved without him.

Furthermore, I need to thank my roommates Mikhail Lemeshko and Moritz Kirste for many helpful discussions. I would like to thank Phil Bunker, Gerd von Helden, Andre Fielicke and Andreas Osterwalder for their advice on various topics.

All other diploma students should not go unmentioned. Thomas Middelmann, Fabian Grätz and Peter Zieger provided me with the latest information from the lab and inspiring discussions.

And of course I want to thank all the people in the department, who provide such a great atmosphere.

Ein besonderer Dank gilt meinen Eltern, die mich immer unterstützt haben und mir das Studium ermöglicht haben.

Die selbstständige und eigenständige Anfertigung versichert an Eides statt.

Berlin, den

_____

Unterschrift